Coherent multiple scattering: from atomic matter waves to light and vice versa

Nicolas Cherroret

Laboratoire Kastler Brossel
Sorbonne Université

Mémoire d'Habilitation à Diriger des Recherches

Présenté par

Nicolas Cherroret

Coherent multiple scattering: from atomic matter waves to light and vice versa

---

soutenue le 14 novembre 2018 devant la commission d'examen:

M. Denis Basko	Rapporteur
Mme Isabelle Bouchoule	Rapportrice
M. Jean Dalibard	Invité
M. Dominique Delande	Invité
M. Robin Kaiser	Examinateur
M. Gilles Montambaux	Rapporteur
Mme Aleksandra Walczak	Présidente du jury

Avant propos

Mon parcours professionnel a débuté par une thèse effectuée sous la direction de Sergey Skipetrov au Laboratoire de Physique et Modélisation des Milieux Condensés à Grenoble entre 2006 et 2009. Pendant cette période je me suis intéressé au transport cohérent des ondes classiques dans les milieux désordonnés, avec l'objectif notable de chercher et caractériser théoriquement des signatures expérimentalement mesurables de la localisation d'Anderson de la lumière dans les milieux de taille finie.

Suite à l'obtention d'une bourse post-doctorale de la fondation Alexander von Humboldt, j'ai ensuite rejoint le groupe d'Andreas Buchleitner à l'Université de Freiburg. Pendant ce post-doctorat, ma recherche s'est orientée vers des problèmes d'optique quantique en présence de désordre. Un des enjeux était alors de comprendre les manifestations de propriétés purement quantiques de la lumière telles que l'intrication ou l'indiscernabilité des photons dans les speckles optiques observés en sortie de milieux désordonnés. Ces travaux étant quelque peu différents de mes activités ultérieures, ils ne seront pas évoqués dans ce manuscript.

En 2011, j'ai eu la chance de rencontrer Christian Miniatura et Cord Müller au Centre de Technologies Quantiques (CQT) de Singapour. C'est à cette époque que mon activité de recherche sur le désordre a sérieusement basculé dans le domaine des atomes froids. La collaboration avec le CQT qui a suivi a été extrêmement fructueuse. Elle a conduit à la proposition d'un schéma expérimental visant à détecter la rétro-diffusion cohérente des ondes de matière, observée peu après par Vincent Josse et ses collaborateurs à l'Institut d'Optique. Nous avons ensuite découvert théoriquement le phénomène de diffusion cohérente vers l'avant. Ces travaux sont présentés dans les chapitres 2 et 3 de ce manuscript.

Au cours de nos tentatives de compréhension de la diffusion cohérente vers l'avant en 2012, j'ai été amené à entrer en contact avec Dominique Delande, qui m'a proposé de le rejoindre au Laboratoire Kastler Brossel. Cela a été pour moi le début d'un second post-doctorat, écourté par mon recrutement au CNRS en 2013. Pendant ce post-doctorat, ma recherche s'est brièvement portée sur l'effet des interactions sur l'expansion des paquets d'ondes d'atomes dans les potentiels désordonnés. Ce sujet est discuté dans le chapitre 5.

Depuis 2013, je poursuis mon étude des ondes de matière désordonnées, qui a notamment donné lieu à une collaboration avec le groupe de Jean Claude Garreau et Pascal Szriftgizer à Lille, dont quelques résultats sont mentionnés dans le chapitre 4. Néanmoins, je travaille désormais également sur d'autres projets comme:

- la diffusion de la lumière dans les nuages d'atomes
- les forces de Casimir impliquant des matériaux hétérogènes
- les systèmes analogues optiques simulant les ondes de matière.

Mon travail sur les systèmes optiques simulant les ondes de matière, en particulier, est récent et amené à prendre plus de place dans mes activités futures. Pour cette raison il est évoqué dans le chapitre 6 avec quelques résultats. En revanche, par souci de maintenir une cohérence thématique j'ai choisi de ne pas discuter dans ce manuscript mes travaux sur la diffusion de la lumière dans les nuages atomiques et sur les forces de Casimir, bien qu'ils constituent une partie non négligeable de mon activité de recherche. Le lecteur intéressé par ces sujets pourra consulter la page web https://sites.google.com/site/nicolascherroret/publications, où toutes les publications associées sont listées.

Contents

CHAPTER 1

Introduction

1.1 Coherent multiple scattering of waves

Waves in disordered media do not propagate along straight lines but are scattered in all directions. If the source that emits the wave is coherent, this multiple scattering process produces an interference pattern known as a speckle, which results from the coherent sum of scattered wavelets with random phases. Speckles are the fingerprint of a disordered material and are frequently encountered in optics. In mesoscopic solids where conduction electrons behave like coherent waves, the question of how interference in multiple scattering manifest themselves in routinely measured observables like the conductance has been a central question in the 1980s [Datta 95]. In conductors at room temperature, these manifestations are usually negligible due to the very small electron coherence length L_ϕ: the conductance faithfully obeys the well known Ohm's law, which describes electron multiple scattering as a classical diffusive (random walk) process through the material's impurities. The conductance is also self-averaging: its value is independent of the specific configuration of impurities because the material behaves as a superposition of many incoherent sub-systems of size L_ϕ (the speckle is averaged out). The situation changes in the mesoscopic regime where L_ϕ exceeds the conductor size and electrons genuinely behave like coherent waves: the conductance is no longer self-averaging and fluctuates from a sample to another, so that its determination requires a proper statistical approach. An important theoretical contribution to this problem is due to Gor'kov, Larkin, and Khmel'nitskii [Gor'kov 79], who calculated the disorder-average conductivity of a mesoscopic sample and found a small negative deviation from the classical Drude result (i.e. from the Ohm's law). This deviation, known as the weak localization correction, stems from the enhanced probability for electrons to return to a point already explored by constructive interference between reversed multiple scattering trajectories. The weak localization correction was observed in many systems, especially in 2D thin films where a magnetic field can be applied perpendicular to the film and used a knob to turn weak localization on and off in a controlled way

[Bergmann 84]. As the weak localization correction also depends on L_ϕ, its measurement constitutes a valuable tool to assess electronic coherence in mesoscopic conductors, still used today [Niimi 09, Capron 13].

One reason for the smallness of the weak localization correction is the global character of the conductivity as a transport quantity. In the early 1980s though, it was realized that if single incident $\boldsymbol{k}_{\rm in}$ and outgoing $\boldsymbol{k}_{\rm out}$ particle directions could be addressed, one would be able to observe a large weak localization effect when $\boldsymbol{k}_{\rm out} = -\boldsymbol{k}_{\rm in}$. Performing such a local measurement is hard with electrons in solids but easy in optics, where one can illuminate a disordered material with a plane wave and measure the average intensity in the exact backscattering direction. In this setup, the constructive interference between reversed paths leads to a coherent enhancement of intensity in the vicinity of backscattering known as the coherent backscattering (CBS) effect. CBS of light was first described theoretically in [Golubentsev 84, Akkermans 85], and observed experimentally soon after [Albada 85, Maret 85]. CBS subsequently gave rise to an impressive amount of works, especially in optics (for a review see, e.g., [Aegerter 09]) and even found applications in daily life [Verma 14].

Beyond weak localization and coherent backscattering, many other "mesoscopic" effects in disorder have been investigated, both for electrons in dirty conductors or for classical waves (light, microwaves, ultrasound etc.) in various heterogeneous media. We may cite, without pretending to be exhaustive: universal conductance fluctuations [Stone 85, Licini 85] or nonlinear current-voltage characteristics [Altshuler 85] in mesoscopic conductors, spatial [Feng 91, Berkovits 94] or temporal [Scheffold 97, Scheffold 98] intensity correlations in optical speckle patterns or mesoscopic echoes in reverberant chaotic cavities [Rosny 00, Weaver 00]. In optics and acoustics, the understanding of mesoscopic effects in wave transport has led to many applications such as focusing or imaging through complex media [Rotter 17].

1.2 Anderson localization

1.2.1 Electron localization

Anderson discovered in 1958 that conduction of non-interacting electrons is stopped in certain disordered networks [Anderson 58]. In three dimensions, Anderson localization manifests itself as a quantum phase transition: the electron spectrum displays a mobility edge (a concept introduced by Mott soon after Anderson's paper), a critical energy above which the eigenstates of the disordered system are spatially extended, and below which they are exponentially localized.

The activity on Anderson localization surged after a seminal article by Abrahams et al. [Abrahams 79], who developed a phenomenological scaling theory of Anderson localization in conductors of finite size, based on precursory works by Thouless [Thouless 74]. Beyond providing a very elegant description of Anderson localization in terms of scaling arguments, this approach also predicted, in addition to the presence of a mobility edge in 3D, the localization of *all* eigenstates in 1D and 2D disordered systems. Furthermore, the scaling theory made contact between Anderson localization and the weak localization correction to the conductivity, describing the latter as a precursor of the former. Soon after, the first experimental signatures of the Anderson transition in 3D solids appeared, usually observed as

a vanishing of the electron conductivity for a critical value of the carrier density [Hertel 83, Paalanen 83, Rosenbaum 94, Katsumoto 87]. On the theoretical side, several descriptions of the localization problem were also developed, based on diagrammatic formalisms [Berezinskii 74], random-matrix approaches [Dorokhov 82, Mello 88], field theories [Efetov 80], and self-consistent treatments [Vollhardt 80a]. Since the late 2000s finally, a broad class of localization phenomena and Anderson transitions have been identified beyond the historical "Wigner-Dyson" ensembles of disordered systems where only the fundamental time-reversal and spin-rotation symmetries matter [Altland 97, Evers 08], and continue to be explored in a large spectrum of condensed-matter systems.

1.2.2 The success of classical waves, the question of light

Today, it is well established that Anderson localization stems from the proliferation of destructive interference of multiply scattered waves in a disordered medium. As such, it is not specific to electrons in solids but may, on paper, occur for classical waves as well [John 84, Anderson 85, John 87]. Searching for Anderson localization of classical waves has several advantages as compared to electrons in solids: one avoids particle interactions which modify the localization scenario (see below) and uncontrolled coupling to other degrees of freedom like phonons. Experiments with classical waves also allow to probe local observables (specific intensity, spatial correlations etc.), to perform time-resolved measurements and to engineer various types of incident beams. The description of Anderson localization of classical waves is however more delicate, for classical waves are easily absorbed in materials. Moreover, unlike de Broglie waves they cannot be bound in potential wells, which prevents their localization at low energies [Skipetrov 09]. Despite these difficulties, several successful experimental observations of localization of microwaves [Chabanov 00, Laurent 07, Peña 14] and light [Schwartz 07, Lahini 08, Mookherjea 08, Boguslawski 13] have been reported in 1D and 2D. Recently, a series of experiments on ultrasound in elastic networks also beautifully demonstrated Anderson localization and the associated phase transition in 3D [Hu 08, Faez 09, Cobus 16].

The question of Anderson localization of light in 3D has a more turbulent history. First observations based of stationary transmission measurements [Wiersma 97] (see also [Genack 91]) were questioned [Scheffold 99] due to the presence of absorption in the samples, which mimics the effect of Anderson localization. This difficulty was later circumvented by time-resolved measurements carried out in the group of G. Maret in Konstanz [Störzer 06, Sperling 13]. Unfortunately, it was eventually realized that the observed presumed signatures of 3D Anderson localization were in fact due to fluorescence [Sperling 16, Skipetrov 16]. At the same time, it was demonstrated numerically that in 3D random ensembles of point scatterers the vector nature of light prevents localization [Skipetrov 14, Bellando 14]. This surprising result was so far missed by theoreticians, for almost all descriptions of Anderson localization relied on scalar models for light. At the moment, it is not yet clear on which precise microscopic mechanism(s) the absence of 3D light localization found in [Skipetrov 14, Bellando 14] is based on, and whether it constitutes an exception or a general rule. A clear experimental observation of 3D localization of light is, on the other hand, still lacking.

1.3 Atomic matter waves in random potentials

1.3.1 Anderson localization of cold atoms

The first experimental studies on Anderson localization of atomic matter waves date back from the early 2000s. These experiments involve clouds of cold atoms evolving in far-detuned spatially disordered optical potentials usually produced from laser speckles or bichromatic lattices. As compared to classical waves, cold-atom setups have the decisive advantage of offering for a great control of the disorder. In addition, while the detection of classical-wave localization most often involves transmission or reflection measurements whose interpretation is severely complicated by interface effects, experiments on cold atoms allow to probe localization *inside* the disordered environment ("bulk" measurements). Last, but not least, atomic interactions can be to some extent controlled in cold gases, and therefore studied in a systematic way [Bloch 08, Sanchez-Palencia 10]. This has to be contrasted with electronic conductors, where interactions are always present and cannot be turned off.

Anderson localization of non-interacting atomic matter waves was observed in 1D in [Billy 08, Roati 08] after several attempts. These experiments were accompanied by a number of theoretical works, [Sanchez-Palencia 07, Kuhn 07, Skipetrov 07] to cite few. In 3D, three experiments reported on Anderson localization of cold atoms as well [Jendrzejewski 12b, Kondov 11, Semeghini 15], although the results of [Kondov 11] have been severely questioned [Pasek 17]. These experimental achievements were all based on the direct observation of a fundamental signature of Anderson localization, the temporal freezing of the diffusive spreading of wave packets. Though rather successful, these works were nevertheless not able to characterize precisely the properties of the Anderson quantum phase transition. This task was accomplished in a different setup, known as the "atomic kicked rotor", in a series of beautiful experiments at the PhLAM laboratory in Lille [Chabé 08, Lemarié 10, Lopez 12] (see also [Manai 15] for a recent experiment in 2D). Interestingly, in the cold-atom context the observations of Anderson localization predated the detection of weak localization. The latter was first observed and characterized in 2012 via the (atomic) coherent backscattering effect [Jendrzejewski 12, Labeyrie 12], followed a few years later by an observation of a related effect, the mesoscopic echo [Hainaut 17], in an experiment of atomic kicked rotor. Along with these works, a recent experimental feat was the ability to selectively break the interference between time-reversed trajectories at play in weak localization by means of a controlled dephasing or an artificial gauge field for cold atoms [Müller 15, Hainaut 17], in the spirit of the conductivity measurements performed in mesoscopic physics.

1.3.2 Cold atoms as a tool for probing interacting disordered systems

The interplay between disorder and interactions is a rich and multiform problem on which we presently have only a fragmentary picture. The great potential of cold-atom setups for addressing this question was quickly identified, for in certain atomic species interactions can be tuned via Feschbach resonances. On the effect of interac-

tions, different types of questions may be asked. A first one concerns the *equilibrium properties* of interacting disordered gases. In this context, the low-temperature phase diagram of bosons attracted a lot attention to identify insulating, superfluid or Bose-glass phases [Fallani 07, White 09, Deissler 10, Pasienski 10]. Another type of problem concerns the *out-of equilibrium* properties of interacting disordered gases ensuing from a quench [Polkovnikov 11, Altman 12]. A central question is then how and to which state the quenched system will evolve at long times. Generally speaking, this type of question is ultimately connected with the localization properties of isolated many-body disordered systems. Since 2006 an important theoretical activity has flourished on this topic, motivated by pioneering works [Gornyi 05, Basko 06] which established that the spectrum of 1D disordered many-body systems may display a transition between a conducting phase and an insulating "many-body localized" phase characterized, in particular, by nonthermal states. Seminal experiments already reported on its observation [Schreiber 15, Bordia 16, Choi 16]. The number of theoretical articles exploring the physics of many-body localization is today enormous and listing them here would not be reasonable. The interested reader may consult the recent reviews [Nandkishore 15, Altman 15, Alet 18].

1.4 Content of the manuscript

This manuscript presents a selection of works carried out between my arrival at Laboratoire Kastler Brossel as a postdoc in 2012 and today on the coherent evolution of atomic matter waves in random potentials. Precisely, a number of interference, "mesoscopic" phenomena surviving a disorder average in these systems is discussed, in particular in the regime where Anderson localization shows up: the coherent backscattering effect (chapter 2), the coherent forward scattering effect (chapter 3), the mesoscopic echo and the quantum boomerang effect (chapter 4). Two of those (the coherent forward scattering effect and the quantum boomerang) were not known until these works. The interplay between weak atomic interactions and Anderson localization is touched upon in chapter 5, for the particular problem of atomic wave packets spreading in random potentials, a scenario frequently considered in experiments. Chapter 6, finally, gives an overview of very recent works by the author, some not yet published, on multiple scattering of light in media of dimension "(2+1)". These peculiar systems, originally introduced to demonstrate Anderson localization of light in 2D [Raedt 89, Schwartz 07, Boguslawski 13], have sparked a growing interest in the recent years for light propagation is governed by an effective Schrödinger equation and thus mimics the behavior of a matter wave. In chapter 6, it is shown that when the vector character of light is properly taken into account these systems in fact display a physics much richer than the one pertained to this sole analogy.

CHAPTER 2

Coherent backscattering of matter waves

This chapter is based on the following articles:

- N. Cherroret, T. Karpiuk, C. A. Müller, B. Grémaud, C. Miniatura, *Coherent backscattering of ultracold matter waves: momentum space signatures*, Phys. Rev. A **85**, 011604 (2012)
- N. Cherroret, D. Delande, *Backscattering echo of correlated wave packets*, Phys. Rev. A **88**, 035602 (2013)
- S. Ghosh, D. Delande, C. Miniatura, N. Cherroret, *Coherent backscattering reveals the Anderson transition*, Phys. Rev. Lett. **115**, 200602 (2015)

Coherent backscattering is an essential marker of the coherent nature of wave transport in a disordered medium. While this phenomenon was routinely observed with classical waves since the late 1980s, its first experimental observation with (atomic) matter waves dates back to 2012 only. It was achieved at Institut d'Optique in Palaiseau, following a proposal imagined by the author and his coworkers. Motivated by this success and by the first experimental observations of 3D Anderson localization of cold atoms that appeared in the same period, in 2015 we decided to investigate theoretically the behavior of the atomic coherent backscattering peak across the Anderson transition. I summarize these developments in this chapter.

2.1 Coherent backscattering in a nutshell

Coherent backscattering (CBS) is an interference peak visible near the backscattering direction of the far-field, average intensity pattern produced by a collimated beam reflected from a spatially disordered material. This phenomenon was observed in a number of experiments involving classical waves, in particular in optics [Albada 85, Maret 85, Wolf 88, Wiersma 95, Labeyrie 99] and in acoustics [Bayer 93,

Tourin 97, Cobus 16]. Let us first remind the qualitative description of CBS. Consider a short wave pulse of well-defined wave vector $\boldsymbol{k}_0$, emitted at $t = 0$ through a semi-infinite disordered material. Within the latter, the wave field $\Psi = \sum_i \psi_i$ can be decomposed into a superposition of elementary amplitudes $\psi_i = |\psi_i| \exp(i\phi_i)$ associated with multiple scattering paths i. The intensity $|\Psi|^2 = \sum_{i,j} |\psi_i \psi_j| e^{i(\phi_i - \phi_j)}$ then consists of a complicated interference pattern known as a speckle. Now consider the disorder average of this quantity. The phases differences $\phi_i - \phi_j$ typically fluctuate by an amount $k_0\ell$, where ℓ is the mean free path. In usual situations this product is very large[1], so that one expects only the paths $i = j$ to survive the average, $\overline{|\Psi|^2} \simeq \sum_i \overline{|\psi_i|^2}$. These "incoherent" contributions are displayed in Fig. 2.1(a), in a typical configuration where the signal is detected in reflection at time t, in a direction $\boldsymbol{k}$ around $-\boldsymbol{k}_0$. In time-reversal invariant systems however, incoherent

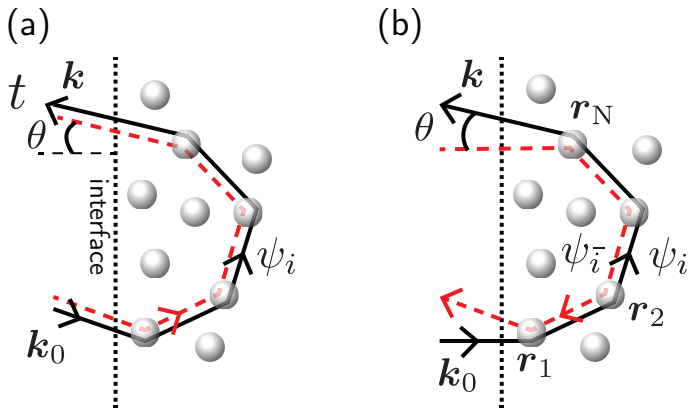

Figure 2.1: (a) Incoherent ($j = i$) and (b) coherent ($j = \bar{i}$) contributions to the average intensity reflected from a disordered medium. (b) involves the interference between two counter-propagating wave paths and gives rise to the CBS peak.

terms are only one part of the reflection signal. Indeed, one must also take into account pairs of time-reversed paths $j = \bar{i}$. Such contributions are displayed in Fig. 2.1(b). At exact backscattering $\boldsymbol{k} = -\boldsymbol{k}_0$ they satisfy $\phi_i = \phi_{\bar{i}}$ so that eventually

$$\overline{|\Psi|^2} = 2 \sum_i \overline{|\psi_i|^2} \quad (\boldsymbol{k} = -\boldsymbol{k}_0). \tag{2.1}$$

The doubling of intensity at backscattering due to the interference of time-reversed paths constitutes the CBS effect. The reasoning can pushed one step further to evaluate the angular shape of the CBS peak: when $\boldsymbol{k} \neq -\boldsymbol{k}_0$, the two time-reversed paths accumulate the finite phase shift

$$\Delta\phi = (\boldsymbol{k}_0 + \boldsymbol{k}) \cdot (\boldsymbol{r}_N - \boldsymbol{r}_1). \tag{2.2}$$

For a given disorder configuration, the interference pertained to Eq. (2.2) produces a cosine-like fringe pattern in reflection, Fig. 2.2(a). Since $|\boldsymbol{k}_0 + \boldsymbol{k}| \sim k_0\theta$ at small backscattering angle, the fringe spacing is $\Delta\theta \sim 2\pi/(k_0|\boldsymbol{r}_N - \boldsymbol{r}_1|)$. The CBS peak appears when summing over disorder configurations: the fringes add up to

[1]For electrons in a good metal like gold, $k_F\ell > 100$. For light in clouds or fog, $k\ell \sim 10^8$.

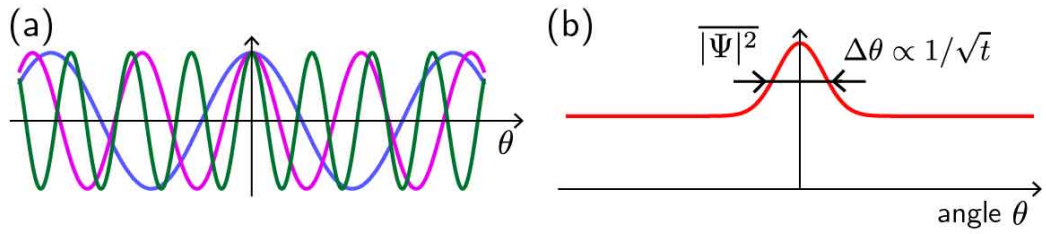

Figure 2.2: (a) For each disorder configuration, the interference between time-reversed paths produces a periodic pattern with random fringe spacing. The central fringe is bright for all configurations. (b) CBS results from averaging over all fringe patterns.

zero except near $\theta = 0$ where the fringe is always bright. Since the propagation is diffusive on average ($|\boldsymbol{r}_\mathrm{N} - \boldsymbol{r}_1| \sim \sqrt{Dt}$), adding up the fringe patterns yields a CBS peak of angular width

$$\Delta\theta \sim \frac{1}{k_0\sqrt{Dt}}. \tag{2.3}$$

The width decreases with time because waves detected at longer times have traveled along longer paths, corresponding to a smaller fringe spacing. The total reflection profile (CBS and incoherent background) is sketched in Fig. 2.2(b).

The CBS peak described here follows from the reflection of a short pulse, a scenario that was experimentally realized in acoustics [Bayer 93, Tourin 97, Cobus 16]. It is also the closest to the matter-wave setup that will be discussed in the next section. In optics, it is more customary to measure CBS using continuous beams. Formally, such a situation amounts to summing the profile in Fig. 2.2(b) over all times. This results in a stationary CBS peak of width $\Delta\theta \sim 1/(k_0\ell)$, displaying a triangular cusp near $\theta = 0$ ("CBS cone") [Golubentsev 84, Akkermans 85, Akkermans 88].

2.2 Coherent backscattering of matter waves

In experiments using classical waves (light, acoustics etc), the detection of CBS in reflection involves an interface separating the disordered medium from the region the wave is coming from. In general, this interface severely complicates the quantitative description of CBS. In 2012, in the context of a collaboration with Cord Müller, Tomasz Karpiuk, Benoît Grémaud and Christian Miniatura, we proposed a new setup for detecting CBS of an atomic matter wave in a disordered potential *without* resorting to any interface [Cherroret 12]. This approach is well suited for cold-atom systems but, as we will see in chapter 6, it can be adapted to optics as well.

2.2.1 Observing CBS with cold atoms

In the setup of Fig. 2.1, CBS is observed by sending a beam of well-defined direction $\boldsymbol{k}_0$ into a disordered material and looking at the angular distribution of the reflected signal. In the language of cold atoms, having a well-defined direction means

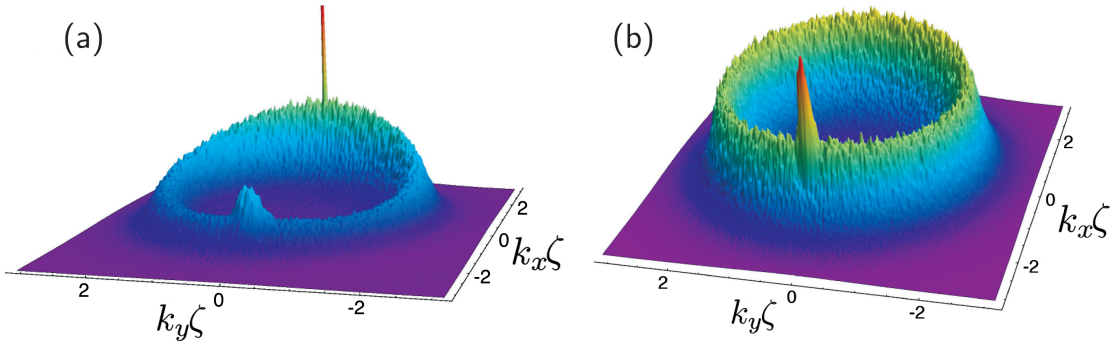

Figure 2.3: Disorder-average momentum distribution (2.5) obtained by numerical propagation of a quasi plane-wave state of mean momentum $\boldsymbol{k}_0$ in a 2D speckle potential. Here $k_0/\Delta k \gg 1$ and $k_0\ell \gg 1$. (a) Distribution at short times $t \sim \tau$ and (b) after a few τ.

preparing an atomic cloud in a state $|\Psi(t=0)\rangle \simeq |\boldsymbol{k}_0\rangle$, which can be done by communicating a mean momentum to the gas while making its dispersion of momenta around $\boldsymbol{k}_0$ very small. Information about the angular distribution of scattered particles is then contained in the average momentum distribution $n_{\boldsymbol{k}}(t) \equiv \overline{|\langle \boldsymbol{k}|\Psi(t)\rangle|^2}$. This suggests the following experimental protocol. A gas is prepared in the state $|\boldsymbol{k}_0\rangle$, let evolve in a spatially disordered potential and finally imaged by time of flight at the desired time. The good point is that no interface is involved in this scenario, as the time-of-flight imaging technique naturally provides a measurement $n_{\boldsymbol{k}}(t)$ *inside* the disorder! Let us now be more precise on the initial state of the gas to be used. To detect a well contrasted CBS peak, the dispersion Δk of particle momenta must be smaller than the CBS width $k_0\Delta\theta \sim 1/\ell$, imposing

$$(\Delta k)^{-1} \gg \ell. \tag{2.4}$$

Typical disordered optical potentials used in cold-atom setups have mean free paths on the order of a few μm [Fallani 08]. For a thermal gas of Rubidium atoms ($\Delta k \sim \sqrt{2mk_{\rm B}T}/\hbar$), condition (2.4) then leads to a temperature $T \lesssim$ few nK. Therefore, a clean observation of CBS requires to use an *ultracold* cloud.

2.2.2 Numerical experiment

In [Cherroret 12] we computed the distribution $n_{\boldsymbol{k}}(t)$ in two dimensions, by numerically evolving in time a quasi plane-wave state $|\Psi(t=0)\rangle$ with the Hamiltonian $H = \boldsymbol{p}^2/(2m) + V(\boldsymbol{r})$, choosing a speckle statistics for the random potential $V(\boldsymbol{r})$ to stick to real experimental conditions:

$$n_{\boldsymbol{k}}(t) = \overline{|\langle \boldsymbol{k}|e^{-iHt/\hbar}|\Psi(t=0)\rangle|^2}. \tag{2.5}$$

In these simulations we started from a Gaussian distribution $n_{\boldsymbol{k}}(t=0) \equiv |\langle \boldsymbol{k}|\Psi(t=0)\rangle|^2 \propto \exp[-(\boldsymbol{k}-\boldsymbol{k}_0)^2/2\Delta k^2]$ of width Δk satisfying Eq. (2.4), and chose disorder parameters so that $k_0\ell \gg 1$ (weak disorder). The distributions obtained at two different times are reproduced in Fig. 2.3. At short times $t \sim \tau$, Fig. 2.3(a), the initial distribution, centered on $\boldsymbol{k}_0$, gets depleted as $\exp(-t/\tau)$ because atoms are

elastically scattered out of the initial mode at a rate given by the scattering mean free time $\tau \equiv \ell/(\hbar k_0/m)$. These scattered atoms populate all other accessible k-space modes and thus distribute within a ring of radius $|\boldsymbol{k}| = |\boldsymbol{k}_0|$. Even for a perfect plane wave and although scattering is elastic, this ring as a finite width: the atomic energy is broadened due to the dispersion of potential's energies. After a few[2] τ, the dynamics becomes diffusive: the memory of the initial direction of propagation gets erased and the momentum distribution becomes more and more isotropic on average, except for the CBS peak that grows around $\boldsymbol{k} = -\boldsymbol{k}_0$. Eventually, at $t \gg \tau$ the initial state is totally depleted, the diffusive background is fully isotropic and the CBS peak is the dominant feature, Fig. 2.3(b).

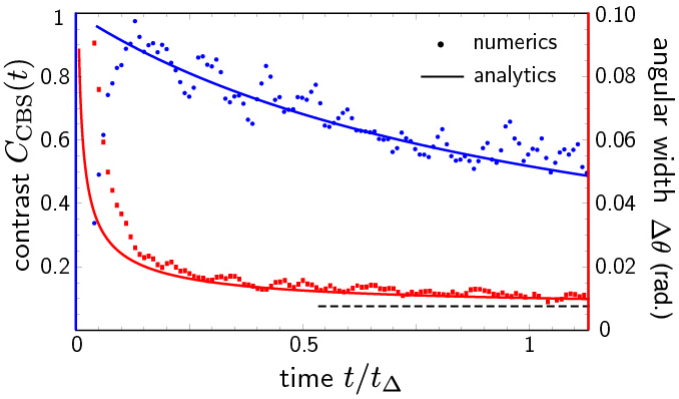

Figure 2.4: CBS contrast (blue dots) and angular width (red dots) deduced from numerical momentum distributions like the one in Fig. 2.3(b). Solid curves are the theoretical prediction for the contrast, Eq. (2.7), and the width, extracted from Eq. (2.7). Deviation of the initial state from a plane wave makes the contrast decay algebraically and the width saturate at $\Delta k/k_0$ when $t \gg t_\Delta$ (dashed line).

2.2.3 Theory

At weak disorder the momentum distribution can be also calculated analytically with the impurity-diagram technique [Montambaux 07]. In the hydrodynamic limit $t \gg \tau$ where atomic momenta are fully randomized, this leads to [Cherroret 12]

$$n_{\boldsymbol{k}}(t) \simeq \frac{A(E_k, \boldsymbol{k}_0)}{2\pi\nu}\left[1 + \int \frac{d^d\boldsymbol{k}'}{(2\pi)^d} \exp\left[-D(\boldsymbol{k}+\boldsymbol{k}')^2 t\right] n_{\boldsymbol{k}'}(0)\right], \tag{2.6}$$

where ν stands for the density-of-states per unit volume and d is the dimensionality. The quantity $A(E_k, \boldsymbol{k}_0)$ is called the spectral function. It can be interpreted as the probability for an atom of initial momentum $\boldsymbol{k}_0$ to acquire the energy $E_k \equiv \hbar^2\boldsymbol{k}^2/2m$ in the random potential[3]. The spectral function describes the ring in Fig. 2.3(b). At weak disorder it has a Lorentzian shape, $A(E_k, \boldsymbol{k}_0) = (2\hbar/\tau)/[(E_k - E_0)^2 + \hbar^2/\tau^2]$, indicating a broadening $\sim \hbar/\tau$ of atomic energies with respect to the free-space

[2]Precisely when t is on the order of the transport mean free time.

[3]The formal definition is $A(E, \boldsymbol{k}) \equiv 2\pi\overline{\langle\boldsymbol{k}|\delta(E-H)|\boldsymbol{k}\rangle}$. A recent experiment reported on the direct measurement of this quantity for cold atoms in disordered potentials [Volchkov18].

value $E_0 \equiv \hbar^2 k_0^2/2m$. The second term in the brackets is the contribution of the CBS peak. Its contrast (ratio of the CBS and ring heights) is

$$C_{\rm CBS}(t) = \int \frac{d^d\boldsymbol{k}'}{(2\pi)^d} \exp\left[-D(\boldsymbol{k}_0+\boldsymbol{k}')^2 t\right] n_{\boldsymbol{k}'}(0). \tag{2.7}$$

The exponential in Eq. (2.7) stems from the averaging of the phase factor $e^{i(\boldsymbol{k}+\boldsymbol{k}')\cdot\Delta\boldsymbol{r}}$ accumulated by a plane-wave component $|\boldsymbol{k}'\rangle$ of the initial cloud between $\boldsymbol{r}_1$ and $\boldsymbol{r}_{\rm N} = \boldsymbol{r}_1 + \Delta\boldsymbol{r}$ [see Fig. 2.1(b)] over the distribution $\exp(-\Delta\boldsymbol{r}^2/2dDt)/(4\pi Dt)^{d/2}$ of diffusive path lengths. The total CBS peak then results from of the incoherent sum of all $\boldsymbol{k}'$ components. This sum can be interpreted as a lack of "spatial coherence" of the initial cloud as it deviates from a pure plane wave. In practice this deviation shows up at a characteristic time

$$t_\Delta \sim (D\Delta k^2)^{-1}. \tag{2.8}$$

When $t \ll t_\Delta$, the CBS peak is fully contrasted and its width coincides with the result (2.3) expected for a perfect plane wave. When $t \gg t_\Delta$ on the other hand, the peak contrast is reduced by a factor $(t_\Delta/t)^{d/2} \ll 1$ and $\Delta\theta$ saturates at $\Delta k/k_0$. Fig. 2.4 compares the prediction (2.7) for the CBS contrast and the CBS width with numerical simulations at weak disorder. The agreement is good, except at short times $t \sim \tau$ where the hydrodynamic description breaks down. The description of short times requires a special treatment that was undertaken in [Plisson 13].

2.2.4 Experiments

CBS of cold atoms was experimentally observed in 2012 at Institut d'Optique [Jendrzejewski 12] and at INLN [Labeyrie 12] shortly after our initial proposal. We first focus on the results of [Jendrzejewski 12], obtained in somewhat cleaner conditions. This experiment used a non-interacting Rb atomic gas, obtained after dilution of an interacting Bose-Einstein condensate (BEC) by a preliminary free expansion. To achieve the quasi plane-wave state required for observing CBS, the gas was subjected to a brief harmonic pulse so to narrow its momentum distribution down to

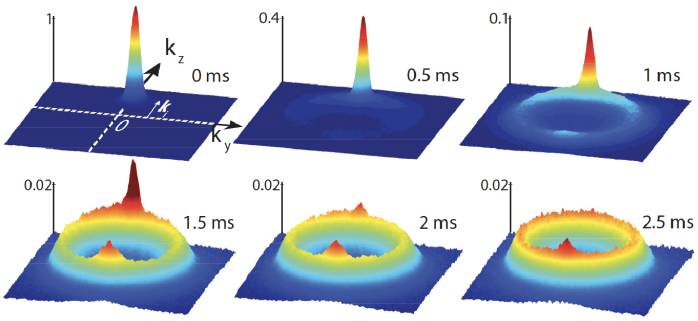

Figure 2.5: Experimental momentum distribution measured at different times in [Jendrzejewski 12], for a non-interacting gas evolving in a 2D optical speckle potential. In this experiment $\tau \simeq 0.33$ ms and $k_0\ell \simeq 5$. The isotropization of the distribution and the CBS peak are well visible.

$\Delta v = \Delta k/\hbar = 0.12$ mm.s^{-1} ("delta-kick cooling" technique [Ammann 97]). In addition to cooling the cloud, the kick also breaks the atom position-momentum correlations that accumulate during the initial cloud's expansion, which turns out to facilitate the characterization of CBS. This point will be discussed in Sec. 2.3. A magnetic-field gradient was subsequently applied to cloud, transferring him a mean velocity $v_0 = 3.3$ mm.s^{-1}. The momentum distribution was finally measured by time-of-flight imaging. It is displayed in Fig. 2.5 at various experimental times. These images nicely reproduce the dynamical scenario discussed in Sec. 2.2.2: a rapid isotropization of momenta over a few τ, and a diffusive ring accompanied by a CBS peak at times $t \sim$ a few ms $\gg \tau$. The exceptional resolution achieved in this experiment is due to a long time-of-flight duration ($T_{\rm tof} \sim 150$ ms), made possible by the use of a levitation setup to compensate for gravity.

2.3 The backscattering echo

In 2012, the group of G. Labeyrie at INLN (now INPHYNI) also reported on an observation of CBS of cold atoms in a 2D speckle potential [Labeyrie 12]. A major difference with the Palaiseau setup was the absence of magnetic levitation, which imposed a smaller time of flight ($\sim$ 42 ms). More crucially, in this experiment no delta-kick cooling was applied to the cloud after its initial expansion, so that significant position-momentum correlations were present in the gas. To understand why such correlations may be problematic for identifying the CBS peak unambiguously, we sketch in Fig. 2.6 the complete experimental protocol of [Labeyrie 12], in 1D for clarity. At $t = 0$ first, a BEC of mean momentum k_0 is released from its trap and starts a free expansion[4] of duration T_i. During this stage, the cloud develops

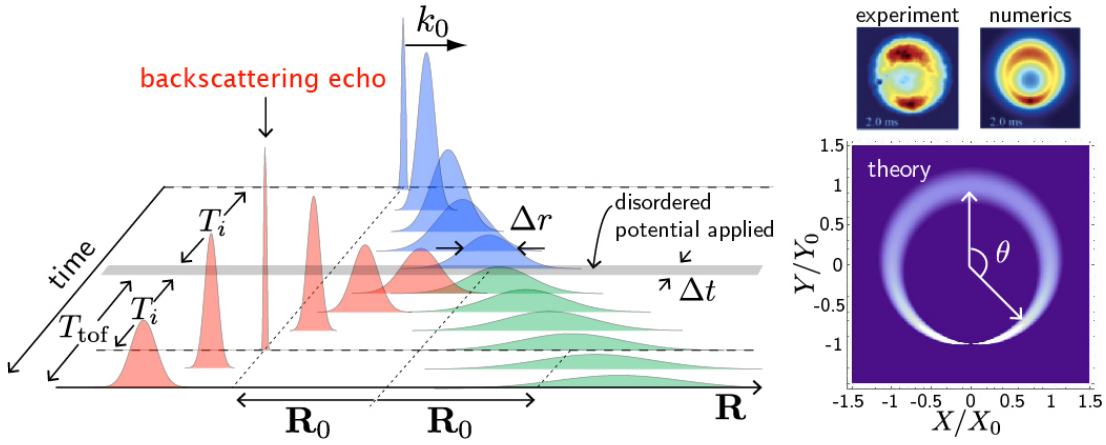

Figure 2.6: Left: in [Labeyrie 12], a BEC is first let expand freely from $t = 0$ to T_i (blue profiles), and thereby develops position-momentum correlations. It is then subjected to a disordered potential for a short duration Δt. When the latter is turned off, the wave packet experiences a free flight of duration $T_{\rm tof}$. At $T_{\rm tof} \simeq T_i$, particles scattered forward (in green) generate a broad density profile, while backscattered particles (in red) refocus: this is the BSE effect. Right: density plot of Eq. (2.9) together with experimental and numerical distributions of [Labeyrie 12].

[4] We here forget particle interactions, which do not play an essential role in the reasoning.

strong position-momentum correlations: atomic positions $\boldsymbol{r}$ and momenta $\boldsymbol{k}$ are related through $\boldsymbol{r} = \hbar \boldsymbol{k} T_i/m$. At $t = T_i$, the speckle potential is applied, say for a duration Δt. Particles are scattered either in the forward direction $+x$ or in the backward direction $-x$. Then when the random potential is turned off, at $T_i + \Delta t$, backscattered particles (depicted in red in Fig. 2.6) all refocus and reform the initial wave packet after a time of flight $T_{\rm tof} \sim T_i$. We have called this (classical) phenomenon the *backscattering echo* (BSE). It is only when $T_{\rm tof} \gg T_i$ that time-of-flight imaging indeed captures the true momentum distribution (2.6). In [Labeyrie 12], the time of flight used was not too far from T_i, so that a BSE was present together with the CBS peak in the measured distribution.

In this description, a BSE shows up only if position-momentum correlations survive the evolution in the speckle potential, which is indeed the case when the cloud size $\Delta r \ll \sqrt{D\Delta t}$. In this limit, it is possible to derive an analytical expression of the spatial distribution detected at $T_{\rm tof} \simeq T_i$ [Cherroret 13]:

$$n_{\mathbf{R}}(T_i) \simeq \frac{1}{2\pi^{3/2}\Delta r|\mathbf{R}+\mathbf{R}_0|} \exp\left[-\frac{(\mathbf{R}^2-\mathbf{R}_0^2)}{4\Delta r^2(\mathbf{R}+\mathbf{R}_0)^2}\right], \tag{2.9}$$

where $\boldsymbol{R}_0 \equiv \hbar \boldsymbol{k}_0 T_i/m$. A density plot of Eq. (2.9) is shown in the right panel of Fig. 2.6 (lower plot). It features a squeezed ring that displays a singularity around the backscattering direction $\theta = \pi$. This singularity signals the BSE [CBS is not accounted for in Eq. (2.9)]. For comparison we also show in the figure a typical experimental distribution as well as a numerical simulation obtained with the same parameters in [Labeyrie 12]. These distributions do display a squeezing and an enhancement at $\theta = \pi$ due to the BSE. Note, however, that Eq. (2.9) corresponds to a limit where the refocusing of the cloud is perfect (infinitely narrow BSE). This idealized scenario originates from the assumption that correlations fully survive the application of the disordered potential ($\Delta r/\sqrt{Dt} \to 0$) and is of course never strictly realized. A refined calculation [Cherroret 13] shows that the BSE has in fact a finite width $\sim \sqrt{D\Delta t}$, which *increases* with the time spent by the cloud in the disorder. Such a scaling is markedly different from the one of the CBS width, Eq. (2.3).

2.4 CBS across the Anderson transition

Motivated by the experimental observations of atomic CBS and the first realizations of 3D Anderson localization of atomic wave packets in the same period (see chapter 5) [Jendrzejewski 12b, Semeghini 15], we later investigated numerically the behavior of the atomic CBS peak in the vicinity of the Anderson phase transition. This work was done during the PhD thesis of Sanjib Ghosh, co-supervised by Christian Miniatura (Majulab), Dominique Delande and myself (LKB) [Ghosh 15].

A quantum particle of energy E evolving in a 3D random potential experiences an Anderson transition at a critical energy E_c known as the mobility edge. Its motion is diffusive when $E > E_c$, spatially localized when $E < E_c$, and sub-diffusive when $E = E_c$. In Eq. (2.6), these different behaviors manifest themselves as a change in the path-length distribution $\exp(-\Delta \boldsymbol{r}^2/6Dt)/(4\pi Dt)^{3/2}$, whose mean square width $\langle \Delta \boldsymbol{r}^2 \rangle \propto Dt$ becomes $\propto \xi^2$ in the localization regime (with ξ the localization length)

and $\propto t^{2/3}$ at the mobility edge (these properties will be discussed in detail in chapter 5). This modifies the CBS angular width as:

$$k_0\Delta\theta \sim \begin{cases} 1/\sqrt{Dt} & E > E_c \\ 1/t^{1/3} & E = E_c \\ 1/\xi & E < E_c. \end{cases} \tag{2.10}$$

The different temporal scalings (2.10) can be used to pinpoint the Anderson transition. This task was accomplished by S. Ghosh during its PhD, through numerical simulations of the momentum distribution in a 3D speckle potential [Ghosh 15]. The CBS angular width extracted from these simulations is shown in the left plot of Fig. 2.7 for three energies[5] E around E_c, and confirms the scaling laws (2.10).

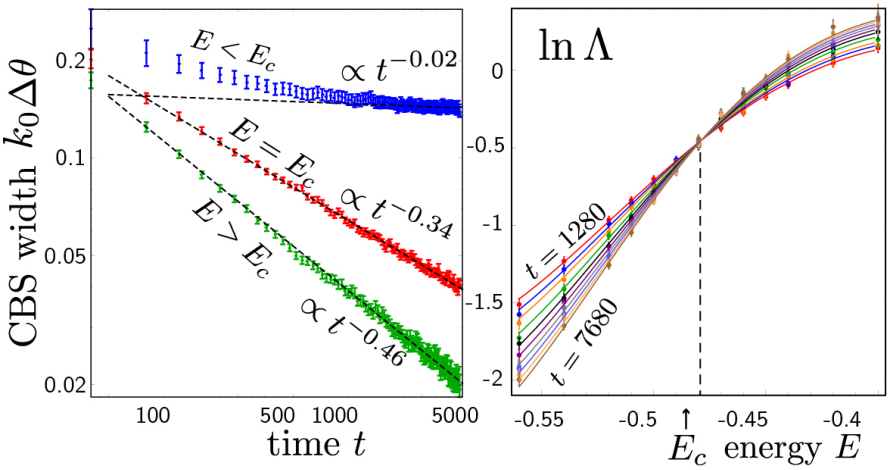

Figure 2.7: Left: CBS angular width as a function of time extracted from numerical simulations of CBS in a 3D speckle potential, for three energies around the mobility edge [Ghosh 15]. Right: Parameter Λ, defined in Eq. (2.11), computed numerically from the CBS width and plotted as a function of energy for various times. All curves cross at the mobility edge E_c. Here times and energies are respectively measured in units of the correlation time and of the correlation energy of the speckle potential.

In the vicinity of E_c, $D(E) \propto |E - E_c|^\nu$ and $\xi(E) \propto |E - E_c|^{-\nu}$, where ν is the critical exponent of the Anderson transition. The three laws (2.10) can then be recast under the unified form

$$\Lambda \equiv \frac{1}{t^{1/3}k_0\Delta\theta} = F\left[\chi(E)t^{1/3\nu}\right], \tag{2.11}$$

where $\chi(E) \propto E - E_c$ and F is a function characteristic of the transition. Eq. (2.11) indicates that the dynamics of the CBS width is governed by a *single* parameter, which was not a priori obvious since the problem involves at least the two parameters E and t. This property is reminiscent of the celebrated single-parameter scaling theory Anderson localization [Abrahams 79]. A direct consequence is that when

[5] In the diffusion regime, the spectral function is narrow so the energy E is roughly $\hbar^2k_0^2/2m$. In the localization regime on the other hand, energy is strongly broadened and the selection of a well-defined E is more tricky. In [Ghosh 15] this was achieved by application of a numerical filter.

$\ln \Lambda$ is plotted against E, the curves at different times should cross at $E = E_c$. This is indeed observed numerically, see the right plot in Fig. 2.7.

The CBS width in 3D can also be exploited to extract an accurate numerical estimate of the mobility edge and of the critical exponent. To achieve this goal, a strategy consists in postulating that the single-parameter scaling law (2.11) holds not only in the close vicinity of the mobility edge, but also away from it, with the functions χ and F unknown. One then Taylor expands χ and F in powers of $E - E_c$ and $t^{1/3\nu}$, and fits this expansion with numerical data of Λ, using E_c, ν and the coefficients of the Taylor expansion as fit parameters. Applying this procedure to the CBS width yields $\nu = 1.61 \pm 0.03$ and, for instance, $E_c \simeq -0.48$ for a disorder amplitude $V_0 = 1$ [Ghosh 15][6]. These values are in good agreement with the best numerical estimates available based on transfer-matrix calculations [Slevin 14, Delande 14] which give, in particular $\nu = 1.57 \pm 0.01$ [Slevin 14].

The idea of using the CBS width for characterizing the Anderson transition was implemented experimentally recently in [Cobus 16]. This experiment did not use cold atoms but elastic waves propagating in a network of Aluminium beads, see Fig. 2.8(a). To detect the Anderson transition, an acoustic pulse is sent through this

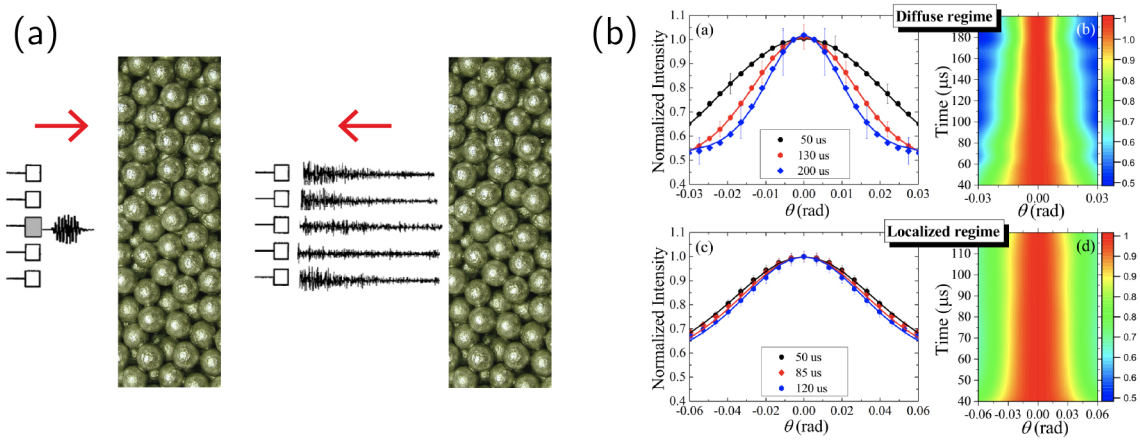

Figure 2.8: (a) Principle of the measurement of CBS with acoustic waves carried out in [Cobus 16]. (b) CBS profiles measured in the diffusion (top) and localization (bottom) regimes at increasing times.

network, and the reflected signal is detected as a function of time by an array of transducers. Fig. 2.8(b) shows measured CBS profiles in the diffusion (top) and localization (bottom) regimes[7]. The saturation of the CBS width in the localization regime is well visible. A critical exponent was also extracted from the data, although a too low value $\nu \simeq 1$ was found. It should be noted, however, that in this setup the data analysis is complicated by the interface and by the finite thickness of the sample, which alter the CBS profile. In this respect, cold atoms again constitute an asset.

[6]These value of E_c and V_0 refer to a blue-detuned speckle potential, and are measured with respect to the average value of the potential and in units of the speckle correlation energy.

[7]Here one switches from a regime to the other by changing the carrier frequency of the pulse (the energy E in the language of matter waves).

CHAPTER 3

The coherent forward scattering effect

This chapter is based on the following articles:

- T. Karpiuk, N. Cherroret, K. L. Lee, B. Grémaud, C. A. Müller, C. Miniatura, *Coherent forward scattering peak induced by Anderson localization*, Phys. Rev. Lett. **109**, 190601 (2012)
- S. Ghosh, N. Cherroret, B. Grémaud, C. Miniatura, D. Delande, *Coherent forward scattering in two-dimensional disordered systems*, Phys. Rev. A **90**, 063602 (2014)
- S. Ghosh, C. Miniatura, N. Cherroret, D. Delande, *Coherent forward scattering as a signature of Anderson metal-insulator transitions*, Phys. Rev. A **95**, 041602(R) (2017)

We discovered the coherent forward scattering (CFS) effect in 2012, shortly after our characterization of CBS in momentum space. CFS refers to an interference peak that grows symmetrically to the CBS peak in the momentum distribution of a matter wave released with a finite mean momentum in a disordered potential. Unlike CBS, which is triggered by weak localization, the full growth of the CFS peak is associated with Anderson localization. In this chapter I summarize its physics, to which I devoted a significant part of my activity since 2012.

3.1 A numerical experiment

We discovered the CFS peak when seeking the manifestations of Anderson localization in the momentum distribution of Fig. 2.3. This question was partly answered in Sec. 2.4: Anderson localization qualitatively modifies the shape of the CBS peak, in particular the time dependence of its angular width. There is, however, another manifestation: at the onset of Anderson localization, which occurs at a characteristic time $t_{\rm loc}$ in general much longer than the scattering time, a new peak grows around the forward direction $\boldsymbol{k} \simeq +\boldsymbol{k}_0$. We first observed this phenomenon in 2D numerical

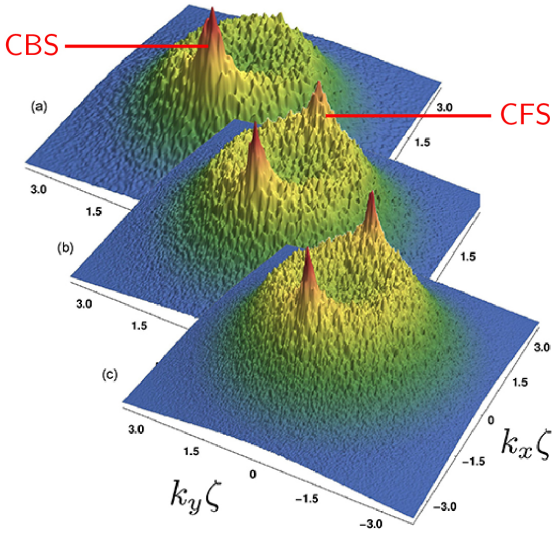

Figure 3.1: Momentum distribution (2.5) obtained by numerical propagation of a plane-wave state $|\boldsymbol{k}_0\rangle$ in a 2D speckle potential. The disorder amplitude is here five times larger than in Fig. 2.3. At long times, a "CFS" peak grows around $\boldsymbol{k} = +\boldsymbol{k}_0$.

momentum distributions [Karpiuk 12], reproduced in Fig. 3.1. These distributions were obtained for a disorder (speckle) amplitude five times larger than in Fig. 2.3 so to reduce the localization time $t_{\rm loc}$. Incidentally, the scattering mean free time is also smaller than in Fig. 2.3, which explains why the ring looks thicker. The distributions in Fig. 3.1 correspond to three successive times beyond the establishment of the structure {ring+CBS peak}. In the upper plot, only the ring and the CBS peak are present. In the middle plot, the CFS peak grows around $\boldsymbol{k} = \boldsymbol{k}_0$. The lower distribution is the asymptotic one: the CFS peak has grown to its maximum value and has become symmetric to the CBS peak.

3.2 Theory

3.2.1 Insufficiency of the one-loop approximation

To understand the origin of the CFS peak, let us come back to the description of atom transport in terms of scattering paths. In chapter 2 we modeled $n_{\boldsymbol{k}}(t)$ as the sum of an incoherent –Fig. 2.2(a)– and a coherent –Fig. 2.2(b)– contribution, in which the paths ψ_i and ψ_j propagate along the same scattering sequence respectively in the same or in opposite directions. These contributions are known as "diffuson" and "cooperon". They are reproduced diagrammatically in Figs. 3.2(a) and (b) in two equivalent representations (the upper ones explicitly display the dotted impurity lines that connect the scattering events shared by the two paths).

As a matter of fact, diagrams (a) and (b) are only the leading-order (zeroth and first-order) terms of a weak-localization perturbation expansion of $n_{\boldsymbol{k}}(t)$. These diagrams have a different spatial structure in $\boldsymbol{k}$ space: the diffuson (a) is smooth while the cooperon (b) is peaked around $\boldsymbol{k} = -\boldsymbol{k}_0$. Higher-order terms involve diagrams with these two structures as well. Those that are peaked around $\boldsymbol{k} = -\boldsymbol{k}_0$ modify

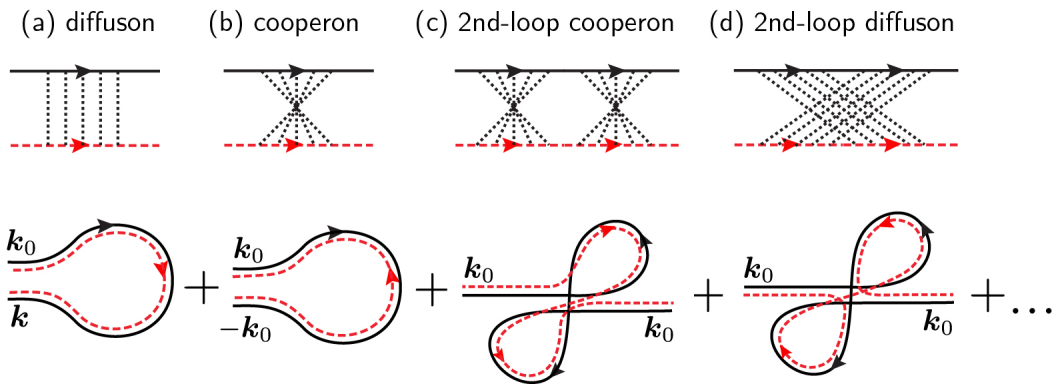

Figure 3.2: Diagrams describing (a) classical diffusion and (b) CBS. (c) and (d) are the leading-order diagrams contributing to the CFS peak.

the CBS peak (they are precisely responsible for the change of the CBS shape at the onset of Anderson localization discussed in Sec. 2.4), while the smooth ones modify the diffusive background, we will discuss them in chapter 5. There exists, however, another interesting category of diagrams : their spatial structure is peaked around $\boldsymbol{k} = +\boldsymbol{k}_0$. At second order there are two such diagrams. They are shown in Figs. 3.2(c) and (d), again in two equivalent representations. The approximation that consists in taking them into account is referred to as a "two-loop approximation" [Hikami 81]. Diagram (c) involves the direct concatenation of two cooperons. For this reason, an atom with initial momentum $\boldsymbol{k}_0$ is twice backscattered and ends up with a momentum $\boldsymbol{k}_0$ after the multiple scattering sequence: the diagram is peaked around $\boldsymbol{k} = +\boldsymbol{k}_0$. The other correction (d) is the time-reversed version of diagram (c): both are thus strictly equal in a time-reversal invariant system.

The two-loop interference diagrams (c) and (d), peaked around $\boldsymbol{k} = \boldsymbol{k}_0$, constitute the leading-order contributions to the CFS peak. This was initially postulated in [Karpiuk 12][1], and later proven rigorously in [Micklitz 14] with the field-theoretic approach to disordered systems (nonlinear σ-model) in a quasi-1D geometry, by perturbation of the σ-model action.

3.2.2 Emergence of CFS at the localization time

It remains to clarify why the CFS diagrams apparently manifest themselves only at long times, in general well beyond the establishment of the CBS peak as observed in numerical simulations. For this purpose, we can make use of a simple geometrical argument where an atom trajectory in the random potential is seen as a semi-classical"tube" of cross-section λ_0^2 and length $v_0 t$ ($v_0 = \hbar k_0/m$, $k_0 = 2\pi/\lambda_0$) [Montambaux 07]. The probability for the interference in Fig. 3.2(c) to occur is then essentially the geometrical probability for the cooperon loop (b) to *cross itself* at some point along the trajectory. This probability $P_{\text{2-loop}} \sim (\lambda_0^{d-1} v_0 t)/V_{\text{tot}}$ is given by the ratio of the tube volume to the total volume accessible to the atom. The latter is $V_{\text{tot}} \sim (Dt)^{d/2}$ in the diffusion regime, and $V_{\text{tot}} \sim \xi^d$ in the Anderson localization

[1]In fact, only diagram (c) was identified in this paper. It is only in subsequent works [Micklitz 14, Ghosh 14] that it was realized that diagram (d) should be also accounted for.

regime, so that:

$$P_{\text{2-loop}} \sim \begin{cases} \dfrac{1}{(k_0\ell)^{d-1}} \left(\dfrac{t}{\tau}\right)^{1-d/2} & \text{diffusion} \\ \dfrac{k_0\ell}{(k_0\xi)^d}\dfrac{t}{\tau} & \text{localization.} \end{cases} \tag{3.1}$$

In the diffusion regime, this prediction reproduces the result of a rigorous, microscopic calculation of diagrams 3.2(c) and (d) [Karpiuk 12], and shows that the probability for a two-loop interference to occur is negligible when $d = 2, 3$ (in 3D $P_{\text{2-loop}}$ even decays with time). In the localization regime, the result (3.1) is only qualitative, but nevertheless clearly indicates that $P_{\text{2-loop}}$ *increases* with time. This confirms that the CFS peak appears when Anderson localization sets in. The characteristic time at which the CFS peak is fully contrasted can be estimated by extrapolating the result obtained in the localization regime to $P_{\text{2-loop}} \sim 1$:

$$t \sim \frac{mk_0^{d-2}}{\hbar}\xi^d \sim h\nu\xi^d \equiv t_{\text{loc}}, \tag{3.2}$$

which is precisely the general expression of the localization time in dimension d.

3.2.3 Beyond perturbation theory: the long-time limit

Strictly speaking, the perturbative diagrams (c) and (d) solely describe the CFS peak as long as their magnitude $P_{\text{2-loop}}$ remains small compared to 1, i.e. as long as $t \ll t_{\text{loc}}$. When $t \sim t_{\text{loc}}$, higher-order loop diagrams come into play to build up the full structure of the CFS peak. Re-summing the complete series of CFS diagrams is a formidable task that has not been accomplished yet. Nonetheless, it turns out that some insight about the long-time limit $t \gg t_{\text{loc}}$ can be inferred from a simple non-perturbative argument based on the expansion of the state vector $|\Psi(t)\rangle$ of the gas over the basis of the disordered system's eigenstates, $|\Psi(t)\rangle = \sum_n \langle\phi_n|\boldsymbol{k}_0\rangle e^{-iE_nt/\hbar}|\phi_n\rangle$ [Lee 14, Ghosh 14]. From this expansion it follows that:

$$n_{\boldsymbol{k}}(t) = \sum_{m,n} \overline{\phi_n^*(\boldsymbol{k}_0)\phi_m(\boldsymbol{k}_0)\phi_n(\boldsymbol{k})\phi_m^*(\boldsymbol{k})e^{-i(E_n-E_m)t/\hbar}} \underset{t\gg t_{\text{loc}}}{\simeq} \sum_n \overline{|\phi_n(\boldsymbol{k}_0)|^2|\phi_n(\boldsymbol{k})|^2}. \tag{3.3}$$

To write the second equality, we explicitly used that the atomic motion becomes confined to a volume ξ^d at long times, due to Anderson localization. In this regime, localized eigenstates are typically separated by $|E_n - E_m| \sim (\nu\xi^d)^{-1} \equiv 2\pi\hbar/t_{\text{loc}}$. Therefore, when $t \gg t_{\text{loc}}$ the off-diagonal phase factors oscillate very fast and vanish after disorder averaging. Eq. (3.3) immediately tells us how the momentum distribution looks like at $t \gg t_{\text{loc}}$. Indeed, in a generic disordered system the eigenstates $\phi_n(\boldsymbol{k})$ are complex random Gaussian variables[2], uncorrelated at different $\boldsymbol{k}$. Furthermore, due to time-reversal invariance the additional symmetry relation $\phi_n(\boldsymbol{k}) = \phi_n^*(-\boldsymbol{k})$ applies. Put together, these two properties lead to:

$$n_{\boldsymbol{k}_0}(t \gg t_{\text{loc}}) = n_{-\boldsymbol{k}_0}(t \gg t_{\text{loc}}) = 2n_{\boldsymbol{k}\neq\pm\boldsymbol{k}_0} \equiv 2n_{\text{ring}}. \tag{3.4}$$

[2]This statistical property can be inferred from the spatial structure of localized modes: $\phi_n(\boldsymbol{r}) \sim e^{i\varphi_n(\boldsymbol{r})}e^{-|\boldsymbol{r}|/\xi}$, where the random phases $\varphi_n(\boldsymbol{r})$ fluctuate at the scale of $\ell \ll \xi$.

In other words, the asymptotic distribution consists of a smooth background $n_{\rm ring}$ and of two peaks at $\boldsymbol{k} = \pm\boldsymbol{k}_0$, in agreement with the numerical result of Fig. 3.1[3]. In passing, time-reversal invariance also implies that $n_{\boldsymbol{k}} = n_{-\boldsymbol{k}}$ in the long-time limit, which confirms the symmetric structure of the asymptotic CBS and CFS peaks visible in the lower distribution of Fig. 3.1.

We now have an almost complete picture of the behavior of CFS in time: its contrast, $C_{\rm CFS}(t) \equiv [n_{\boldsymbol{k}_0}(t) - n_{\rm ring}]/n_{\rm ring}$, grows at times $t \sim t_{\rm loc}$ [Eq. (3.1)] and then saturates at 1 when $t \gg t_{\rm loc}$ [Eq. (3.4)]. The question of how it evolves in between these two limits is more tricky. It can be reformulated in a slightly different way by inserting the density of states (dos) ρ in the mode expansion (3.3), assuming a statistical independence of eigenfunctions and eigenenergies [Lee 14, Ghosh 14]. This procedure leads to

$$C_{\rm CFS}(t) = 2\pi\hbar\rho \int \frac{d\omega}{2\pi} e^{-i\omega t} \frac{\overline{\delta\rho(E_0)\delta\rho(E_0+\hbar\omega)}}{\overline{\rho(E_0)}^2}. \tag{3.5}$$

Eq. (3.5) underlines an interesting –and unexpected– connection between the CFS peak contrast and the Fourier transform of the correlator of dos fluctuations, a quantity known as the form factor. This relation could be exploited experimentally to get information about the statistics of energy levels of a disordered system from measurement of the CFS peak. From a more theoretical point of view, the time dependence of the CFS contrast can conversely be inferred from the calculation of the dos correlator. Such a calculation is still a complicated theoretical problem in general. It was nevertheless recently solved by means of the field-theoretic approach to disordered systems [Micklitz 14, Marinho 18], albeit the analytical results obtained in these works are only valid for quasi-1D geometries. In 2D and 3D, only approximate expressions are available, and only for $t \gg t_{\rm loc}$. Indeed, in this limit the form factor is dominated by the correlation of nearby levels in the spectrum ($|\hbar\omega| \ll 1/\nu\xi^d$). This correlation can be estimated by diagonalizing the 2×2 hybridization Hamiltonian coupling such pairs of levels, with a coupling strength governed by the overlap of the two associated localized wave functions [Mott 70, Sivan 87, Altland 14, Ghosh 14]. In 2D, this approach gives:

$$C_{\rm CFS}(t \gg t_{\rm loc}) \simeq 1 - \alpha \frac{\ln(t/t_{\rm loc})}{t/t_{\rm loc}}, \tag{3.6}$$

where α is a phenomenological prefactor whose precise determination would require a microscopic calculation. Fig. 3.3 compares numerical results for the CFS contrast as a function of time with Eq. (3.6) (α and $t_{\rm loc}$ are taken as fit parameters). Note that at the time scale of the figure, the CBS contrast is always equal to 1 (we remind that the CBS peak grows over a few τ, where the scattering time $\tau \ll t_{\rm loc}$ in 2D).

[3]Strictly speaking, the CFS peak is a consequence of Anderson localization in *unbounded* systems only. Indeed, the attentive reader will notice that in the reasoning leading to (3.4), what matters is the existence of a finite mean-level spacing. Therefore, a CFS peak will also show up for a gas evolving in a spatially-limited disordered potential, for instance in a steep trap, even in the absence of Anderson localization. In this case however, the localization time is replaced by the Heisenberg time and the CFS peak has different dynamical properties [Ghosh 14].

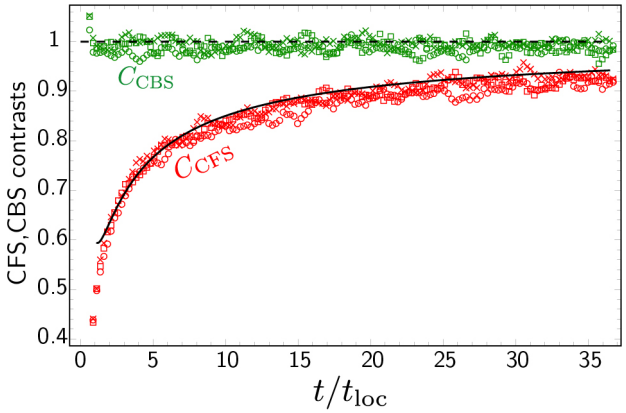

Figure 3.3: Contrast of the CBS (green symbols) and CFS (red symbols) peaks as a function of $t/t_{\rm loc}$, obtained from numerical simulations in a 2D speckle potential. The solid curve is a fit to Eq. (3.6). The dashed line is a guide to the eye.

The CFS peak has not yet been observed experimentally in disordered potentials. In particular, it was not visible in the distributions measured in [Jendrzejewski 12] (see Fig. 2.5) because the evolution time was limited to a few ms in this experiment (for comparison, in experiments that reported on 3D localization of cold atoms $t_{\rm loc}$ was on the order of a few seconds; in 2D under the same conditions it would be much longer). Nevertheless, the counterpart of the CFS peak in position space, the mesoscopic echo in the localization regime (see next chapter), was observed in 2018, in an experimental setup based on the atomic kicked rotor [Hainaut 18]. We will briefly discuss this experiment in Sec. 4.2.2.

3.3 CFS across the Anderson transition

The arguments of Sec. 3.2 indicate that the CFS peak shows up only beyond the localization time, when Anderson localization of eigenstates gives rise to a finite mean-level spacing. In the diffusion regime, states are extended: no mean-level spacing can be defined and no CFS peak is expected. Applied to 3D, this reasoning suggests that the CFS peak can be used as a clear marker of the Anderson transition: on the diffusive side of the transition, no CFS peak should be visible in the momentum distribution, whereas on the localized side a CFS peak should be present (at $t \gg t_{\rm loc}$). In other words, at a fixed (long) time the CFS peak contrast should display a jump as the critical point is crossed. In [Ghosh 17] we indeed observed this phenomenon in numerical simulations of the 3D Anderson model, which describes the hopping of a quantum particle (hopping strength J) on a cubic lattice with random onsite energies uniformly distributed over an interval W [Anderson 58]. At energy $E = 0$, this model displays an Anderson transition at a critical value $W = W_c \simeq 16.5J$.

Numerical momentum distributions obtained for this model at a fixed long time are displayed in Fig. 3.4(a,b,c) in the diffusion ($W < W_c$), critical ($W = W_c$) and localization ($W > W_c$) phases, and confirm the CFS jump. These distributions were calculated by S. Ghosh during his PhD. Panels (d-f) also display the CFS contrast as a function of time. In the localization regime we recover the slow growth seen in

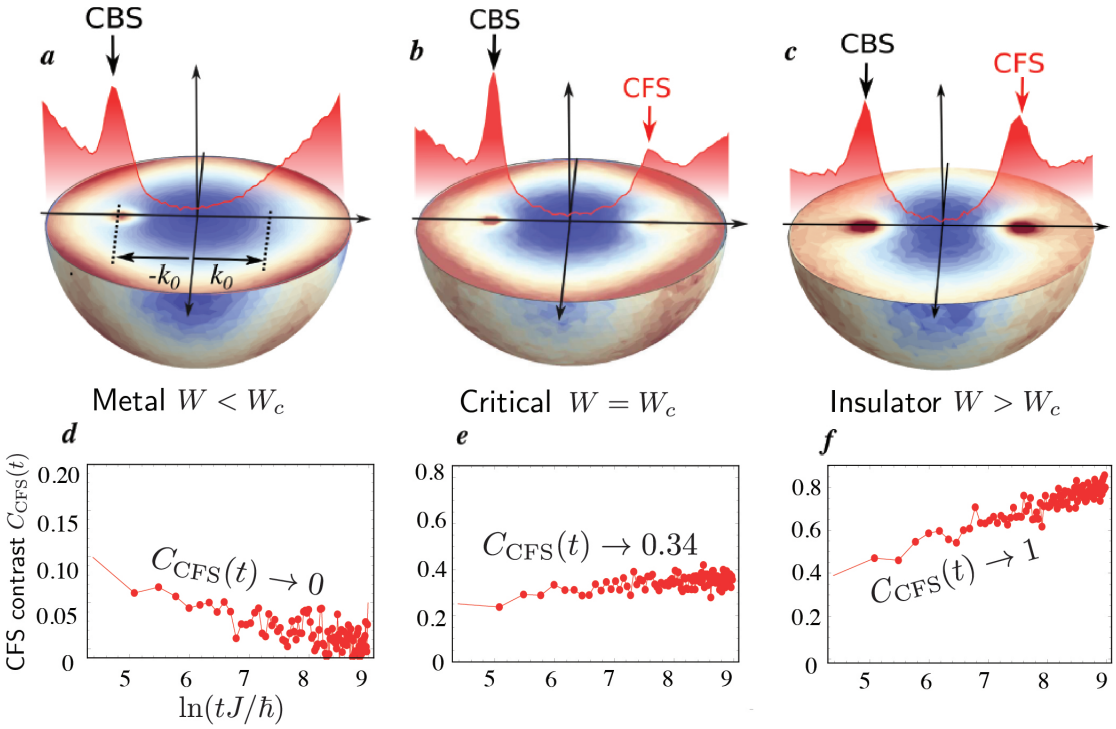

Figure 3.4: (a-c): Long-time limit of the average momentum distribution $n_{\boldsymbol{k}}(t)$ calculated numerically in the diffusion ($W < 12J$), critical ($W = 16.5J$) and localization ($W > W_c = 20J$) phases of the cubic 3D Anderson model (tunneling rate J, disorder strength W, energy $E = 0$). The CFS and CBS peaks are visible at $+\boldsymbol{k}_0$ and $-\boldsymbol{k}_0$ respectively. The solid curve is a cut along the direction of $\boldsymbol{k}_0$. (d-f): Evolution of the CFS contrast with time in the three phases.

2D. In the diffusion regime, a small CFS peak shows up a short times, but it quickly fades away as predicted by Eq. (3.1) for $d = 3$. What happens at the critical point is more surprising: a CFS peak is present at long times, though with a reduced contrast $C_{\rm CFS} \simeq 0.34$. By assuming that the equality (3.5) between the CFS contrast and the form factor still holds at the critical point, one can show that the value of CFS contrast at long times in fact coincides with the *spectral compressibility* χ of the disordered system [Chalker 96a, Chalker 96b]. In a complex system, this quantity quantifies the fluctuations of the number of levels with respect to their mean in a given energy interval. It plays, in particular, an important role in the context of random-matrix theory [Mehta 91, Bohigas 91]. The level-number fluctuations are typically suppressed in the diffusion regime ($\chi = 0$, the spectrum is said to be "rigid"), whereas they are typically strong in the localization regime ($\chi = 1$). The intermediate critical value $\chi \simeq 0.34$ carries information on the multifractal character of eigenstates at the mobility edge and appears to be universal [Zharekeshev 95]. This universality was indeed observed numerically in [Ghosh 17], where the CFS contrast was calculated at the critical point of the Anderson transition for various types of disorder potentials.

CHAPTER 4

Mesoscopic echo and quantum boomerang

This chapter is based on the following articles:

- C. Hainaut, I. Manai, R. Chicireanu, J.-F. Clément, S. Zemmouri, J. C. Garreau, P. Szriftgiser, G. Lemarié, N. Cherroret, and D. Delande, *Return to the origin as a probe of atomic phase coherence*, Phys. Rev. Lett. **118**, 184101 (2017)
- C. Hainaut, I. Manai, J.-F. Clément, J. C. Garreau, P. Szriftgiser, G. Lemarié, N. Cherroret, D. Delande, and R. Chicireanu, *Controlling symmetry and localization with an artificial gauge field in a disordered quantum system*, Nature Comm. **9**, 1382 (2018)
- T. Prat, D. Delande, and N. Cherroret, *The Quantum Boomerang: an unexpected signature of Anderson localization*, arXiv 1704.05241 (2018)

Coherent back and forward scattering are manifestations of weak and Anderson localization in momentum space. Their observation with cold atoms requires a specific procedure to prepare the gas in a plane-wave state. So far however, the majority of experiments that reported on atom localization considered it in *position* space, exploiting another of its signatures: the "freezing" of wave-packet spreading. This phenomenon, which was observed experimentally in 1D [Billy 08, Roati 08] and 3D [Jendrzejewski 12b, Semeghini 15] disordered potentials as well as in clouds subjected to pulsed standing waves (a system known as the kicked rotor) [Chabé 08, Manai 15], will be the object of the next chapter. Beyond the freezing of spreading wave packets however, it is also interesting to investigate how the CBS and CFS peaks of chapters 2 and 3 manifest themselves in position space. This question, perhaps less known, is addressed in the present chapter.

4.1 The mesoscopic echo

4.1.1 Diffusion regime

When a wave packet is let spread in a random potential, the weak localization interference at play in CBS manifests itself as a narrow peak at the origin of the

density profile, standing on top of a diffusive background. This peak is due to the enhanced probability for the particles to return to their starting point by constructive interference between counter-propagating trajectories. In the following we refer to this phenomenon as the "mesoscopic echo", borrowing the terminology introduced in [Prigodin 94]. The mesoscopic echo can be observed in the density distribution of a wave packet evolving according to the Hamiltonian $H = \boldsymbol{p}^2/(2m) + V(\boldsymbol{r})$:

$$n_{\boldsymbol{r}}(t) \equiv \overline{|\langle \boldsymbol{r}|\Psi(t)\rangle|^2} = \overline{|\langle \boldsymbol{r}|e^{-iHt/\hbar}|\Psi(t=0)\rangle|^2}. \tag{4.1}$$

Fig. 4.1(a) shows the distribution (4.1) obtained after a few mean free times by numerically propagating a Gaussian wave packet $n_{\boldsymbol{r}}(0) \propto \exp[-(\boldsymbol{r}-\boldsymbol{r}_0)^2/2\Delta r^2]$ in a 2D speckle potential $V(\boldsymbol{r})$. It displays a broad diffusive pedestal and a narrow peak around the origin $\boldsymbol{r} = \boldsymbol{r}_0$. Note that the initial state considered here is the exact

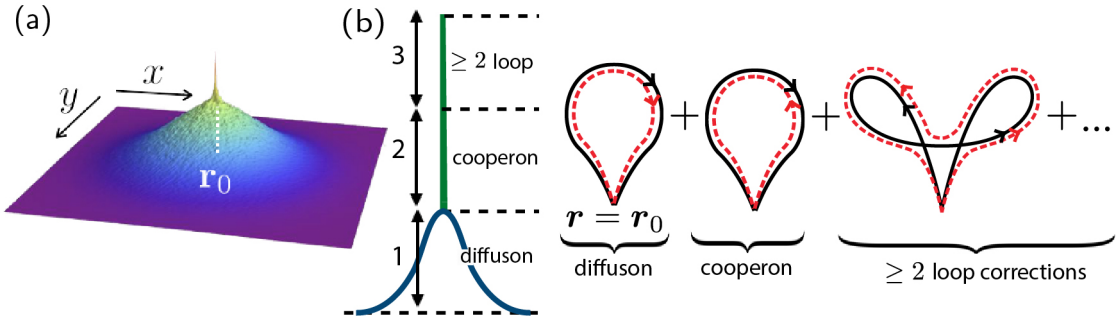

Figure 4.1: (a) Spatial distribution (4.1) obtained by numerical propagation of a narrow wave packet in a 2D speckle potential after a few τ. The mesoscopic echo is visible. (b) Shape of the distribution at long times. When $t \ll t_{\rm loc}$ the mesoscopic echo is due to the cooperon diagram, yielding an enhancement factor of 2. When $t \gg t_{\rm loc}$, higher-loop diagrams proliferate, yielding an enhancement factor of 3.

opposite of the plane-wave state needed to observe CBS in the far field. Precisely, the wave-packet width Δr must be much *smaller* than the mean free path ℓ [compare with criterion (2.4) for CBS]. When this condition is fulfilled, the density distribution in the diffusion regime is given by [Montambaux 07]:

$$n_{\boldsymbol{r}}(t) = \frac{e^{-(\boldsymbol{r}-\boldsymbol{r}_0)^2/2dDt}}{(4\pi Dt)^{d/2}} \left[1 + \int d^d\boldsymbol{r}' g^2(|\boldsymbol{r}-\boldsymbol{r}'|) n_{\boldsymbol{r}'}(0)\right], \tag{4.2}$$

where the function $g(|\boldsymbol{r}|)$ decays on the scale of the mean de Broglie wavelength $\lambda_0 = 2\pi/k_0$ of the wave packet: $g(|\boldsymbol{r}|) = J_0(k_0|\boldsymbol{r}|)\exp(-|\boldsymbol{r}|/2\ell)$ in 2D[1]. The Gaussian prefactor in Eq. (4.2) is the classical diffusive background associated with pairs of paths propagating along the same scattering sequence (diffuson). The second term in the brackets is the mesoscopic echo, associated with pairs of paths propagating along the same scattering sequence but in opposite directions (cooperon), see Fig. 4.1(b). The peak contrast (ratio of the cooperon and diffuson at $\boldsymbol{r} = \boldsymbol{r}_0$) is

$$C_{\rm ME} = \int d^d\boldsymbol{r}' g^2(|\boldsymbol{r}_0 - \boldsymbol{r}'|) n_{\boldsymbol{r}'}(0). \tag{4.3}$$

[1] see, e.g., [Montambaux 07] for the expression of $g(|\boldsymbol{r}|)$ in any dimension.

$C_{\rm ME} = 1$ in the ideal case of a initial wave packet of width $\Delta r \ll \lambda_0$. When this condition is not met, the peak contrast is reduced by the convolution (loss of spatial coherence). With classical waves, the condition $\Delta r \ll \lambda_0$ can be readily realized by using a narrow quasi-monochromatic pulse impinging on a disordered sample. The mesoscopic echo was thus observed long ago in acoustics [Rosny 00, Weaver 00][2]. A beautiful experiment also reported on this phenomenon in the near-field intensity profile of seismic waves propagating in earth's crust [Larose 04].

4.1.2 Localization regime

The description of the mesoscopic echo in terms of a cooperon must be revisited at the onset of Anderson localization $t \sim t_{\rm loc}$, where interference diagrams involving more than one loop start to proliferate. One of them is shown in Fig. 4.1(b): it is the exact counterpart of the CFS diagram (c) in Fig. 3.2. In position space, such a higher-loop diagram makes the contrast of the mesoscopic echo grow *beyond* 1. The fate of the peak in the limit $t \gg t_{\rm loc}$ can be inferred by a mode decomposition analog to that used in Sec. 3.2.3: $|\Psi(t)\rangle = \sum_n \langle\phi_n|\boldsymbol{r}_0\rangle e^{-iE_n t/\hbar}|\phi_n\rangle$. From this decomposition we can express the spatial density $n_{\boldsymbol{r}}(t) = \overline{|\langle\boldsymbol{r}|\Psi(t)\rangle|^2}$ and, as in Sec. 3.2.3, neglect the oscillating phase factors beyond the localization time:

$$n_{\boldsymbol{r}}(t) \underset{t\gg t_{\rm loc}}{\simeq} \sum_n \overline{|\phi_n(\boldsymbol{r}_0)|^2|\phi_n(\boldsymbol{r})|^2}. \tag{4.4}$$

We then use that the localized wave functions are random Gaussian variables, uncorrelated at different positions. This is the same argument as in momentum space, except for one detail: the spatial eigenstates are here *real* due the time-reversal invariance of the disordered system. This implies:

$$n_{\boldsymbol{r}_0}(t \gg t_{\rm loc}) = 3n_{\boldsymbol{r}\neq\boldsymbol{r}_0}. \tag{4.5}$$

In other words, from $t \sim t_{\rm loc}$ onward, the mesoscopic echo grows beyond the factor-2 enhancement expected from the sole account of the cooperon, and reaches a factor-3 enhancement at long times. This phenomenon, which is the counterpart of the growth of the CFS peak in momentum space, is schematized in Fig. 4.1(b). As for CFS it constitutes a signature of Anderson localization in unbounded disordered media[3]. The growth of the mesoscopic echo in time is governed by the same curves as in Fig. 3.3: the factor-2 enhancement due to the cooperon shows up over a few scattering times τ, while the establishment of the factor 3 takes place over $t_{\rm loc}$.

4.2 Experimental observations with cold atoms

Observing the mesoscopic echo with an atomic matter wave is challenging because the spatial distributions of cold gases in optical traps are in general too large for the criterion $\Delta r \ll \lambda_0$ to be satisfied. Even worse, the energy distribution of cold gases

[2]These experiments did not involve disorder in the strict sense but a chaotic cavity.

[3]As for the CFS peak, a similar enhancement can be observed for diffusive waves in *closed* systems. This was shown experimentally with ultrasound in a chaotic cavity [Weaver 00].

in random potentials is not naturally peaked around a well-defined $E_0 = \hbar^2 k_0^2/2m$, as we implicitly assumed so far [in particular when writing Eq. (4.2)], but is instead rather smooth. For these reasons, the mesoscopic echo is in general poorly contrasted and, incidentally, it was not visible in any of the experiments on disordered cold gases reported in the past ten years. The first successful observation is recent, and was achieved in an experimental realization of the atomic "kicked rotor" that we discuss below.

4.2.1 Diffusion regime

The mesoscopic echo was first measured with cold atoms in the diffusion regime in 2017, during the PhD thesis of Clément Hainaut at PhLAM [Hainaut 17]. In this experiment no spatial disorder was used, but rather a temporal form of disorder where the atoms are subjected to an optical standing wave modulated by a periodic sequence of pulses. This setup, known as the atomic kicked rotor, has played an important role in the quest for Anderson localization of cold atoms (more details will be given in chapter 5). Its physics is the following. When subjected to a kick, an atom undergoes a change in momentum, whose value becomes quickly unpredictable after a few kicks. This corresponds to a chaotic motion, similar to a multiple scattering process but in momentum space. Like in spatially disordered systems, interference between scattering paths may also occur and lead to localization. In the atomic kicked rotor, the mesoscopic echo shows up around the point $p = 0$ of the momentum distribution $n_p(t) \equiv \overline{|\langle p|\Psi(t)\rangle|^2}$. Observing a well-contrasted peak in this system requires $n_p(t = 0)$ to be as narrow as possible, i.e. a gas as cold as possible.

The experiment [Hainaut 17] used a gas a of Cs atoms cooled down to $\sim 2\mu$K. Even at this low temperature though, the contrast of the mesoscopic echo is significantly decreased. For this reason, a *differential* measurement of the peak was proposed. Precisely, the following Hamiltonian[4], inspired of [Tian 05], was realized:

$$H = \frac{p^2}{2} + K \sum_n \left[\cos x \ \delta(t-2n) + \cos(x+a) \ \delta(t-2n+1)\right]. \tag{4.6}$$

Eq. (4.6) slightly differs from the standard kicked-rotor Hamiltonian [Casati 79], owing to the additional spatial phase a (the usual kicked rotor is recovered when $a = 0$). In [Hainaut 17], the blinking standing wave is produced by two counter-propagating lasers periodically switched on and off. The phase a is obtained by spatially shifting the standing wave every second pulse. The mesoscopic echo, then, is observed by time-of-flight imaging of the momentum distribution $n_p(t) \equiv \overline{|\langle p|\Psi(t)\rangle|^2}$. Experimental distributions at two successive kicks are shown in Fig. 4.2 (left panel). The value of the distribution at $p = 0$ is also shown in the right panel as a function of time. The interest of using a phase shift a appears: the mesoscopic echo periodically disappears and reappears every second kick. It can therefore be well identified, despite its low contrast. The blinking of the mesoscopic echo is due to an additional

[4] In Eq. (4.6) time is measured in units of the standing-wave pulse period T, space in units of the laser wave number $(2k_L)^{-1}$ and momenta in units of $m/(2k_L T)$.

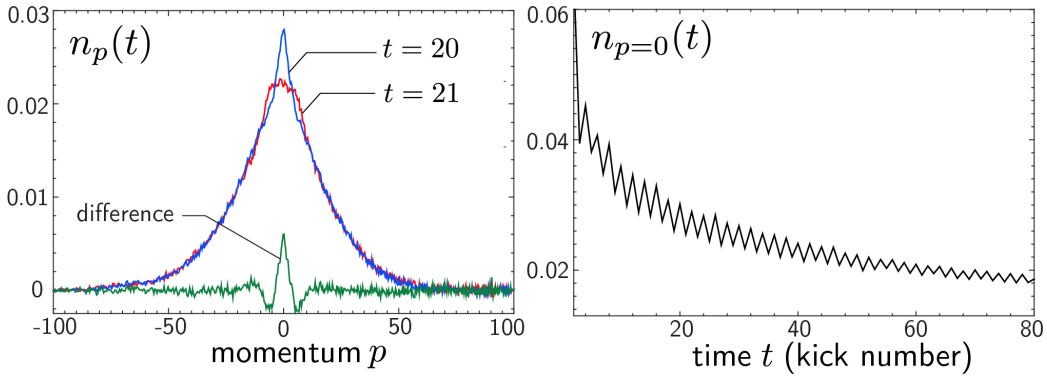

Figure 4.2: Left: experimental distribution $n_p(t)$ measured in [Hainaut 17] at two successive kicks. Right: $n_{p=0}(t)$ as a function of time, which shows an oscillation of the mesoscopic echo.

phase $\exp(i\Phi) = \exp(ia\delta p)$ imprinted to an atom when its momentum is scattered by δp. The effect of this phase on the interference between time-reversed paths is illustrated in Fig. 4.3. Panel (a) shows an interference sequence of 4 kicks. The

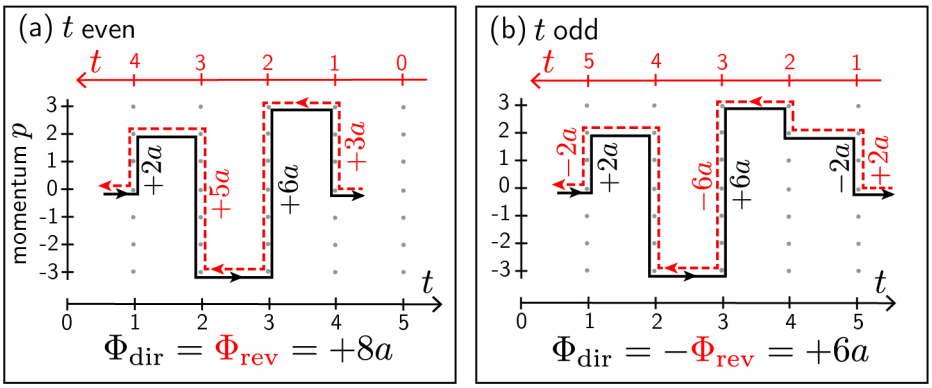

Figure 4.3: Cooperon diagram in the kicked-rotor model (4.6), at an even (a) and an odd (b) kick number. Vertical lines refer to the kicks, which change the momentum, and horizontal lines to free propagation between the kicks. For an even kick number, the two counter-propagating paths accumulate the same phase, so that the interference is constructive. For an odd kick number, the two paths accumulate opposite phases, yielding a finite phase difference and a suppression of the mesoscopic echo.

direct (black) and reversed (dashed red) paths accumulate the same total phase $\Phi_{\rm dir} = \Phi_{\rm rev} = 8a$: the interference is constructive, $\Phi \equiv \Phi_{\rm dir} - \Phi_{\rm rev} = 0$. In contrast, for a sequence of 5 kicks, panel (b), the accumulated phases $\Phi_{\rm dir}$ and $\Phi_{\rm rev}$ have opposite signs, so that a finite phase difference Φ subsists: the interference is not constructive and the average over all paths suppresses the mesoscopic echo in general (provided a is large enough, see below).

The periodic suppression and revival of the peak can also be analytically calculated with the impurity-diagram technique. This approach, originally developed for spatially disordered systems, was adapted to the kicked rotor by A. Altland in [Altland 93]. We used it to calculate the contrast of the mesoscopic echo pertained to model (4.6). This calculation requires to consider separately the series of

crossed diagrams for an odd and an even number of kicks. In the ideal case of an infinitely narrow initial wave packet, this yields, in the diffusion regime:

$$n_{p=0}(t) \simeq \frac{1}{\sqrt{4\pi Dt}} \left[1 + \begin{cases} 1 & t \text{ even} \\ \mathrm{e}^{-a^2 Dt} & t \text{ odd} \end{cases} \right], \tag{4.7}$$

where D is the diffusion coefficient. The second term in the brackets is the contribution of the mesoscopic echo. We recover that for finite a this contribution is only visible at even kicks. At odd kicks, the peak has a low contrast $\mathrm{e}^{-a^2 Dt}$, which stems from the average of the phase factor $\exp(ia\delta p)$ accumulated by the time-reversed sequences in Fig. 4.3(b) over the diffusive distribution of path lengths δp.

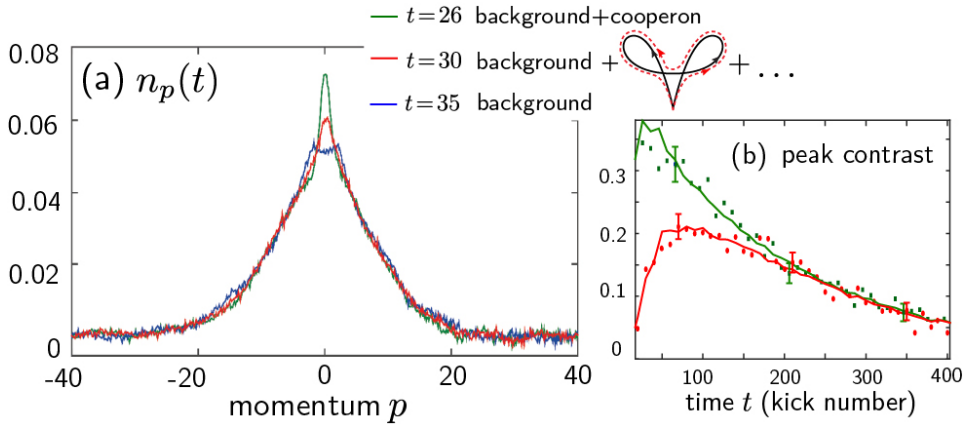

Figure 4.4: (a) Experimental distributions $n_p(t)$ measured in [Hainaut 18]. In this experiment the kick strength K is modulated periodically in time so to temporally separate the contributions of the cooperon and of higher-loop diagrams to the mesoscopic echo. (b) Contributions of the cooperon (green) and of higher-loop diagrams (red) to the contrast of the mesoscopic echo, extracted with this procedure. The difference with Fig. 3.3 is due to the presence of decoherence.

4.2.2 Localization regime

In Sec. 4.1.2 we saw that the enhancement factor of the mesoscopic echo crosses-over from a factor 2 to a factor 3 at the onset of Anderson localization. At first sight, distinguishing experimentally between these two regimes seems hard since the peak is anyhow strongly suppressed by the too broad size of the initial wave packet. A clever way to circumvent this difficulty was proposed in [Hainaut 18], based on the idea that the cooperon disappears when the temporal symmetry of the kick sequence is broken. Precisely, in [Hainaut 18] the kick amplitude K in Eq. (4.6) was further *periodically modulated* in time. This modulation was chosen so to break the time-reversal symmetry of the kick sequence except at specific kicks where the cooperon becomes nonzero. Fig. 4.4(a), for instance, shows a configuration with a period-5 modulation, where the cooperon is only visible at kicks $t = 6 \bmod 10$ (again no echo shows up at even kicks). With this strategy it becomes possible to *temporally separate* the contributions of the cooperon and of higher-loop diagrams, and in particular to access their individual time dependence. Those are shown in Fig. 4.4(b). The difference with Fig. 3.3 is explained by the presence of stray decoherence, which kills the mesoscopic echo exponentially at long times.

4.3 The quantum boomerang

We have so far discussed two configurations corresponding to two ways of preparing a cold gas in a disordered potential. In chapters 2 and 3, we considered a cloud prepared in a (quasi) plane-wave state, $n_{\boldsymbol{k}}(t=0) \simeq \delta(\boldsymbol{k}-\boldsymbol{k}_0)$. The interesting physics then takes place in momentum space. In the second scenario (this chapter), the cloud is prepared in a wave-packet state, $n_{\boldsymbol{r}}(t=0) \simeq \delta(\boldsymbol{r}-\boldsymbol{r}_0)$, and the interesting physics is in position space. In between these two limits however, there is a third intermediate configuration. Suppose, indeed, that one prepares the gas in a wave-packet state to which a finite momentum is impulsed:

$$\langle \boldsymbol{r}|\Psi(t=0)\rangle \propto e^{-\boldsymbol{r}^2/2\Delta r^2 + i\boldsymbol{k}_0\cdot\boldsymbol{r}} \equiv \langle \boldsymbol{r}|\Psi_{\boldsymbol{k}_0}\rangle, \tag{4.8}$$

where the width $\Delta r \ll \ell$ (we here set $\boldsymbol{r}_0 = 0$ without loss of generality). Describing the dynamics of such a state in a random potential was the objet of the PhD thesis of Tony Prat, defended in 2017. Because the wave packet now has a finite mean momentum $\boldsymbol{k}_0$ (unlike in Sec. 4.1), we intuitively expect that it will not only spread but also *move* along the direction of $\boldsymbol{k}_0$ when released in the random potential. To characterize this motion, a natural observable is the average center of mass, $\langle \boldsymbol{r}\rangle \equiv \overline{\langle \Psi(t)|\boldsymbol{r}|\Psi(t)\rangle}$, where the overbar again refers to disorder averaging.

To begin with, let consider the time evolution of the center mass within a purely classical description where the atoms in the cloud behave like Boltzmann particles. Upon application of the random potential, these particles experience a diffusive motion which randomizes the directions of their momenta. This randomization roughly takes place over a transport mean free time τ, and during this process the wave packet typically moves of one transport mean free path ℓ. A simple calculation based on the Boltzmann kinetic equation confirms this scenario [Prat 18]:

$$|\langle \boldsymbol{r}\rangle| = \ell\left(1 - e^{-t/\tau}\right). \tag{4.9}$$

The Boltzmann picture, however, neglects interference and in particular localization effects. In the left plot of Fig. 4.5, the classical prediction (4.9) is compared with exact numerical simulations of the Schrödinger equation in 1D. The difference between the two results is striking: in the quantum system, the center of mass does not saturate at ℓ but goes to zero at long times. In other words, despite the wave packet has been initially "pushed" forward, it *returns to its starting point* at long times. We have called this phenomenon the quantum boomerang. To understand why the wave packet returns to the origin, one can again resort to the eigenstate expansion $|\Psi(t)\rangle = \sum_n \langle \phi_n|\Psi_{k_0}\rangle e^{-iE_n t/\hbar}|\phi_n\rangle$ to express the center of mass $\overline{\langle \Psi(t)|x|\Psi(t)\rangle}$. At times longer than $t_{\rm loc}$ (which is on the order of τ in 1D), we infer:

$$\langle x\rangle \underset{t\gg t_{\rm loc}}{\simeq} \sum_n \overline{|\langle \phi_n|\Psi_{k_0}\rangle|^2 \langle \phi_n|x|\phi_n\rangle}. \tag{4.10}$$

To see that quantity is actually zero, we have to make use of the symmetry properties of the system. Due to time-reversal invariance, first, the eigenfunctions $\phi_n(x)$ are real. This implies that $\langle \phi_n|\Psi_{k_0}\rangle = \langle \phi_n|\Psi_{-k_0}\rangle^*$, such that Eq. (4.10) is invariant upon $k_0 \to -k_0$. In other words, the long-time limit of the average center of mass

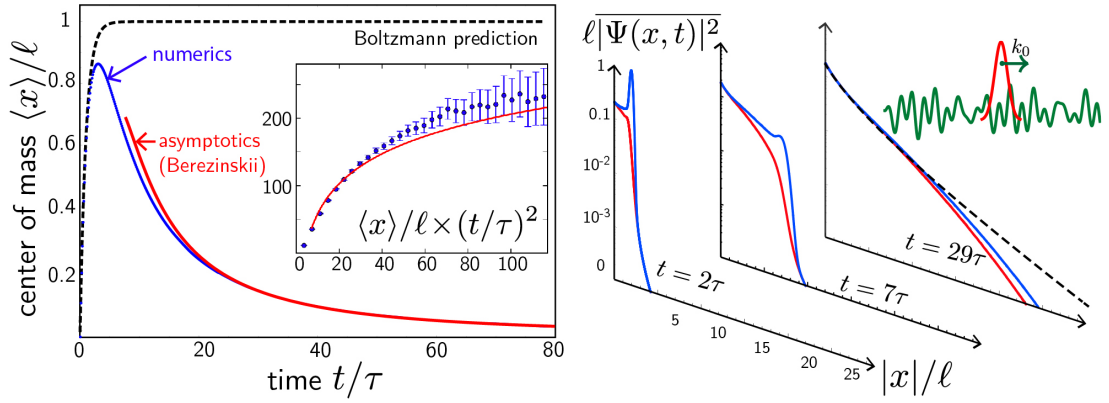

Figure 4.5: Left: numerical center of mass compared with the analytical result of Berezinskii approach at long times. The dashed curve is the classical prediction (4.9). Right: $x > 0$ (blue) and $x < 0$ parts of the density profile of the moving wave packet at three successive times. The dashed curve is the asymptotic distribution calculated by Gogolin in [Gogolin 82].

is the same for right- and left-moving wave packets. Due to the parity-invariance of the system on average, this property necessarily implies that $\langle x\rangle$ is zero. Note that the argument presented here is not specific to 1D but also applies to the localization regime of 2D and 3D systems [Prat 18].

The quantum boomerang is a manifestation of Anderson localization that mixes both large and short scales (the motion takes place within one mean free path but over long times). This makes its quantitative description difficult in general. In particular, usual diagrammatic approaches or nonlinear σ-models seem of limited use as they apply to scales beyond ℓ in general. In 1D nevertheless, $\langle x\rangle$ be calculated analytically by means of an exact solution of the localization problem due to Berezinskii [Berezinskii 74]. This approach consists in a complete resummation of interference contributions based on an ordering of 1D impurity diagrams. For $t \gg \tau$, it leads to $\langle x\rangle \simeq 64\ell \ln(t/4\tau)(\tau/t)^2$. This prediction agrees well with the numerics, see the red curve in the left panel of Fig. 4.5. The logarithm is captured as well, as shown in the inset.

The right panel of Fig. 4.5 finally shows how the density profile $n_x(t)$ evolves as the boomerang effect occurs. $n_x(t)$ is displayed at three successive times, for a wave packet of initial momentum along $+x$. Blue curves are the $x > 0$ part of the profile, and red curves the $x < 0$ part. The profiles exhibit a ballistic peak responsible for the increase of $\langle x\rangle$ at short times. After this peak has been attenuated, the profile re-symmetrizes itself around $x = 0$. This demonstrates that the boomerang effect does not rely on a global forth-and-back motion of the wave packet, as one could have expected, but rather on a re-symmetrization of the profile around $x = 0$. Precisely, at very long times $n_x(t)$ converges to the same asymptotic distribution as for $k_0 = 0$, the so-called Gogolin profile [Gogolin 82], shown as a dashed curve in the right panel of Fig. 4.5.

CHAPTER 5

Weakly interacting disordered matter waves

This chapter is based on the following articles:

- N. Cherroret, B. Vermersch, J. C. Garreau, D. Delande, *How nonlinear interactions challenge the 3D Anderson transition*, Phys. Rev. Lett. **112**, 170603 (2014)
- N. Cherroret, *A self-consistent theory of localization in nonlinear random media*, J. of Phys.: Cond. Mat. **20**, 024002 (2016)
- N. Cherroret, T. Karpiuk, B. Grémaud, C. Miniatura, *Thermalization of matter waves in random potentials*, Phys. Rev. A **92**, 063614 (2015)

The effect of particle interactions on localization phenomena is a difficult problem for which we do not have yet a general understanding. In weakly disordered conductors, one effect of electron-electron collisions is to introduce decoherence in the counter-propagating interference trajectories responsible for weak localization [Altshuler 82][1]. In systems of atomic bosons, interactions were also shown to partially destroy coherent backscattering [Hartung 08]. The interplay between interactions and Anderson localization is, on the other hand, a much more complicated problem. Since 2006, an important theoretical activity on the general localization properties of isolated many-body disordered systems has flourished (see [Nandkishore 15, Altman 15, Alet 18] for reviews), motivated by seminal works [Gornyi 05, Basko 06] which established that the spectrum of 1D disordered many-body systems may display a transition between a conducting phase and an insulating "many-body localized" phase. The experimental observation of many-body localization has already been claimed [Schreiber 15, Bordia 16, Choi 16]. In this chapter though, we will be less ambitious and only touch upon the question of interactions. To this aim we will restrict ourselves to weakly interacting gases of bosons at the mean-field (single-particle) level, and address the particular question of the dynamical evolution of atomic wave packets in random potentials.

[1] Electron interactions also bring an additional (negative) coherent contribution to the conductivity, known as the Altshuler-Aronov correction [Altshuler 80].

5.1 Localization of non-interacting wave packets

5.1.1 Reminders

When subjected to a random potential, a non-interacting atomic wave packet of mean energy E spreads according to Eq. (4.2) in the diffusion regime. In the previous chapter, we were mostly interested in the mesoscopic echo that grows around $\boldsymbol{r} = \boldsymbol{r}_0$. We now focus on the shape of the profile at $\boldsymbol{r} \neq \boldsymbol{r}_0$. In the diffusion regime, this profile is $n_{\boldsymbol{r}}(t) \equiv P_E(\boldsymbol{r}, \boldsymbol{r}_0, t) \simeq \exp[-(\boldsymbol{r}-\boldsymbol{r}_0)^2/2dDt]/(4\pi Dt)^{d/2}$. It is governed by the diffusion coefficient $D = v\ell/d$ and has a mean square width

$$\langle \Delta \boldsymbol{r}^2 \rangle \equiv \int d^d\boldsymbol{r}\, (\boldsymbol{r}-\boldsymbol{r}_0)^2 n_{\boldsymbol{r}}(t) \simeq 2dDt. \tag{5.1}$$

At the onset of Anderson localization, diffusion breaks down, the wave packet stops expanding and its spatial distribution becomes exponentially localized, $P_E(\boldsymbol{r}, \boldsymbol{r}_0, t) \propto \exp(-|\boldsymbol{r}-\boldsymbol{r}_0|/\xi)$, with

$$\langle \Delta \boldsymbol{r}^2 \rangle \propto \xi^2. \tag{5.2}$$

The condition for wave-packet localization strongly depends on dimensionality. In 2D this happens through a cross-over: localization occurs when $t \sim t_{\rm loc} \gg \tau$. In 1D the localization time is on the order of τ, so that the diffusion regime does not even exist and localization is the rule. In 3D finally, localization shows up through a phase transition at a critical energy E_c, the mobility edge: a wave packet of mean energy $E > E_c$ spreads according to Eq. (5.1) up to arbitrarily long times, whereas if $E < E_c$ it gets localized. At the mobility edge $E = E_c$ finally, there is no characteristic time scale and the expansion is sub-diffusive:

$$\langle \Delta \boldsymbol{r}^2 \rangle \propto t^{2/3}. \tag{5.3}$$

The critical properties of the Anderson transition manifest themselves in the energy dependence of D and ξ. The diffusion coefficient vanishes in the vicinity of the critical point, while the localization length diverges: $D \propto (E-E_c)^\nu$ and $\xi \propto (E_c-E)^{-\nu}$. These scalings are algebraic, governed by the critical exponent $\nu \simeq 1.58$.

5.1.2 Experiments

The first experimental observation of the three laws (5.1), (5.2) and (5.3) for cold atoms was achieved in 2008, exploiting a modified version of the atomic kicked-rotor [Chabé 08]. We remind that the kicked-rotor Hamiltonian, $\hat{H} = \hat{p}^2/2 + K\cos\hat{x}\sum_n \delta(t-n)$, describes a particle subjected to a blinking standing wave. Its quantum dynamics displays a phenomenon known as dynamical localization [Casati 79], which is formally equivalent to 1D Anderson localization except that it takes place in momentum space [Fishman 84]. When the kick strength is additionally modulated in a quasi-periodic fashion, $K \to K[1+\epsilon\cos(\omega_1 t)\cos(\omega_2 t)]$, see Fig. 5.1(a), the dynamics of the kicked rotor becomes equivalent to the one of a *3D* disordered system [Shepelyansky 89, Lemarié 09], the Anderson transition taking place at a critical value $K = K_c$. Fig. 5.1(b) shows experimental mean square

widths $\langle \Delta p^2 \rangle$ of a cloud of Cs atoms measured in [Chabé 08] for three values of K in the diffusion ($K > K_c$), localization ($K < K_c$) and critical ($K = K_c$) regimes. The three scaling laws (5.1), (5.2) and (5.3) are well visible.

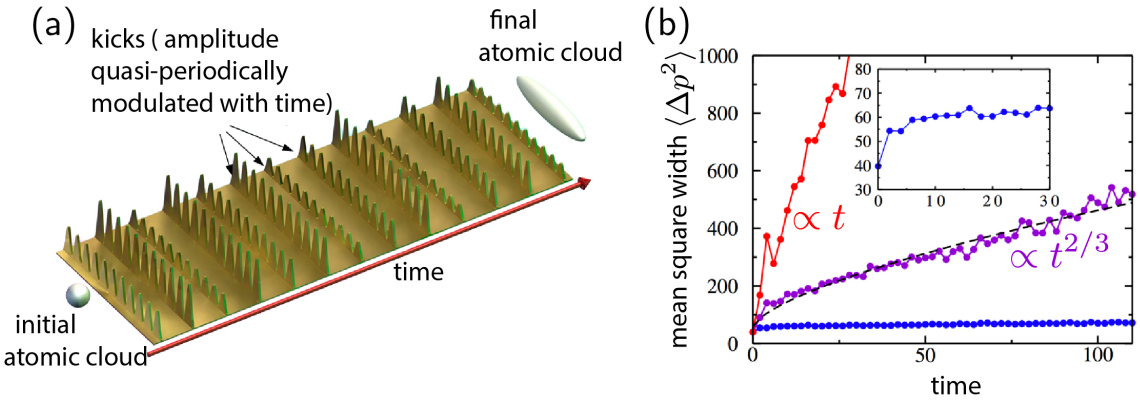

Figure 5.1: (a) In [Chabé 08], a cold gas is subjected to a periodic sequence of pulsed standing waves, the amplitude of which are quasi-periodically modulated in time. This leads to an effective 3D dynamical spreading of the momentum distribution of the gas. (b) Mean square width of the momentum distribution measured in this experiment, for three kick strengths K around the critical point K_c.

After this work, several experiments reported on Anderson localization of atomic wave packets in spatially disordered optical potentials in 1D [Billy 08, Roati 08] and 3D [Jendrzejewski 12b, Semeghini 15]. These observations were all based on the saturation criterion (5.2), see Fig. 5.2. An important bottleneck of these experiments, however, is that atoms of various energies around E_c were present in the clouds. For this reason a clear separation of the three regimes (5.1), (5.2) and (5.3) was not seen in 3D. We will come back to this point in Sec. 5.3.

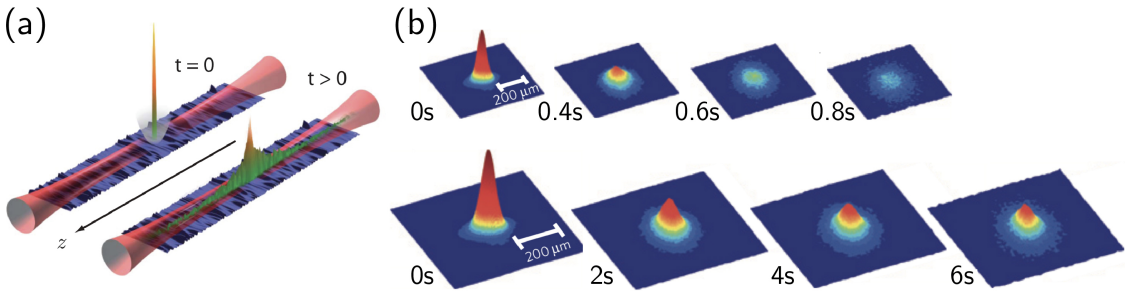

Figure 5.2: (a) 1D Anderson localization observed in [Billy 08]. A Bose-Einstein condensate is released from its trap at $t = 0$, and constrained to spread along a 1D optical guide on which an optical speckle potential is superimposed. The spreading is observed as a function of time by fluorescence imaging. (b) 3D Anderson localization of a condensate observed in [Jendrzejewski 12b]. At weak disorder (top), the atomic wave packet is essentially above the mobility edge and thus spreads diffusively. At stronger disorder (bottom), the wave packet is essentially below the mobility edge and gets spatially localized.

5.1.3 Self-consistent theory of Anderson localization

On the theory side, Eqs. (5.1), (5.2) and (5.3) can be proven in the framework of the self-consistent theory (SCT) of localization. We here briefly remind the spirit of this approach. As seen in chapter 4, in the diffusion regime pairs of counter-propagating

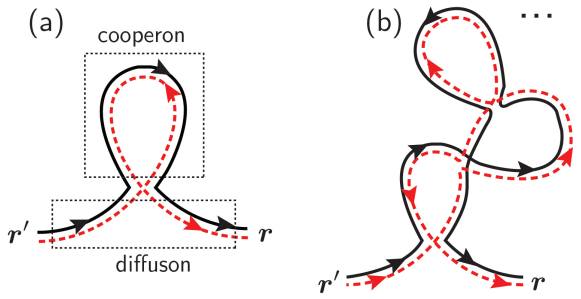

Figure 5.3: (a) Diagrammatic representation of weak localization: the diffusion coefficient is reduced owing to the occurrence of cooperon loops in the propagation. (b) At the onset of Anderson localization, interference proliferate. In the SCT, this proliferation is treated by a nesting of cooperon loops.

paths (cooperon) give rise to a mesoscopic echo at the center $\boldsymbol{r} = \boldsymbol{r}_0$ of the profile $n_{\boldsymbol{r}}(t)$. To leading-order however, the cooperon also affects the diffusive profile at $\boldsymbol{r} \neq \boldsymbol{r}_0$ by virtue the mechanism in Fig. 4.1(a)[2]: two amplitudes travel from $\boldsymbol{r}'$ by diffusion, then undergo a crossing followed by a propagation sequence along reversed paths, and finally recombine before detection at $\boldsymbol{r}$. The net effect of the loop thus constructed is a decrease of the diffusion coefficient from $D_0 \equiv v\ell/d$ to $D_0+\delta D<D_0$ known as weak localization [Gor'kov 79, Bergmann 84]. The relative change $\delta D/D_0$ can be estimated from the geometrical probability for an atom trajectory to cross itself at some point. This probability is given by the product of the semi-classical volume $\lambda^{d-1}vdt$ spanned by an atom over a time t with the probability density $P_E(\boldsymbol{r},\boldsymbol{r},t)$ of making a loop, integrated over all possible times:

$$\frac{\delta D}{D_0} = \int \lambda^{d-1} v dt \times P_E(\boldsymbol{r},\boldsymbol{r},t) \sim \frac{1}{\pi\nu\hbar} \int \frac{d^d\boldsymbol{Q}}{-i\omega + D_0\boldsymbol{Q}^2}\bigg|_{\omega\to 0}. \tag{5.4}$$

The perturbative correction (5.4) contains the premises of Anderson localization. Indeed, the integral over $\boldsymbol{Q}$ displays an infrared divergence in 1D and 2D, which signals that diffusion always break down in the thermodynamic limit in these dimensions. In 3D on the other hand, $\delta D/D_0 \sim -1/(k\ell)^2$, which suggests the critical point of the Anderson transition ($D \equiv D_0 + \delta D \to 0$) if one extrapolates to $k\ell \sim 1$.

A prescription to go beyond the perturbative result (5.4) and thus to describe Anderson localization was proposed by Vollhardt and Wölfle in 1980 [Vollhardt 80a, Vollhardt 80b, Vollhardt 92, Wolfle 10], and is today known as the SCT of localization. The strategy consists in substituting the renormalized D for D_0 in the weak localization correction:

$$\frac{1}{D} = \frac{1}{D_0} + \frac{1}{\pi\nu\hbar D_0} \int \frac{d^d\boldsymbol{Q}}{(2\pi)^d} \frac{1}{-i\omega + D\boldsymbol{Q}^2}. \tag{5.5}$$

[2]These processes indeed minimize the path-length difference ($\sim \ell$) between the two paths.

This procedure describes a nesting of localization loops, as illustrated in Fig. 5.3(b). Although approximate, the SCT rather accurately predicts the phase diagram of the Anderson model [Kroha 90], can be engineered to describe real systems (with various shapes/boundary conditions etc.) [van Tiggelen 07, Cherroret 08], and provides a quantitative basis for the phenomenological scaling theory [Vollhardt 82]. A consequence of the renormalization procedure (5.5) is that the diffusion coefficient D naturally acquires an ω dependence. Once $D(\omega)$ is found from Eq. (5.4), the density distribution of a wave packet follows from $P_E(\boldsymbol{r}, \boldsymbol{r}_0, t) = \int d\omega d^d\boldsymbol{q}/(2\pi)^{d+1} e^{i\boldsymbol{q}\cdot(\boldsymbol{r}-\boldsymbol{r}_0)-i\omega t} \times 1/[-i\omega + D(\omega)\boldsymbol{q}^2]$. In 1D for instance, the resolution of Eq. (5.5) leads to $D(\omega) = -i\omega\xi^2$, from which we immediately recover $P_E(x, x_0, t) \propto \exp(-|x - x_0|/\xi)$ and Eq. (5.2). In 3D, Eq. (5.5) also predicts a critical point at a certain value[3] $E = E_c$ with $D(\omega) = -i\omega\xi^2$ for $E < E_c$, $D(\omega) = D_0$ for $E \gg E_c$ and $D(\omega) \propto (-i\omega)^{1/3}$ for $E = E_c$, which again leads Eqs. (5.1), (5.2) and (5.3). The SCT thus fairly well describes the dynamics of wave packets at the onset of Anderson localization. One should keep in mind, however, that the approach remains approximate since only a certain class of diagrams is accounted for while many others are neglected[4]. In particular, it fails to describe the large fluctuations in the vicinity of the critical point in 3D, and in particular gives the wrong estimation $\nu = 1$ of the critical exponent.

5.2 Spreading of weakly-interacting bosons

5.2.1 Sub-diffusion

Clarifying how weak particle interactions modify the spreading of wave packets in disorder has occupied several groups since two seminal articles published in 2008 [Pikovsky 08, Kopidakis 08]. From a theoretical point of view, this problem is most easily tackled with bosons, which obey the nonlinear Gross-Pitaevskii equation at low temperatures. Despite the relative simplicity of the Gross-Pitaevskii equation, the problem turned out to be non-trivial, even in 1D, at both the numerical and theoretical levels. In [Pikovsky 08, Kopidakis 08], it was numerically found that for a small nonlinearity and at strong disorder, wave packets are no longer localized at long times but spread sub-diffusively, $\langle \Delta \boldsymbol{r}^2 \rangle \propto t^\alpha$ with $\alpha < 1$. In other words, Anderson localization is destroyed, but diffusion is not fully recovered. The precise value of α was somewhat debated [Pikovsky 08, Kopidakis 08, Flach 09, Garcia-Mata 09], for the sub-diffusion process establishes very slowly and the precise estimation of α requires to run simulations over enormously long times[5]. Numerics nevertheless seems to suggest $\alpha = 0.3 - 0.4$. The question is not fully clarified though, since other works also put forward that sub-diffusion could be non-algebraic and eventually become slower than any power law at arbitrarily long times [Wang 09, Basko 11]. Experimentally, signatures of sub-diffusion of a weakly interacting Bose-Einstein condensate were found in [Lucioni 11].

[3] The value of E_c depends on the ultraviolet cutoff needed to regularize Eq. (5.5) at short scales, and is thus non-universal: it must be determined for each model of disorder.

[4] In particular, the 2-loop diagrams responsible for the CFS peak are *not* included in the SCT.

[5] In the latest numerical experiment aimed to determine α [Vakulchyk 18], the time scale probed would correspond to 10^9s in a real experiment!

5.2.2 Nonlinear self-consistent theory

In 2014 we developed a generalized SCT of localization aimed to take into account the interaction potential $g|\Psi(\boldsymbol{r},t)|^2$ ($g>0$) of the Gross-Pitaevskii equation [Cherroret 14, Cherroret 16]. This approach is based on previous theoretical works which established, in a context of nonlinear optics, that for continuous light beams propagating in disordered materials a weak Kerr nonlinearity dephases the cooperon but leaves the diffuson unaffected. A consequence is, in particular, that the coherent backscattering peak is reduced, while diffusion is hardly affected [Agranovich 91, Hartung 08, Wellens 08]. In short, nonlinear interactions can be implemented into the SCT (5.5) by adding a dephasing-like term of the type $ign_{\boldsymbol{r}}(\omega)$ in the denominator of the weak localization correction in Eq. (5.5)[6]. Such an approach however relies on the essential assumption that the wave packet energy distribution is peaked around a mean energy E and that it remains so in the course of time (absence of thermalization), an approximation that cannot be true up to arbitrarily long times. We will address this point in Sec. 5.3. Even with this approximation, the nonlinear SCT thus designed [see Eq. (5.6)] is involved and can only be solved using an homogeneity approximation for the nonlinear term [Cherroret 16]. In 1D, this leads to the curves in Fig. 5.4(a) for the mean square width $\langle\Delta x^2\rangle$ of a spreading wave packet. They show that when $g\neq 0$ $\langle\Delta x^2\rangle$ starts to increase sub-diffusively beyond a characteristic time[7] $\tau_{\rm NL}\sim\xi/gN$, reaching $\langle\Delta x^2\rangle\sim t^{1/2}$ when $t\gg\tau_{\rm NL}$. This behavior is qualitatively similar to the predictions of numerical simulations [Pikovsky 08, Kopidakis 08, Flach 09, Garcia-Mata 09]. The obtained sub-diffusive exponent is however slightly too large (0.5 instead of $0.3-0.4$), which may be explained, in particular, by the neglect of energy thermalization.

5.2.3 Sub-diffusion in 3D

In 3D, the nonlinear SCT provides interesting predictions for $\langle\Delta\boldsymbol{r}^2\rangle$, shown in Fig. 5.4(b): the nonlinearity has no visible effect for $E\geqslant E_c$. In particular, the asymp-

[6] More quantitatively, one must take into account that in the self-consistent scheme of Fig. 5.3 loops are nested according to a diffuson/cooperon alternation. The non-equivalence between diffuson P and cooperon P' when $g\neq 0$ then requires to introduce a *set* of self-consistent equations, with a renormalized diffusion coefficient D for P and another D' for P', leading to:

$$\begin{cases} \left[-i\omega - D\boldsymbol{\nabla}_{\boldsymbol{r}}^2\right] P(\boldsymbol{r}',\boldsymbol{r},\omega) = \delta(\boldsymbol{r}-\boldsymbol{r}') \\ \dfrac{1}{D} = \dfrac{1}{D_0} + \dfrac{1}{\pi\nu D_0} P'(\boldsymbol{r},\boldsymbol{r},\omega) \\ \left[-i\omega - D'\boldsymbol{\nabla}_{\boldsymbol{r}}^2 - i\dfrac{g}{\hbar} n_{\boldsymbol{r}}(\omega)*\right] R'(\boldsymbol{r}',\boldsymbol{r},\omega) = \dfrac{1}{2\pi\nu\tau^2}\delta(\boldsymbol{r}-\boldsymbol{r}') \\ \dfrac{1}{D'} = \dfrac{1}{D_0} + \dfrac{1}{\pi\nu D_0} P(\boldsymbol{r},\boldsymbol{r},\omega), \end{cases} \tag{5.6}$$

where $P'(\boldsymbol{r}',\boldsymbol{r},t) = 2\pi\nu\tau^2 \mathrm{Re}\left[R'(\boldsymbol{r}',\boldsymbol{r},t)\right]$ and the wave-packet density is $n_{\boldsymbol{r}}(t) = \int d^d\boldsymbol{r}' P(\boldsymbol{r}',\boldsymbol{r},t) n_{\boldsymbol{r}'}(t=0)$. Eqs. (5.6) highlight the dephasing $\phi\propto gn_{\boldsymbol{r}}$ by which interactions compete with localization: ϕ alters the Cooperon P' via a frequency convolution $*$ reminiscent of the multiplicative potential $g|\Psi(\boldsymbol{r},t)|^2$ in the Gross-Pitaevskii equation. In the limit $g=0$, the equations for (P,D) and (P',D') become identical and Eq. (5.5) is recovered.

[7] $\hbar/\tau_{\rm NL}$ can be interpreted as the interaction energy in a localization volume. A similar time scale $\sim 1/g$ beyond which sub-diffusion prevails was predicted in [Iomin 09].

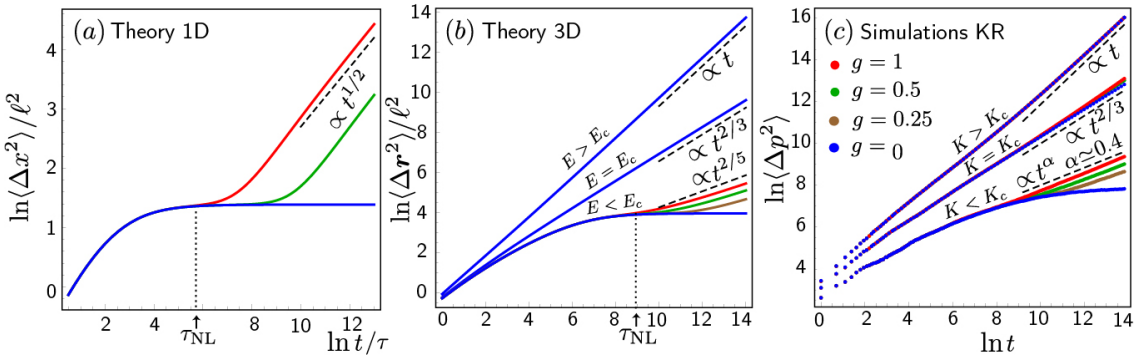

Figure 5.4: (a) Mean square width $\langle \Delta x^2 \rangle$ predicted by the nonlinear SCT for $g = 0$ (blue curve), $gN\ell/D_0 = 10^{-4}$ (green curve) and 10^{-3} (red curve) in 1D. (b) $\langle \Delta \boldsymbol{r}^2 \rangle$ predicted by the SCT in 3D, for $E > E_c$, $E < E_c$ and $E = E_c$. Colored curves correspond to different values of $gN/(D_0\ell)$, increasing from bottom to top. Only for $E < E_c$ do interactions qualitatively modify the long-time asymptotics, indicated by dashed lines. (c) $\langle \Delta p^2 \rangle$ obtained from numerical simulations of the nonlinear quasi-periodic kicked rotor.

totic laws (5.1) and (5.3) are robust against interactions. In contrast, for $E < E_c$ localization is destroyed in favor of sub-diffusion at times $t \gg \tau_{\rm NL} \sim \xi^3/gN$. The robustness of Eqs. (5.1) and (5.3) can be qualitatively understood by the fact that the nonlinear dephasing $\phi \sim g n_{\boldsymbol{r}}(t)$ quickly tends to zero as the wave packet gets diluted in these regimes. On the contrary, the emergence of sub-diffusion below the critical point is the result of a trade-off between interference due to disorder and dephasing due to interactions as the packet spreads: on the one hand, interference tend to localize the packet and thus to reinforce the dephasing mechanism by preventing ϕ from decreasing to zero as time grows. On the other hand, interactions tend to delocalize the packet, which makes ϕ decrease and in turn reinforces interference.

Fig. 5.4(c) shows simulations of wave-packet spreading performed by Benoît Vermersch during his PhD [Vermersch 13]. These simulations do not use a 3D disordered potential though, but are based on the quasi-periodic kicked-rotor model discussed in Sec. 5.1.2, to which a nonlinear potential $g|\Psi(p,t)|^2$ is added. Although this system is not strictly identical[8], the results qualitatively reproduce the prediction of the nonlinear SCT: interactions do not affect much the dynamics in the diffusion regime and at the critical point, while they turn localization into sub-diffusion[9].

To analyze more closely the effect of nonlinear interactions on the Anderson transition, a possible strategy consists in probing the scaling properties of the system, in the spirit of the scaling theory of localization [Abrahams 79]. The latter was originally developed to provide a criterion for Anderson localization in disordered electronic conductors of finite size [Abrahams 79], and relies on the scaling of the conductance G with the conductor size L. For instance, in a 3D good metal the conductance $G \propto DL$ increases with L, while in an Anderson insulator $G \propto \exp(-L/\xi)$

[8]The equivalence between the quasi-periodic kicked rotor and a 3D Anderson problem disappears when a local nonlinear term is added in both models.

[9]Note that the fact that both the nonlinear SCT in 3D and the simulations of the nonlinear quasi-periodic kicked rotor give the same sub-diffusive exponent $\alpha \simeq 0.4$ is probably fortuitous.

decreases with L. At the critical point finally, the system is scale-invariant and $G = \text{const}$. These three behaviors are encapsulated in the so-called scaling function

$$\beta(G) = \frac{d \ln G(L)}{d \ln L}. \tag{5.7}$$

In 3D, $\beta(G)$ is positive above the critical point and negative below. In between, the vanishing of $\beta(G)$ signals the presence of the critical point. The same approach can be applied to the scenario of wave-packet spreading. The role of the system size is played by the wave packet width, $L \equiv \langle \Delta \boldsymbol{r}^2 \rangle^{1/2}$, and the "conductance" is defined as $G \propto D \times L = \langle \Delta \boldsymbol{r}^2 \rangle^{3/2}/t$, in analogy with its expression for an electronic conductor. The predictions of the nonlinear SCT for $\beta(G)$ are shown in Fig. 5.5(a),

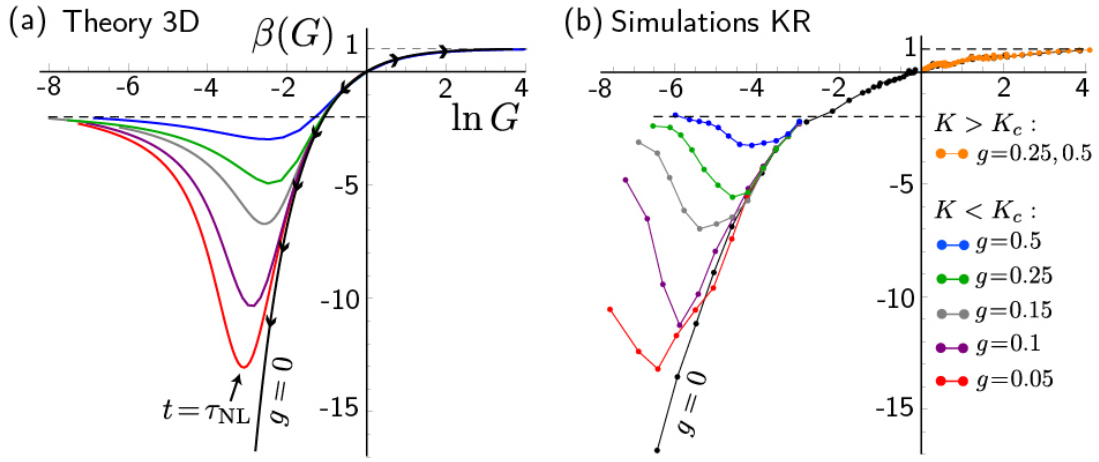

Figure 5.5: (a) Scaling function calculated with the nonlinear SCT for $g = 0$ (black curve) and for five finite values of $gN/(D_0\ell)$ (colored curves, the nonlinearity increases from bottom to top). (b) Numerical simulations of $\beta(G)$ in the nonlinear quasi-periodic kicked rotor.

to be compared with numerical simulations of the nonlinear quasi-periodic kicked rotor, Fig. 5.5(b). For $g = 0$ (black curve) β is monotonic, positive in the diffusion regime, negative in the localization regime and zero at the critical point as expected. Far in the diffusive phase $\beta(G) \to 1$ since $\langle \Delta \boldsymbol{r}^2 \rangle \sim D_0 t$. For $g \neq 0$, we observe that for all curves the point where β vanishes is still present and unmodified, suggesting that a phase transition still exists at $E = E_c$. In the diffusion regime, β remains unaffected by interactions. In contrast, below the critical point the shape of β changes: interactions give rise to a minimum associated with a breakdown of monotonicity. This minimum corresponds to the temporal cross-over $t \sim \tau_{\text{NL}} \equiv \xi^3/gN$ where the system turns from localized to sub-diffusive. The limit $\beta(G \to 0) \to \text{const} < 0$, finally, corresponds to the sub-diffusive law $\langle \Delta \boldsymbol{r}^2 \rangle \sim t^\alpha$ at long times.

We finally mention an interesting feature of the plots in Fig. 5.5: different values of g generate different β functions. This result is in marked contrast with what is expected for non-interacting disordered systems, where the *sole* parameter G is sufficient to describe the scaling of the system with size [Abrahams 79]: in the nonlinear problem, the single-parameter scaling hypothesis breaks down.

5.3 Thermalization

5.3.1 The energy distribution

As mentioned previously, the energy distribution $f(E)$ of atomic clouds in disordered potentials is in general not peaked around a well-defined energy E_0 but is instead broad. For a non-interacting wave packet initially located around $\boldsymbol{r}_0$, the density distribution reads generally [Shapiro 12]:

$$n_{\boldsymbol{r}}(t) = \int dE f(E) P_E(\boldsymbol{r}, \boldsymbol{r}_0, t), \tag{5.8}$$

with an energy distribution $f(E) \equiv 1/(2\pi) \times \int d^d\boldsymbol{k}' n_{\boldsymbol{k}'}(t=0) A(E, \boldsymbol{k}') \neq \delta(E - E_0)$. $f(E)$ depends on both the momentum distribution of the gas at $t = 0$, $n_{\boldsymbol{k}'}(t = 0)$, and on the spectral function $A(E, \boldsymbol{k}')$. The latter carries information on how atomic energies $\hbar^2\boldsymbol{k}'^2/2m$ are broadened when the atoms are subjected to the disordered potential at $t = 0$ (see footnote 3 in chapter 2). We emphasized in the previous chapter that a broad energy distribution makes the mesoscopic echo hard to observe in spatially disordered potentials. A similar experimental difficulty arises when one aims to probe the Anderson transition in 3D from the freezing of a wave packet, since a broad mixture of atom energies around E_c gives rise to a complicated wave-packet dynamics in place of Eqs. (5.1), (5.2) and (5.3) [Jendrzejewski 12b, Semeghini 15]. This issue also makes the determination of the mobility edge E_c quite challenging, and partly explains the remaining discrepancy between theory and experiments regarding the value of E_c in speckle potentials [Pasek 17].

5.3.2 Thermalization of interacting clouds

For non-interacting atoms, the energy distribution $f(E)$ is set once for all after disorder has been turned on. In the presence of interactions on the contrary, $f(E, t)$ *changes in time* owing to particle collisions. Thermalization of atomic energies was not accounted for in the nonlinear SCT of spreading wave packets discussed in Sec. 5.2.2, but it definitely occurs at long times. A consequence of thermalization, in particular, might be a smoothing of the nonlinear transition in Fig. 5.5.

To our knowledge, an exact theory describing the spreading of weakly interacting wave packets in a random potential is not yet available. The specific question of thermalization, however, can be more straightforwardly investigated in momentum space, following the time evolution of plane-wave states as in chapters 2 and 3. In 1D it was addressed in nonlinear discrete disordered chains in [Oganesyan 09, Mulansky 09, Kottos 11, Mulansky 13, Basko 11]. In 2015, we also briefly explored this problem in 2D, by revisiting the setup discussed in chapters 2 and 3 in the presence of weak interactions: we considered the evolution of the average momentum distribution $n_{\boldsymbol{k}}(t)$ of a gas prepared in the state $|\boldsymbol{k}_0\rangle$ and evolving in a 2D speckle potential according to the Gross-Pitaevskii equation [Cherroret 15]. Fig. 5.6(a) shows numerical simulations of $n_{\boldsymbol{k}}(t)$ carried out in this way by a colleague, Tomasz Karpiuk. At short times, the distribution displays the ring and the CBS peak discussed in chapter 2. At longer times, the picture changes: the CBS peak

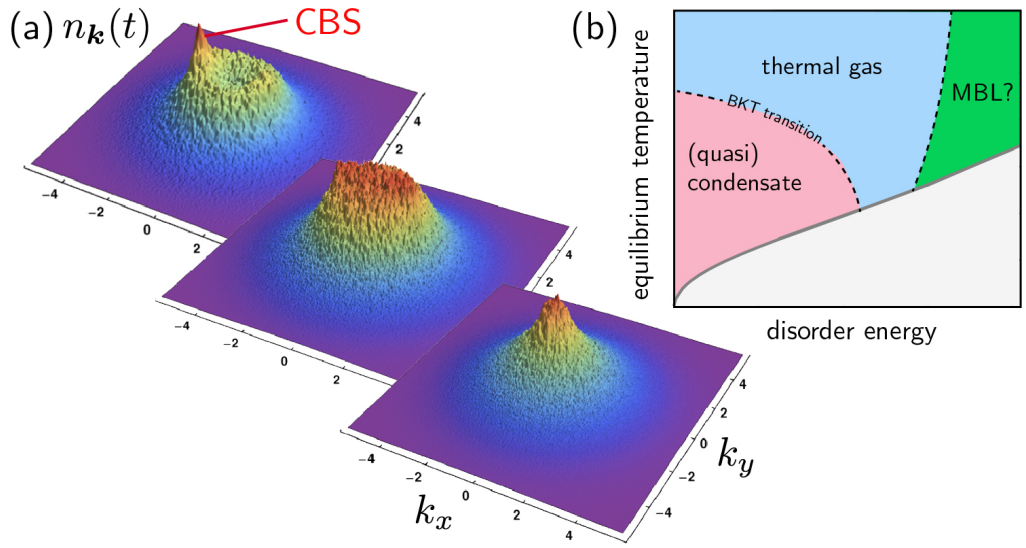

Figure 5.6: (a) Momentum distribution of a cold gas after time evolution of the state $|\boldsymbol{k}_0\rangle$ with the Gross-Pitaevskii equation (courtesy of Tomasz Karpiuk). At short times we distinguish the diffusive ring and the CBS peak discussed in chapter 2. At longer times both disappear and the distribution becomes smooth and centered on $\boldsymbol{k} = 0$. (b) Possible equilibrium phase diagram of a quenched interacting boson gas after it has evolved over long times in a 2D random potential.

disappears and, eventually, the diffusive ring itself evolves toward a smooth distribution centered on $\boldsymbol{k} = 0$. This phenomenon is due to slow evolution of $f(E,t)$ to a *thermal* profile.

Beyond the mean-field level however, it is not yet clear (at least to the author) to what state a quenched interacting gas of bosons in a 2D random potential should converge at long times. A possible equilibrium phase diagram is sketched in Fig. 5.6(b). We conclude this chapter by briefly commenting on it. For generic initial conditions first (i.e. initial values of the kinetic $\hbar^2 k_0^2/2m$, disorder and interaction energies), we expect $f(E,t)$ to converge to a thermal distribution, characterized by an effective temperature and a chemical potential that depend on these initial conditions[10]. At small disorder strengths, the equilibrium temperature is correspondingly small so that a BKT transition should occur. What are the precise properties of the gas in this phase is not well known (see however [Allard 12] and [Carleo 13] for recent experimental and theoretical works addressing this question for a disordered gas at equilibrium in a trap). What happens at strong disorder is even less clear, but one might find there a many-body localized phase, known to be present in the spectrum of certain many-body disordered systems at strong enough disorder [Alet 18]. If this phase exists[11], the associated distribution $f(E, t \to \infty)$ should display a non-thermal character.

[10]Note that since the equilibrium temperature in particular depends on the amplitude of the disorder potential the gas is initially subjected to, it is strictly positive as soon as disorder is nonzero, hence the forbidden gray region in Fig. 5.6(b).

[11]This statement is open for at least two reasons: it is not yet clear whether many-body localization can occur in dimensions larger than 1 [Alet 18], as well as in continuous systems [Gornyi 17].

CHAPTER 6

Light scattering in (2+1) dimensions

This chapter is based on the following article:

- N. Cherroret, *Coherent multiple scattering of light in (2+1) dimensions*, Phys. Rev. A **98**, 013805 (2018)

In chapter 2 we discussed a configuration where the coherent backscattering peak is observed in the momentum space of a bulk disordered system by propagation of a plane atomic matter wave. It turns out that this configuration is not restricted to cold atoms but can be realized in optics as well, in media of dimension "(2+1)", which display spatial fluctuations of their refractive index in two directions but are homogeneous along the third one[1]. In fact, beyond the mere question of disorder this type of medium has attracted a growing interest in the recent years, for in the paraxial limit light mimics the behavior of a matter wave in an external potential, with the possible implementation of effective photon interactions [Carusotto 13]. In 2017 I started a theoretical analysis of these systems, which turn out to be extremely rich, in particular when the polarization degree of freedom is taken into account.

6.1 Paraxial scattering in (2+1) dimensions

6.1.1 The paraxial approximation

The propagation of a beam in a disordered dielectric medium of dimension (2+1) is illustrated in Fig. 6.1(a). Such a medium is characterized by a permittivity profile $\epsilon = \bar{\epsilon} + \delta\epsilon(\boldsymbol{r}_\perp)$, which displays spatial variations in the plane $\boldsymbol{r}_\perp \equiv (x, y)$ around an average value $\bar{\epsilon}$ but is, on the other hand, homogeneous along the "optical axis" z. Evolution of the electric field is described by the Helmholtz equation

$$\left[\Delta\delta_{ij} - \nabla_i\nabla_j + k^2\delta_{ij} - V(\boldsymbol{r}_\perp)\delta_{ij}\right] E_j(\boldsymbol{r}) = 0, \tag{6.1}$$

[1]Let us also mention the case of exciton-polaritons in 2D microcavities, which offer a third alternative [Langbein 02].

where $k^2 = \omega^2\bar{\epsilon}/c^2$, with ω the light carrier frequency, and the "potential" $V(\boldsymbol{r}_\perp) \equiv -k^2\delta\epsilon(\boldsymbol{r}_\perp)/\bar{\epsilon}$. For a beam almost aligned with the z-axis, it is common, in this geometry, to make use of a *paraxial approximation*. The latter consists in writing the electric field as $\mathbf{E}(\boldsymbol{r}) = \boldsymbol{\mathcal{E}}(\boldsymbol{r})e^{ikz}$ $[\boldsymbol{r} \equiv (\boldsymbol{r}_\perp, z)]$ and assuming slow variations of its envelope along z, $|\partial^2\mathcal{E}/\partial z^2| \ll k|\partial\mathcal{E}/\partial z|$, and of the in-plane permittivity, $|\nabla_\perp\epsilon| \ll k$ [Agrawal 95, Rosanov 02]. Under these conditions, the envelope $\boldsymbol{\mathcal{E}}$ is mostly transverse and the Helmholtz equation (6.1) simplifies to

$$i\frac{\partial\mathcal{E}}{\partial z} = \left[-\Delta_\perp + \frac{1}{2k}V(\boldsymbol{r}_\perp)\right]\mathcal{E}(\boldsymbol{r}), \tag{6.2}$$

which constitutes the paraxial wave equation. The latter is similar to a 2D time-dependent Schrödinger equation, where z plays the role of time and the permittivity profile $\delta\epsilon(\boldsymbol{r}_\perp)$ the one of an external potential.

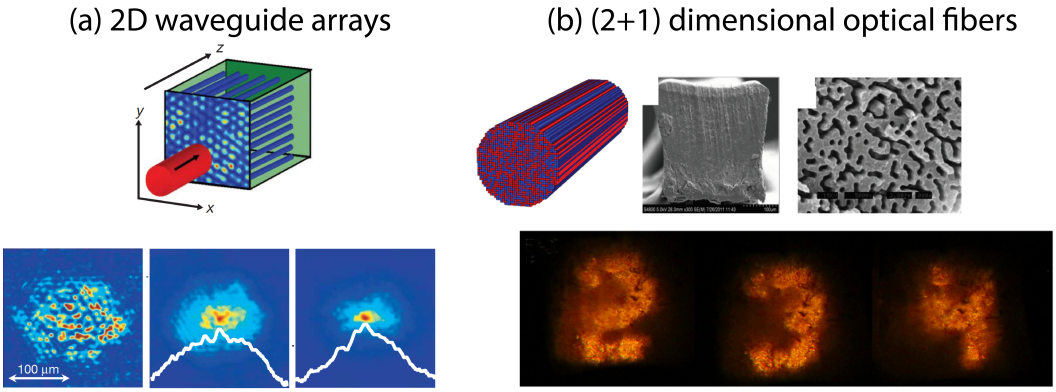

Figure 6.1: (a) Photo-refractive disordered material of dimension (2+1) (from [Schwartz 07]). The medium displays spatial variations of its permittivity in the plane (x, y) but is homogeneous along z. Here a narrow, focused incident beam at $z = 0$ undergoes a spreading in the plane (x, y). 2D localization of its spatial profile $\overline{|\mathcal{E}(\boldsymbol{r}_\perp, z)|^2}$ is observed when $\delta\epsilon(\boldsymbol{r}_\perp)$ is made sufficiently disordered. (b) Transverse localization observed in a disordered optical fiber [Karbasi 12, Karbasi 14, Mafi 14]. Here many points constituting an image ("2", "3", or "4") are transported along the fiber thanks to transverse localization.

6.1.2 Experiments

When $\delta\epsilon(\boldsymbol{r}_\perp)$ is made random, the correspondence between Eq. (6.2) and a Schrödinger equation provides a strategy to study, within an optical context, bulk time-dependent localization phenomena like in cold-atom setups. For instance, by illuminating the medium with a stationary focused beam one effectively produces a narrow wave packet whose subsequent spreading in the plane (x, y) can display localization at large enough z, an idea originally proposed in the group of A. Lagendijk [Raedt 89]. This configuration was first implemented in [Schwartz 07] to demonstrate 2D transverse Anderson localization of light in a photo-refractive crystal on which a (2+1)-dimensional random refractive-index distribution was imprinted with

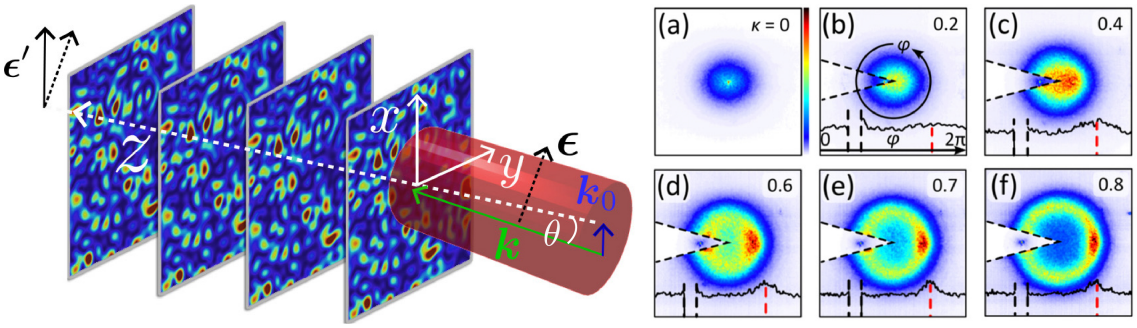

Figure 6.2: Left: medium of dimension (2+1) illuminated by a tilted collimated ("plane-wave") beam of transverse wave vector $\boldsymbol{k}_0$ and polarization $\boldsymbol{\epsilon}$ at $z = 0$. Right: optical distribution $\overline{|\mathcal{E}(\boldsymbol{k}_\perp, z)|^2}$ of transverse momenta measured in [Boguslawski 13] in a such a geometry, at fixed z and for increasing tilts of the incident beam (i.e. increasing k_0). A diffusive ring and a CBS peak appear at large enough tilts.

a writing beam. This phenomenon is shown in the lower-right image of Fig. 6.1(a): one observes a spatial localization of the wave packet profile $\overline{|\mathcal{E}(\boldsymbol{r}_\perp, z)|^2}$ at strong enough disorder. Note that the observation of 2D Anderson localization is here facilitated by the fact that the localization length $\xi \propto \exp(\pi \Delta k_\perp \ell/2)$ is controlled by the inverse width $\Delta k_\perp$ of the wave packet rather than by the wave number $k \gg \Delta k_\perp$ itself, and can thus easily be made small[2]. Transverse localization of light was also observed in [Boguslawski 13] in a photo-refractive material, as well as in disordered optical fibers in [Karbasi 12]. In [Karbasi 14, Mafi 14], transverse localization was even proposed as a means for transporting multiplexed signals through disorder fibers, see Fig. 6.1(b).

One can also take advantage of the paraxial equation to study the CBS peak in the 2D bulk configuration of chapter 2, by illuminating the medium with a broad, tilted collimated beam, as illustrated in the left panel of Fig. 6.2. As the beam evolves along the effective time z, the transverse projection $\boldsymbol{k}_0$ of its wave vector is randomized due to multiple scattering in the plane (x, y). The optical distribution $\overline{|\mathcal{E}(\boldsymbol{k}_\perp, z)|^2}$ measured in transmission in the far field then has the structure of Fig. 2.3, with a diffusive ring and a CBS on top of it. This effect was observed experimentally recently [Boguslawski 17]. Momentum distributions observed in this work are reproduced in Fig. 6.2 for various inclinations $\kappa = k_0/k_t$ of the incident beam (k_t is a normalization factor related to the correlation length of the disorder). The diffusive ring and CBS peak become clearly visible at nonzero tilt.

Let us mention, finally, that studying Eq. (6.2) is also very interesting in *nonlinear* Kerr materials where $\delta\epsilon(\boldsymbol{r}_\perp) \propto |\mathcal{E}(\boldsymbol{r}_\perp)|^2$: the paraxial equation becomes formally equivalent to the Gross-Pitaevskii equation that governs weakly-interacting Bose-Einstein condensates. This analogy was recently exploited for studying optical analogues of quantum matter-wave phenomena such as interactions-driven thermalization [Sun 12, Kaiser 18] or superfluidity [Michel 18].

[2]It should be noted, however, that the effective velocity of the transverse beam is proportional to $\Delta k_\perp$, such that the classical diffusion coefficient $D_0 \propto \Delta k_\perp^2$ is *also* very small: there is a risk of confusion between Anderson localization and slow diffusion in this system.

6.2 Beyond the paraxial approximation

6.2.1 Motivation

Although widely used in the literature, the paraxial equation (6.2) should be taken with care. For a disordered potential $V(\boldsymbol{r}_\perp)$ especially, it is not clear when this equation breaks down. In this respect, the assumptions of "slow variations" of the field envelope along z and of the in-plane permittivity mentioned above are not very enlightening. The latter seems even dangerous at the onset of Anderson localization. In addition, the paraxial wave equation completely neglects the vector nature of light. Clarifying how polarization effects manifest themselves beyond the paraxial approximation is essential for experiments that operate close to the paraxial limit. More generally, understanding the role of the vector nature of light in heterogeneous media is required for a proper characterization of disorder-induced interference effects like CBS, known to be sensitive to polarization in general [Stephen 86, Wolf 88]. The question is even crucial for Anderson localization of light, which was shown to be severely altered in random ensembles of scatterers when vector effects are accounted for [Skipetrov 14, Bellando 14, Maximo 15].

6.2.2 Theory

It turns out that electromagnetic wave propagation in a weakly disordered medium of dimension (2+1) can be rigorously described using the tensor impurity-diagram technique based on the Helmholtz equation (6.1). This approach was previously used in 3D isotropic disordered media to unveil the role of light polarization in the physics of diffusion and of CBS [Stephen 86, Barabanenkov 95, Lubatsch 05, Sheng 06]. In (2+1) dimensions the problem is considerably more difficult due to the anisotropic character of the medium on average, but can still be solved. In the configuration of Fig. 6.2 for instance, i.e. for an incident collimated beam of transverse momentum $\boldsymbol{k}_0$ and polarization $\boldsymbol{\epsilon}$, the average distribution of transverse momenta measured at the coordinate z and along a polarization axis $\boldsymbol{\epsilon}'$ is given by [Cherroret 18]

$$\overline{|\boldsymbol{\epsilon}'\cdot\mathbf{E}(\boldsymbol{k}_\perp,z)|^2}=\frac{k/2z_s\epsilon^*_\alpha\epsilon'_\gamma\epsilon'^*_\beta\epsilon_\delta}{(2k/z_s)^2+(\boldsymbol{k}_\perp^2-\boldsymbol{k}_0^2)^2}\sum_{n=1,2,3}e^{-z/z_n}\Big[\Pi^{(n)}_{\alpha\beta,\gamma\delta}+\Pi^{(n)}_{\alpha\delta,\gamma\beta}e^{-D(\boldsymbol{k}_\perp+\boldsymbol{k}_0)^2z}\Big] \quad (6.3)$$

where z_s is the scattering mean free time (analogous to τ in the previous chapters) and $D=\hat{k}_0^2z_s/2$ is the diffusion coefficient[3]. The dimensionless number $\hat{k}_0\equiv k_0/k$ can be interpreted as the effective mean velocity of the incident beam in the plane (x,y). Eq. (6.3) is the optical counterpart of Eq. (2.6)[4]. The Lorentzian prefactor is the optical spectral function and is responsible for the diffusive ring in Fig. 6.2, whose width is governed by the scattering mean free time. The second term in the brackets describes the CBS peak, centered around $\boldsymbol{k}_\perp=-\boldsymbol{k}_0$. As in chapter 2, see Eq. (2.3), the CBS width decays as $1/\sqrt{Dz}$.

[3]Disorder is here assumed uncorrelated.

[4]Like Eq. (2.6), Eq. (6.3) holds in the hydrodynamic limit $z\gg z_s$, i.e. after transverse momenta have been randomized by multiple scattering in the plane (x,y). It also assumes $\hat{k}_0/k\ll 1$, i.e. that the incident beam has a small inclination with the optical axis. The momentum distribution in the regime $\hat{k}_0/k\sim 1$ can be described analytically as well but has a more complicated expression.

6.2.3 Scalar-to-vector cross-over

The most interesting feature of Eq. (6.3) is the polarization dependence of the diffusive ring and CBS peak, governed by three dimensionless four-rank tensors $\Pi^{(n)}_{\alpha\beta,\gamma\delta}$ contracted with the incident $\boldsymbol{\epsilon}$ and detection $\boldsymbol{\epsilon}'$ polarizations vectors. These tensors have lifetimes z_n which obey

$$z_1 \sim z_2 \sim z_p \equiv \frac{z_s}{\hat{k}_0^4} \text{ and } z_3 = \infty, \tag{6.4}$$

The finite lifetime z_p signals that the system undergoes a *cross-over* at $z \sim z_p \gg z_s$. Indeed, when $z \ll z_p$ the exponentials in Eq. (6.3) all approximate to 1. The three tensors $\Pi^{(n)}$ then have equal weights and obey $\sum_n \Pi^{(n)}_{\alpha\beta,\gamma\delta} = \delta_{\alpha\gamma}\delta_{\beta\delta}$, such that

$$\overline{|\boldsymbol{\epsilon}' \cdot \mathbf{E}(\boldsymbol{k}_\perp, z \ll z_p)|^2} \propto |\boldsymbol{\epsilon} \cdot \boldsymbol{\epsilon}'^*|^2 \left[1 + e^{-D(\boldsymbol{k}_\perp + \boldsymbol{k}_0)^2 z}\right]. \tag{6.5}$$

This result characterizes the behavior of a *scalar wave*, and in fact coincides with the prediction of the paraxial equation (6.2): the light polarization stays *fixed* during the multiple scattering process, hence the prefactor $|\boldsymbol{\epsilon} \cdot \boldsymbol{\epsilon}'^*|^2$, which only depends on the relative positions of input and output polarizers. We give in the first two rows of Table 6.1 the explicit value of $|\boldsymbol{\epsilon} \cdot \boldsymbol{\epsilon}'^*|^2$ of both the diffusive and CBS signals in four main experimental setups where linearly polarized light is analyzed along the parallel ($l \parallel l$) or perpendicular ($l \perp l$) channels, or where circularly polarized light is analyzed in channels of same ($\sigma \parallel \sigma$) or opposite ($\sigma \perp \sigma$) polarization. As intuition suggests, the diffusive ring and the CBS peak are visible in the $l \parallel l$ and $\sigma \parallel \sigma$ channels only ($\boldsymbol{\epsilon}' = \boldsymbol{\epsilon}$).

channels	$\sigma \parallel \sigma$	$\sigma \perp \sigma$	$l \parallel l$	$l \perp l$
ring($z \ll z_p$)	1	0	1	0
CBS($z \ll z_p$)	1	0	1	0
ring($z \gg z_p$)	1/2	1/2	1/2	1/2
CBS($z \gg z_p$)	0	1/2	1/2	0

Table 6.1: Diffusive and CBS signals in the four polarization channels, for $z \ll z_p$ (scalar regime) and $z \gg z_p$ (vector regime).

The regime $z \gg z_p$, in strong contrast, *cannot* be described by the paraxial wave equation. In this limit, the tensors $\Pi^{(1)}$ and $\Pi^{(2)}$ have decayed and the polarization structure of the distribution is solely governed by $\Pi^{(3)}_{\alpha\beta,\gamma\delta} = \frac{1}{2}\delta_{\alpha\beta}\delta_{\gamma\delta}$. We then have:

$$\overline{|\boldsymbol{\epsilon}' \cdot \mathbf{E}(\boldsymbol{k}_\perp, z \gg z_p)|^2} \propto \frac{1}{2}\left[1 + |\boldsymbol{\epsilon} \cdot \boldsymbol{\epsilon}'|^2 e^{-D(\boldsymbol{k}_\perp + \boldsymbol{k}_0)^2 z}\right]. \tag{6.6}$$

The amplitudes 1/2 and $|\boldsymbol{\epsilon} \cdot \boldsymbol{\epsilon}'|^2/2$ of the diffusive and CBS signals in the four polarization channels are displayed in the last two rows of Table 6.1: the diffusive signal is visible with the same probability in all channels. This indicates that polarization has

been *randomized* by the multiple scattering process. The behavior of the CBS peak is more unexpected: it is only visible in the channels $l \parallel l$ and, surprisingly, $\sigma \perp \sigma$ ($\boldsymbol{\epsilon}' = \boldsymbol{\epsilon}^*$). This somewhat counter-intuitive behavior can be understood by general arguments based on time-reversal symmetry and on the homogeneity of the medium along z: let us consider the wave amplitude $\mathcal{A}^{1\to \mathrm{N}}(\boldsymbol{k}_0, \boldsymbol{\epsilon}; \boldsymbol{k}_\perp, \boldsymbol{\epsilon}'; k_z)$ associated with a multiple scattering sequence $1 \to \mathrm{N}$ from the initial state $(\boldsymbol{k}_0, \boldsymbol{\epsilon})$ to the final state $(\boldsymbol{k}_\perp, \boldsymbol{\epsilon}')$, with k_z conserved. The CBS interference is constructed by pairing this amplitude with its counter-propagating partner $\mathcal{A}^{\mathrm{N}\to 1}(\boldsymbol{k}_0, \boldsymbol{\epsilon}; \boldsymbol{k}_\perp, \boldsymbol{\epsilon}'; k_z)$. To find the condition of constructive interference, we first apply the reciprocity theorem that pertains to time-reversal symmetry [Saxon 55, Montambaux 07]:

$$\mathcal{A}^{\mathrm{N}\to 1}(\boldsymbol{k}_0, \boldsymbol{\epsilon}; \boldsymbol{k}_\perp, \boldsymbol{\epsilon}'; k_z) = \mathcal{A}^{1\to \mathrm{N}}(-\boldsymbol{k}_\perp, \boldsymbol{\epsilon}'^*; -\boldsymbol{k}_0, \boldsymbol{\epsilon}^*; -k_z). \tag{6.7}$$

Owing to the independence of disorder on the longitudinal coordinate z, the right-hand side of Eq. (6.7) is also parity-symmetric with respect to the variable k_z. The CBS interference is therefore constructive provided $\mathcal{A}^{1\to \mathrm{N}}(\boldsymbol{k}_0, \boldsymbol{\epsilon}; \boldsymbol{k}_\perp, \boldsymbol{\epsilon}'; k_z) = \mathcal{A}^{1\to \mathrm{N}}(-\boldsymbol{k}_\perp, \boldsymbol{\epsilon}'^*; -\boldsymbol{k}_0, \boldsymbol{\epsilon}^*; k_z)$. This equality is obviously satisfied when:

$$\boldsymbol{k}_\perp = -\boldsymbol{k}_0, \;\; \boldsymbol{\epsilon}' = \boldsymbol{\epsilon}^*, \tag{6.8}$$

i.e. the CBS peak is indeed fully contrasted in the channels $l \parallel l$ and $\sigma \perp \sigma$.

6.2.4 Randomization of polarization

The effective time scale $z_p = z_s/\hat{k}_0^4 \sim z_s/\theta^4$ is inversely proportional to the fourth power of the angle θ made by the incident beam with the optical axis (see Fig. 6.2). We have seen that it separates a scalar regime where polarization is fixed, from a vector regime where polarization is randomized. z_p can therefore be interpreted as the time needed to *randomize the direction of polarization* in (2+1) dimensions. This interpretation can be confirmed by the following qualitative argument. The incident beam, of wave vector $\boldsymbol{k} = (\boldsymbol{k}_0, k_z)$, has the polarization $\boldsymbol{\epsilon}$. After the first scattering event on a refractive-index fluctuation, the beam is scattered into a direction $\hat{\boldsymbol{k}}'$ and acquires a unit polarization $\boldsymbol{\epsilon}'$ which fulfills the law of parallel transport [MacKintosh 89]:

$$\boldsymbol{\epsilon}' = \frac{\boldsymbol{\epsilon} - (\hat{\boldsymbol{k}}' \cdot \boldsymbol{\epsilon})\hat{\boldsymbol{k}}'}{\sqrt{1 - |\boldsymbol{k}' \cdot \boldsymbol{\epsilon}|^2}}. \tag{6.9}$$

In the right-hand side, the dot products $\hat{\boldsymbol{k}}' \cdot \boldsymbol{\epsilon} \equiv \boldsymbol{k}'_\perp \cdot \boldsymbol{\epsilon}_\perp + \epsilon_z \hat{k}_z \sim \hat{k}_0$, since $|\hat{k}_z| \sim |\boldsymbol{\epsilon}_\perp| \sim 1$ and $|\epsilon_z| \sim |\hat{\boldsymbol{k}}'_\perp| \sim \hat{k}_0 \equiv k_0/k$ for a paraxial incident beam. To leading order in $\hat{k}_0 \ll 1$, the change in polarization in the plane (x, y), $\Delta\boldsymbol{\epsilon}_\perp \equiv \boldsymbol{\epsilon}'_\perp - \boldsymbol{\epsilon}_\perp$, is thus on the order of

$$|\Delta\boldsymbol{\epsilon}_\perp| \sim \hat{k}_0^2. \tag{6.10}$$

After a random walk of $N = z/z_s$ scattering events, the polarization subsequently changes by an amount $|\Delta\boldsymbol{\epsilon}_\perp(N)| \sim \sqrt{N}|\Delta\boldsymbol{\epsilon}_\perp| \sim \sqrt{N}\hat{k}_0^2$. The randomization of polarization is realized when this quantity is on the order of 1. This happens when

$$N \sim \frac{1}{\hat{k}_0^4} \Leftrightarrow z \sim \frac{z_s}{\hat{k}_0^4} \equiv z_p, \tag{6.11}$$

which confirms the interpretation of z_p given above. It is interesting to note that z_p is much larger than the mean free time z_s in this system. This must be contrasted with conventional 3D disordered media, where both time scales are on the same order[5]. The geometry (2+1) thus offers the opportunity to study separately, within a single setup, the behavior of both scalar and vector light in the presence of disorder. This is particularly appealing in view of the question of Anderson localization of light, which was experimentally observed in (2+1) dimensions in [Schwartz 07], while it was shown to be absent for vector waves, at least in three dimensions [Skipetrov 14].

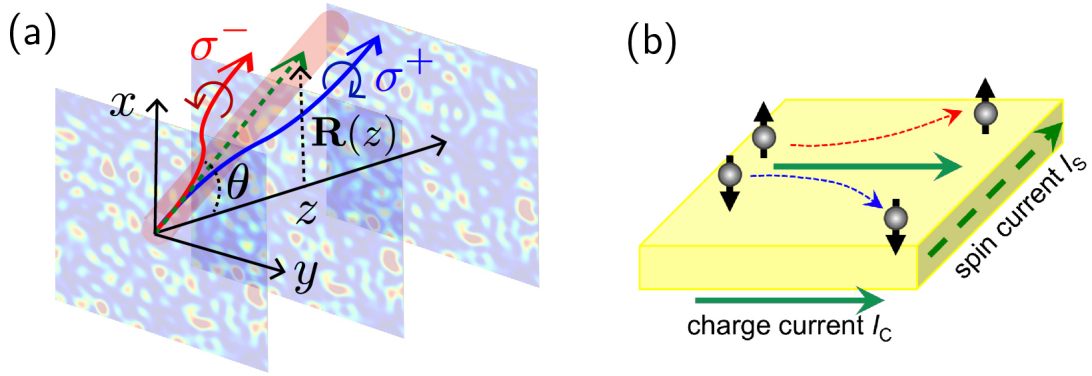

Figure 6.3: (a) In the geometry of Fig. 6.2, the ballistic signal associated with a circularly polarized incident beam experiences an helicity-dependent deflection as it deviates from paraxiality. This phenomenon constitutes an optical version of the electronic spin Hall effect in solids, (b): a charge current is converted into a spin current due to the spin-orbit interaction.

6.3 Disorder and spin-orbit interactions of light

We conclude this chapter by a prospective discussion aiming to emphasize the richness of light propagation in (2+1) dimensions. The results presented from here on are preliminary and should be regarded as such. They are part of the PhD thesis of Tamara Bardon-Brun, which started in 2017.

In (2+1) dimensions, we have seen that the paraxial equation fails to describe diffusive light propagation at long z, when vector effects become important. In the same way, the *ballistic* component of light, i.e. the part of the incident beam that is not scattered, also experiences deviations from the scalar description. We remind that in a disordered medium, the ballistic signal stems from the average component $\overline{\mathbf{E}}$ of the random light field $\mathbf{E} = \overline{\mathbf{E}} + \delta\mathbf{E}$, and constitutes the main contribution to the intensity $\overline{|\mathbf{E}|^2}$ at short times $z \lesssim z_s$, when light has not yet been scattered much. Beyond z_s, the ballistic signal decays exponentially (Beer-Lambert law) as photons are scattered and feed the diffusive halo $\delta\mathbf{E}$, and at long times $z \gg z_s$ the latter becomes the main contribution to $\overline{|\mathbf{E}|^2}$. Let us now come back to the scenario in Fig. 6.2, i.e a collimated beam of small transverse wave vector $\boldsymbol{k}_0$, and consider the

[5]More precisely, in a 3D disorder the time to randomize the polarization direction is on the order of the transport mean free time.

center of mass of the ballistic beam in the the plane (x, y), see Fig. 6.3(a):

$$\mathbf{R}(z) \equiv \frac{\int d^2\boldsymbol{r}_\perp \boldsymbol{r}_\perp |\overline{\mathbf{E}}(\boldsymbol{r}_\perp, z)|^2}{\int d^2\boldsymbol{r}_\perp |\overline{\mathbf{E}}(\boldsymbol{r}_\perp, z)|^2}. \tag{6.12}$$

The impurity-diagram technique [Montambaux 07] applied to the paraxial equation (6.2) readily gives $\mathbf{R}(z) = \hat{\boldsymbol{k}}_0 z$, as expected intuitively: the ballistic signal propagates along a straight line. As the beam deviates from paraxiality however, an interesting phenomenon shows up for circularly polarized light: ballistic light experiences an helicity-dependent *deflection*. This effect is captured by the impurity-diagram technique applied to the Helmholtz equation (6.1), which gives [Bardon-Brun 18]:

$$\mathbf{R}(z) = \hat{\boldsymbol{k}}_0 z + \frac{\sigma}{k_0}\left[1 - \frac{1}{\cosh(z\hat{k}_0^2/2z_s)}\right]\mathbf{e}_y, \tag{6.13}$$

where $\sigma = \pm 1$ is the helicity. The correction term in Eq. (6.13) is a consequence of effective spin-orbit interactions of light in this system: the in-plane spatial inhomogeneity induces a coupling between the optical "spin" (circular polarization) and the beam trajectory[6].

The trajectory described by Eq. (6.13) is illustrated in Fig. 6.3(a): the beam is deflected toward the direction of rotation of the electric field. This deflection constitutes an optical version of the *spin Hall effect* [Sinova 15]. The spin Hall effect arises in certain conductors that display spin-orbit coupling, and is illustrated in Fig. 6.3(b) for a 2D electron gas accelerated by an external electric field. Spin-up electrons are deflected to one side of the conductor and spin-down electrons to the other side, which results in a transverse spin current. At a qualitative level, the electronic spin Hall effect can be described with the semi-classical spin-orbit Hamiltonian $H = \boldsymbol{p}^2/2m + V(\boldsymbol{r}) + \mathcal{A}(\boldsymbol{p} \times \boldsymbol{\nabla} V) \cdot \mathbf{S}$, where $\mathcal{A} > 0$ is a constant that depends on the material and V is the electric-field potential energy [Dyakonov 10]. In the 2D geometry of Fig. 6.3(b), Hamilton's equations lead to the Newton's law

$$m\dot{\mathbf{v}} = -\boldsymbol{\nabla} V(\boldsymbol{r}) + m\mathcal{A}\Delta_\perp V(\boldsymbol{r})(\mathbf{v} \times \mathbf{S}), \tag{6.14}$$

which involves an effective Lorentz force that indeed deflects electron trajectories. The 2D spin Hall effect thus described can be translated to our optical scenario with the following correspondences. The 2D plane of the electron gas corresponds to the plane (x, y) in Fig. 6.2, the initial electron velocity $\mathbf{v}(t = 0)$ to the optical transverse wave vector $\boldsymbol{k}_0$ at $z = 0$, the electric potential $V(\boldsymbol{r}_\perp)$ to the permittivity fluctuations $\delta\epsilon(\boldsymbol{r}_\perp)$ and the electron spin $\mathbf{S}$ to $\sigma = \pm 1$. An important subtlety of the optical scheme, however, is that the deflection is observed on the *disorder-averaged* field $\mathbf{E}$, which normally describes light propagation in an effective (i.e. homogeneous) medium. In other words the deflection survives the disorder average, a result under current investigation. Let us conclude by noting that the spin Hall effect of light is not specific to our system. Similar deflections have been identified in various inhomogeneous media [Liberman 92, Andrews 13, Bliokh 15]. To our knowledge however, Eq. (6.13) constitutes to the first demonstration of the spin Hall effect of light in the presence of disorder, and arises interesting questions regarding the properties of Anderson localization in dimension (2+1).

[6] This coupling is naturally present in the Helmholtz equation, through the term $\boldsymbol{\nabla}\boldsymbol{\nabla} \cdot \mathbf{E}$.

CHAPTER 7

Conclusion and outlook

In this manuscript I have described, essentially in a cold-atom context, a few emblematic interference phenomena that show up when a matter wave evolves in a random potential: coherent backscattering, coherent forward scattering, mesoscopic echo and quantum boomerang. One interesting lesson of these works is that although the physics of non-interacting disordered systems is today relatively well understood, it can still reveal surprises and worth pursuing theoretical and experimental investigations. The coherent forward scattering and the quantum boomerang effects are two clear examples of this statement: although relatively simple, they have been discovered only recently (and are not yet observed experimentally). In the same spirit, the experimental observation and characterization of the mesoscopic echo in the localization regime were only achieved a year ago!

Looking at such mesoscopic effects for probing the localization properties of matter waves is interesting for at least two reasons. First, these phenomena manifest themselves a spectacular signatures of coherent transport and are rather straightforwardly accessible to the experimentalist by measurement of simple transport observables. Second, they are in general highly sensitive to perturbations of the coherent multiple scattering process. The latter property naturally calls for the investigation of the robustness of the coherent backscattering, the coherent forward scattering, the mesoscopic echo or the quantum boomerang against interactions in atomic systems. This task will most probably be part of my future activities. In the context of light scattering, understanding the role of vector effects in media of dimension (2+1) is another of my research perspectives. The preliminary results presented in this manuscript show that there is much to do in this context: exploring the role of vector effects in light localization away from the paraxial regime, the possibility of exploiting the polarization degree of freedom for simulating artificial gauge fields for light or the implementation of effective photon interactions via a $\chi^{(3)}$ nonlinearity are just a few examples of open problems.

Bibliography

[Abrahams 79] E. Abrahams, P. W. Anderson, D. C. Licciardello, and T. V. Ramakrishnan, *Scaling theory of localization: absence of quantum diffusion in two dimensions*, Phys. Rev. Lett. **42**, 673 (1979).

[Aegerter 09] C. M. Aegerter and G. Maret, *Coherent backscattering and Anderson localization of light*, Progress in Optics **52**, 1 (2009).

[Agranovich 91] V. M. Agranovich and V. E. Kravtsov, *Nonlinear backscattering from opaque media*, Phys. Rev. B **43**, 13691 (1991).

[Agrawal 95] G. P. Agrawal, *Nonlinear Fiber Optics* (Academic Press, San Diego, 1995).

[Akkermans 85] E. Akkermans and R. Maynard, *Weak localization of waves*, J. Phys. France **46**, L-1045 (1985).

[Akkermans 88] E. Akkermans, P. E. Wolf, R. Maynard, and G. Maret, *Theoretical study of the coherent backscattering of light by disordered media*, J. Phys. France **49**, 77 (1988).

[Albada 85] M. P. van Albada and A. Lagendijk, *Observation of weak localization of light in a random medium*, Phys. Rev. Lett. **55**, 2692 (1985).

[Alet 18] F. Alet and N. Laflorencie, *Many-body localization: an introduction and selected topics*, Comptes Rendus Physique (2018).

[Allard 12] B. Allard, T. Plisson, M. Holzmann, G. Salomon, A. Aspect, P. Bouyer, and T. Bourdel, *Effect of disorder close to the superfluid transition in a two-dimensional Bose gas*, Phys. Rev. A **85**, 033602 (2012).

[Altland 93] A. Altland, *Diagrammatic approach to Anderson localization in the quantum kicked rotator*, Phys. Rev. Lett. **71**, 69 (1993).

[Altland 97] A. Altland and M. R. Zirnbauer, *Nonstandard symmetry classes in mesoscopic normal-superconducting hybrid structures*, Phys. Rev. B **55**, 1142 (1997).

[Altland 14] A. Altland and D. Fuchs, *Spectral statistics of mesoscopic wires: crossover from Wigner-Dyson to Poisson regime*, Phys. Rev. Lett. **74**, 4269 (1995).

[Altman 12] E. Altman, *Non equilibrium quantum dynamics in ultra-cold quantum gases*, Lecture Notes of the 2012 Les Houches Summer School of Physics "Strongly Interacting Quantum Systems Out of Equilibrium", Oxford University Press.

[Altman 15] E. Altman and R. Vosk, *Universal dynamics and renormalization in many-body-localized Systems*, Ann. Rev. Cond. Matt. **6**, 383 (2015).

[Altshuler 80] B. L. Altshuler, A. G. Aronov, and P. A. Lee, *Interaction effects in disordered Fermi systems in two dimensions*, Phys. Rev. Lett. **44**, 1288 (1980).

[Altshuler 82] B. L. Altshuler, A. G. Aronov, and D. E. Khmelnitskii, *Effects of electron–electron collisions with small energy transfers on quantum localization*, J. Phys. C, **15**, 7367 (1982).

[Altshuler 85] B. L. Al'tshuler and D. E. Khmelnitskii, *Fluctuation properties of small conductors*, JETP Lett. **42**, 359 (1985).

[Ammann 97] H. Ammann and N. Christensen, *Delta kick cooling : a new method for cooling atoms*, Phys. Rev. Lett. **78**, 2088 (1997).

[Anderson 58] P. W. Anderson, *Absence of diffusion in certain random lattices*, Phys. Rev. **109**, 1492 (1958).

[Anderson 85] P. W. Anderson, *The question of classical localization a theory of white paint?*, Philos. Mag. B, **52**, 505 (1985).

[Andrews 13] D. L. Andrews and M. Babiker, *The angular momentum of light*, Cambridge University Press 2013.

[Barabanenkov 95] Yu. N. Barabanenkov and V. D. Ozrin, *Diffusion asymptotics of the Bethe-Salpeter equation for electromagnetic waves in discrete random media*, Phys. Lett. A **206**, 116 (1995).

[Bardon-Brun 18] T. Bardon-Brun and N. Cherroret, in preparation.

[Basko 06] D. M. Basko, I. L. Aleiner, B. L. Altshuler, *Metal–insulator transition in a weakly interacting many-electron system with localized single-particle states*, Annals of Physics **321**, 1126 (2006).

[Basko 11] D. M. Basko, *Weak chaos in the disordered nonlinear schrödinger chain: destruction of Anderson localization by Arnold diffusion*, Annals of Physics **326**, 1577 (2011).

[Bayer 93] G. Bayer and T. Niederdränk, *Weak localization of acoustic waves in strongly scattering media*, Phys. Rev. Lett. **70**, 3884 (1993).

[Bellando 14] L. Bellando, A. Gero, E. Akkermans, and R. Kaiser, *Cooperative effects and disorder: a scaling analysis of the spectrum of the effective atomic Hamiltonian*, Phys. Rev. A **90**, 063822 (2014).

[Berezinskii 74] V. L. Berezinsky, *Kinetics of a quantum particle in a one-dimensional random potential*, Zh. Eksp. Teor. Fiz. **65**, 1251 (1973) [Sov. Phys. JETP **38**, 620 (1974)].

[Bergmann 84] G. Bergmann, *Weak localization in thin films*, Phys. Rep. **107**, 1 (1984).

[Berkovits 94] R. Berkovits and S. Feng, *Correlations in coherent multiple scattering*, Phys. Rep. **238**, 135 (1994).

[Billy 08] J. Billy, V. Josse, Z. Zuo, A. Bernard, B. Hambrecht, P. Lugan, D. Clément, L. Sanchez-Palencia, A. Aspect, and P. Bouyer, *Direct observation of Anderson localization of matter waves in a controlled disorder*, Nature **453**, 891 (2008).

[Bliokh 15] K. Y. Bliokh, F. J. Rodríguez-Fortuño, F. Nori, and A. V. Zayats, *Spin–orbit interactions of light*, Nature Phot. **9**, 796 (2015).

[Bloch 08] I. Bloch, J. Dalibard, and W. Zwerger, *Many-body physics with ultracold gases*, Rev. Mod. Phys. **80**, 885 (2008).

[Boguslawski 13] M Boguslawski, S. Brake, J. Armijo, F. Diebel, P. Rose, and C. Denz, *Analysis of transverse Anderson localization in refractive index structures with customized random potential*, Opt. Exp. **21**, 31713 (2013).

[Boguslawski 17] M. Boguslawski, S. Brake, D. Leykam, A. S. Desyatnikov, and C. Denz, *Observation of transverse coherent backscattering in disordered photonic structures*, Sci. Rep. **7**, 10439 (2017).

[Bohigas 91] O. Bohigas, *Random matrix theories and chaotic dynamics*, in Chaos and Quantum Physics, Proceedings of Les Houches Summer School, eds. M. J. Giannoni, A. Voros and J. Zinn-Justin, Amsterdam: North-Holland, 1991, Session LII, p. 91.

[Bordia 16] P. Bordia, H. P. Lüschen, S. S. Hodgman, M. Schreiber, I. Bloch, and U. Schneider, *Coupling identical one-dimensional many-body localized systems*, Phys. Rev. Lett. **116**, 140401 (2016).

[Capron 13] T. Capron, C. Texier, G. Montambaux, D. Mailly, A. D.Wieck, and L. Saminadayar, *Ergodic versus diffusive decoherence in mesoscopic devices*, Phys. Rev. B **87**, 041307 (2013).

[Carleo 13] G. Carleo, G. Boéris, M. Holzmann, L. Sanchez-Palencia, *Universal superfluid transition and transport properties of two-dimensional dirty bosons*, Phys. Rev. Lett. **111**, 050406 (2013).

[Carusotto 13] I. Carusotto and C. Ciuti, *Quantum fluids of light*, Rev. Mod. Phys. **85**, 299 (2013).

[Casati 79] G. Casati, B.V. Chirikov, J. Ford, and F.M. Izrailev, *Stochastic behavior of a quantum pendulum under a periodic perturbation*, Lecture Notes in Physics, Springer, Berlin, **93**, 334 (1979).

[Chabanov 00] A. A. Chabanov, M. Stoytchev, and A. Z. Genack, *Statistical signatures of photon localization*, Nature **404**, 850 (2000).

[Chabé 08] J. Chabé, G. Lemarié, B. Grémaud, D. Delande, P. Szriftgiser, and J. C. Garreau, *Experimental observation of the Anderson metal-insulator transition with atomic matter waves*, Phys. Rev. Lett. **101**, 255702 (2008).

[Chalker 96a] J. T. Chalker, I. V. Lerner, and R. A. Smith, *Random walks through the ensemble: linking spectral statistics with wave-function correlations in disordered metals*, Phys. Rev. Lett. **77**, 554 (1996).

[Chalker 96b] J. T. Chalker, I. V. Lerner, and R. S. Smith, *Fictitious level dynamics: a novel approach to spectral statistics in disordered conductors*, J. Math. Phys. **37**, 5061 (1996).

[Cherroret 06] N. Cherroret, *Coherent transport of waves in random media: from mesoscopic correlations to Anderson localization*, thèse de doctorat, Laboratoire de Physique et de Modélisation des Milieux Condensés, Université Joseph Fourier, Grenoble (2009).

[Cherroret 08] N. Cherroret and S.E. Skipetrov, *Microscopic derivation of self-consistent equations of Anderson localization in a disordered medium of finite size*, Phys. Rev. E **77**, 046608 (2008).

[Cherroret 12] N. Cherroret, T. Karpiuk, C. A. Müller, B. Grémaud, and C. Miniatura, *Coherent backscattering of ultracold matter waves: momentum space signatures*, Phys. Rev. A **85**, 011604 (2012).

[Cherroret 13] N. Cherroret and D. Delande, *Backscattering echo of correlated wave packets*, Phys. Rev. A **88**, 035602 (2013).

[Cherroret 14] N. Cherroret, B. Vermersch, J. C. Garreau, and D. Delande, *How nonlinear interactions challenge the three-dimensional Anderson transition*, Phys. Rev. Lett. **112**, 170603 (2014).

[Cherroret 15] N. Cherroret, T. Karpiuk, B. Grémaud, C. Miniatura, *Thermalization of matter waves in random potentials*, Phys. Rev. A **92**, 063614 (2015).

[Cherroret 16] N. Cherroret, *A self-consistent theory of localization in nonlinear random media*, J. of Phys.: Cond. Mat. **20**, 024002 (2016).

[Cherroret 18] N. Cherroret, *Coherent multiple scattering of light in (2+1) dimensions*, Phys. Rev. A **98**, 013805 (2018).

[Choi 16] J.-Y. Choi, S. Hild, J. Zeiher, P. Schauß, A. Rubio-Abadal, T. Yefsah, V. Khemani, D. A. Huse, I. Bloch, and C. Gross, *Exploring the many-body localization transition in two dimensions*, Science **352**, 1547 (2016).

[Cobus 16] L. A. Cobus, S. E. Skipetrov, A. Aubry, B. A. van Tiggelen, A. Derode, and J. H. Page, *Anderson mobility gap probed by dynamic coherent backscattering*, Phys. Rev. Lett. **116**, 193901 (2016).

[Datta 95] S. Datta, *Electronic transport in mesoscopic systems*, Cambridge studies in Semiconductor Physics and Micoelectronic Engineering, Cambridge: Cambridge University Press, 1995.

[Deissler 10] B. Deissler, M. Zaccanti, G. Roati, C. D. Errico, M. Fattori, M. Modugno, G. Modugno, and M. Inguscio, *Delocalization of a disordered bosonic system by repulsive interactions*, Nature Phys. **6**, 354 (2010).

[Delande 14] D. Delande and G. Orso, *Mobility edge for cold atoms in laser speckle potentials*, Phys. Rev. Lett. **113**, 060601 (2014).

[Dorokhov 82] O. N. Dorokhov, *Transmission coefficient and the localization length of an electron in N bound disordered chains*, JETP Lett. **36** (1982) 318.

[Dyakonov 10] M. I. Dyakonov, *Spin Hall Effect*, Future Trends in Microelectronics, S. Luryi, J. Xu, and A. Zaslavsky (eds), Wiley 2010, p. 251.

[Efetov 80] K. B. Efetov, A. I. Larkin, and D. E. Kheml'nitskii, *Interaction of diffusion modes in the theory of localization*, Sov. Phys. JETP **52**, 568 (1980).

[Evers 08] F. Evers and A. D. Mirlin, *Anderson transitions*, Rev. Mod. Phys. **80**, 1355 (2008).

[Faez 09] S. Faez, A. Strybulevych, J. H. Page, A. Lagendijk, and B. A. van Tiggelen, *Observation of multifractality in Anderson localization of ultrasound*, Phys. Rev. Lett. **103**, 155703 (2009).

[Fallani 07] L. Fallani, J. E. Lye, V. Guarrera, C. Fort, and M. Inguscio, *Ultracold atoms in a disordered crystal of light : towards a Bose glass*, Phys. Rev. Lett. **98**, 130404 (2007).

[Fallani 08] L. Fallani, C. Fort, and M. Inguscio, *Bose–Einstein condensates in disordered potentials*, Adv. At. Mol. Opt. Phys. **56**, 119 (2008).

[Feng 91] S. Feng and P. A. Lee, *Mesoscopic conductors and correlations in laser speckle patterns*, Science **251**, 633 (1991).

[Fishman 84] D. R. Grempel, R. E. Prange, and S. Fishman, *Quantum dynamics of a nonintegrable system*, Phys. Rev. A **29**, 1639 (1984).

[Flach 09] S. Flach, D. O. Krimer, and Ch. Skokos, *Universal spreading of wave packets in disordered nonlinear systems*, Phys. Rev. Lett. **102**, 024101 (2009).

[Garcia-Mata 09] I. Garcia-Mata and D. L. Shepelyansky, *Delocalization induced by nonlinearity in systems with disorder*, Phys. Rev. E **79**, 026205 (2009).

[Genack 91] A. Z. Genack and N. Garcia, *Observation of photon localization in a three-dimensional disordered system*, Phys. Rev. Lett. **66**, 2064 (1991).

[Ghosh 14] S. Ghosh, N. Cherroret, B. Grémaud, C. Miniatura, and D. Delande, *Coherent forward scattering in two-dimensional disordered systems*, Phys. Rev. A **90**, 063602 (2014).

[Ghosh 15] S. Ghosh, D. Delande, C. Miniatura, and N. Cherroret, *Coherent backscattering reveals the Anderson transition*, Phys. Rev. Lett. **115**, 200602 (2015).

[Ghosh 17] S. Ghosh, C. Miniatura, N. Cherroret, and D. Delande, *Coherent forward scattering as a signature of Anderson metal-insulator transitions*, Phys. Rev. A **95**, 041602(R) (2017).

[Gogolin 82] A. A. Gogolin, *Electron localization and hopping conductivity in one-dimensional disordered systems*, Phys. Rep. **86**, 1 (1982).

[Golubentsev 84] A. A. Golubentsev, *Suppression of interference effects in multiple scattering of light*, Sov. Phys. JETP **59**, 26 (1984).

[Gor'kov 79] L. P. Gor'kov, A. I. Larkin, and D. E. Khmel'nitskii, *Particle conductivity in a two-dimensional random potential*, JETP Lett. **30**, 228 (1979).

[Gornyi 05] I. V. Gornyi, A. D. Mirlin, and D. G. Polyakov, *Interacting electrons in disordered wires: Anderson localization and low-T transport*, Phys. Rev. Lett. **95**, 206603 (2005).

[Gornyi 17] I. V. Gornyi, A. D. Mirlin, M. Müller, and D. G. Polyakov, *Absence of many-body localization in a continuum*, Annalen der Physik **529**, 1600365 (2017).

[Hainaut 17] C. Hainaut, I. Manai, R. Chicireanu, J.-F. Clément, S. Zemmouri, J. C. Garreau, P. Szriftgiser, G. Lemarié, N. Cherroret, and D. Delande, *Return to the origin as a probe of atomic phase coherence*, Phys. Rev. Lett. **118**, 184101 (2017).

[Hainaut 18] C. Hainaut, I. Manai, J.-F. Clément, J. C. Garreau, P. Szriftgiser, G. Lemarié, N. Cherroret, D. Delande, and R. Chicireanu, *Controlling symmetry and localization with an artificial gauge field in a disordered quantum system*, Nature Comm. **9**, 1382 (2018).

[Hartung 08] M. Hartung, T. Wellens, C. A. Müller, K. Richter, and P. Schlagheck, *Coherent backscattering of Bose-Einstein condensates in two-dimensional disorder potentials*, Phys. Rev. Lett. **101**, 020603 (2008).

[Hertel 83] G. Hertel, D. J. Bishop, E. G. Spencer, J. M. Rowell, and R. C. Dynes, *Tunneling and transport measurements at the metal-insulator transition of amorphous Nb: Si*, Phys. Rev. Lett. **50**, 743 (1983).

[Hikami 81] S. Hikami, *Anderson localization in a nonlinear σ-model representation*, Phys. Rev. B **24**, 2671 (1981).

[Hu 08] H. Hu, A. Strybulevych, J. H. Page, S. E. Skipetrov, and B. A. van Tiggelen, *Localization of ultrasound in a three-dimensional elastic network*, Nature Phys. **4**, 945 (2008).

[Iomin 09] A. Iomin, *Dynamics of wave packets for the nonlinear Schrödinger equation with a random potential*, Phys. Rev. E **80**, 037601 (2009).

[Jendrzejewski 12] F. Jendrzejewski, K. Müller, J. Richard, A. Date, T. Plisson, P. Bouyer, A. Aspect, and V. Josse, *Coherent backscattering of ultracold atoms*, Phys. Rev. Lett. **109**, 195302 (2012).

[Jendrzejewski 12b] F. Jendrzejewski, A. Bernard, K. Müller, P. Cheinet, V. Josse, M. Piraud, L. Pezzé, L. Sanchez-Palencia, A. Aspect, and P. Bouyer, *Three-dimensional localization of ultracold atoms in an optical disordered potential*, Nature Phys. **8**, 1 (2012).

[John 84] S. John, *Electromagnetic absorption in a disordered medium near a photon mobility edge*, Phys. Rev. Lett. **53**, 2169 (1984).

[John 87] S. John, *Strong localization of photons in certain disordered dielectric superlattices*, Phys. Rev. Lett. **58**, 2486 (1987).

[Kaiser 18] N. Šantić, A. Fusaro, S. Salem, J. Garnier, A. Picozzi, and R. Kaiser, *Nonequilibrium precondensation of classical waves in two dimensions propagating through atomic vapors*, Phys. Rev. Lett. **120**, 055301 (2018).

[Karbasi 12] S. Karbasi, C. R. Mirr, P. G. Yarandi, R. J. Frazier, K. W. Koch, and A. Mafi, *Observation of transverse Anderson localization in an optical fiber*, Optics Lett. **37**, 2304 (2012).

[Karbasi 14] S. Karbasi, R. J. Frazier, K. W. Koch, T. Hawkins, J. Ballato, and A. Mafi, *Image transport through a disordered optical fibre mediated by transverse Anderson localization*, Nature Comm. **5**, 3362 (2014).

[Karpiuk 12] T. Karpiuk, N. Cherroret, K. L. Lee, B. Grémaud, C. A. Müller, and C. Miniatura, *Coherent forward scattering peak induced by Anderson localization*, Phys. Rev. Lett. **109**, 190601 (2012).

[Katsumoto 87] S. Katsumoto, F. Komori, N. Sano, and S. ichi Kobayashi, *Fine tuning of metal-insulator transition in Al0.3Ga0.7As using persistent photoconductivity*, J. Phys. Soc. Jpn **56**, 2259 (1987).

[Kondov 11] S. S. Kondov, W. R. McGehee, J. J. Zirbel and B. DeMarco, *Three-dimensional Anderson localization of ultracold matter*, Science **334**, 66 (2011).

[Kopidakis 08] G. Kopidakis, S. Komineas, S. Flach, and S. Aubry, *Absence of wave packet diffusion in disordered nonlinear systems*, Phys. Rev. Lett. **100**, 084103 (2008).

[Kottos 11] T. Kottos and B. Shapiro, *Thermalization of strongly disordered nonlinear chains*, Phys. Rev. E **83**, 062103 (2011).

[Kroha 90] J. Kroha, T. Kopp, and P. Wölfle, *Self-consistent theory of Anderson localization for the tight-binding model with site-diagonal disorder*, Phys. Rev. B **41**, 888 (1990).

[Kuhn 07] R. Kuhn, O. Sigwarth, C. Miniatura, D. Delande, and C. A. Müller, *Coherent matter wave transport in speckle potentials*, New. J. Phys. **9**, 161 (2007).

[Labeyrie 99] G. Labeyrie, F. de Tomasi, J.-C. Bernard, C. A. Müller, C. Miniatura, and R. Kaiser, *Coherent backscattering of light by cold atoms*, Phys. Rev. Lett. **83**, 5266 (1999).

[Labeyrie 12] G. Labeyrie, T. Karpiuk, J.-F. Schaff, B. Grémaud, C. Miniatura and D. Delande, *Enhanced backscattering of a dilute Bose-Einstein condensate*, Eur. Lett. **100**, 66001 (2012).

[Lahini 08] Y. Lahini, A. Avidan, F. Pozzi, M. Sorel, R. Morandotti, D. N. Christodoulides, and Y. Silberberg, *Anderson localization and nonlinearity in one-dimensional disordered photonic lattices*, Phys. Rev. Lett. **100**, 013906 (2008).

[Langbein 02] W. Langbein, E. Runge, V. Savona, and R. Zimmermann, *Enhanced resonant backscattering of excitons in disordered quantum wells*, Phys. Rev. Lett. **89**, 157401 (2002).

[Larose 04] E. Larose, L. Margerin, B. A. van Tiggelen, and M. Campillo, *Weak localization of seismic waves*, Phys. Rev. Lett. **93**, 048501 (2004).

[Laurent 07] D. Laurent, O. Legrand, P. Sebbah, C. Vanneste, and F. Mortessagne, *Localized modes in a finite-size open disordered microwave cavity*, Phys. Rev. Lett. **99**, 253902 (2007).

[Lee 14] K. L. Lee, B. Grémaud, and C. Miniatura, *Dynamics of localized waves in one-dimensional random potentials: statistical theory of the coherent forward scattering peak*, Phys. Rev. A **90**, 043605 (2014).

[Lemarié 09] G. Lemarié, J. Chabé, P. Szriftgiser, J.-C. Garreau, B. Grémaud, and D. Delande, *Observation of the Anderson metal-insulator transition with atomic matter waves: theory and experiment*, Phys. Rev. A **80**, 043626 (2009).

[Lemarié 10] G. Lemarié, H. Lignier, D. Delande, P. Szriftgiser, and J. C. Garreau, *Critical state of the Anderson transition: between a metal and an insulator*, Phys. Rev. Lett. **105**, 090601 (2010).

[Liberman 92] V. S. Liberman and B. Y. Zel'dovich, *Spin-orbit interaction of a photon in an inhomogeneous medium*, Phys. Rev. A **46**, 5199 (1992).

[Licini 85] J. C. Licini, D. J. Bishop, M. A. Kastner, and J. Melngailis, *Aperiodic magnetoresistance oscillations in narrow inversion layers in Si*, Phys. Rev. Lett. **55**, 2987 (1985).

[Lopez 12] M. Lopez, J.-F. Clément, P. Szriftgiser, J. C. Garreau, and D. Delande, *Experimental test of universality of the Anderson transition*, Phys. Rev. Lett. **108**, 095701 (2012).

[Lubatsch 05] A. Lubatsch, J. Kroha, and K. Busch, *Theory of light diffusion in disordered media with linear absorption or gain*, Phys. Rev. B **71**, 184201 (2005).

[Lucioni 11] E. Lucioni, B. Deissler, L. Tanzi, G. Roati, M. Zaccanti, M. Modugno, M. Larcher, F. Dalfovo, M. Inguscio, and G. Modugno, *Observation of subdiffusion in a disordered interacting system*, Phys. Rev. Lett. **106**, 230403 (2011).

[MacKintosh 89] F. C. MacKintosh, X. Zhu, D. J. Pine, and D. A. Weitz, *Polarization memory of multiply scattered light*, Phys. Rev. B **40**, 9342 (1989).

[Mafi 14] A. Mafi, S. Karbasi, K. W. Koch, T. Hawkins, and J. Ballato, *Transverse Anderson localization in disordered glass optical fibers: a review*, Materials **7**, 5520 (2014).

[Manai 15] I. Manai, J.-F. Clément, R. Chicireanu, C. Hainaut, J. C. Garreau, P. Szriftgiser, and D. Delande, *Experimental observation of two-dimensional Anderson localization with the atomic kicked rotor*, Phys. Rev. Lett. **115**, 240603 (2015).

[Maret 85] P. E. Wolf and G. Maret, *Weak localization and coherent backscattering of photons in disordered media*, Phys. Rev. Lett. **55**, 2696 (1985).

[Marinho 18] M. Marinho and T. Micklitz, *Spectral correlations in Anderson insulating wires*, Phys. Rev. B **97**, 041406(R) (2018).

[Maximo 15] C. E. Maximo, N. Piovella, P. W. Courteille, R. Kaiser, and R. Bachelard, *Spatial and temporal localization of light in two dimensions*, Phys. Rev. A **92**, 062702 (2015).

[Mehta 91] M. L. Mehta, *Random matrices*, Academic Press, New York (1991).

[Mello 88] P. A. Mello, P. Pereyra, and N. Kumar, *Macroscopic approach to multichannel disordered conductors*, Ann. Phys. (N.Y.) **181**, 290 (1988).

[Michel 18] C. Michel, O. Boughdad, M. Albert, P.-E. Larré, and M. Bellec, *Superfluid motion and drag-force cancellation in a fluid of light* Nature Comm. **9**, 2108 (2018).

[Micklitz 14] T. Micklitz, C. A. Müller, and A. Altland, *Strong Anderson localization in cold atom quantum quenches*, Phys. Rev. Lett. **112**, 110602 (2014).

[Montambaux 07] E. Akkermans and G. Montambaux, *Mesoscopic physics of electrons and photons*, Cambridge University Press, Cambridge, (2007).

[Mookherjea 08] S. Mookherjea, J. S. Park, S.-H. Yang, and P. R. Bandaru, *Localization in silicon nanophotonic slow-light waveguides*, Nature Phot. **2**, 90 (2008).

[Mott 70] N. F. Mott, *Conduction in non-crystalline systems*, Philos. Mag. **22**, 7 (1970).

[Mulansky 09] M. Mulansky, K. Ahnert, A. Pikovsky, and D. L. Shepelyansky, *Dynamical thermalization of disordered nonlinear lattices*, Phys. Rev. E **80**, 056212 (2009).

[Mulansky 13] M. Mulansky and A. Pikovsky, *Energy spreading in strongly nonlinear disordered lattices*, New J. Phys. **15**, 053015 (2013).

[Müller 15] K. Müller, J. Richard, V. V. Volchkov, V. Denechaud, P. Bouyer, A. Aspect, and V. Josse, *Suppression and revival of weak localization through control of time-reversal symmetry*, Phys. Rev. Lett. **114**, 205301 (2015).

[Nandkishore 15] R. Nandkishore and D. A. Huse, *Many-body localization and thermalization in quantum statistical mechanics*, Ann. Rev. Cond. Matt. **6**, 15 (2015).

[Niimi 09] Y. Niimi, Y. Baines, T. Capron, D. Mailly, F.-Y. Lo, A. D. Wieck, T. Meunier, L. Saminadayar, and C. Bäuerle, *Effect of disorder on the quantum coherence in mesoscopic wires*, Phys. Rev. Lett. **102**, 226801 (2009).

[Oganesyan 09] V. Oganesyan, A. Pal, and D. A. Huse, *Energy transport in disordered classical spin chains*, Phys. Rev. B **80**, 115104 (2009).

[Paalanen 83] M. A. Paalanen, T. F. Rosenbaum, G. A. Thomas, and R. N. Bhatt, *Critical ccaling of the conductance in a disordered insulator*, Phys. Rev. Lett. **51**, 1896 (1983).

[Pasek 17] M. Pasek, G. Orso, and D. Delande, *Anderson localization of ultracold atoms: where is the mobility edge?*, Phys. Rev. Lett. **118**, 170403 (2017).

[Pasienski 10] M. Pasienski, D. McKay, M. White, and B. DeMarco, *A disordered insulator in an optical lattice*, Nature Phys. **6**, 677 (2010).

[Peña 14] A. Peña, A. Girschik, F. Libisch, S. Rotter, and A. A. Chabanov, *The single-channel regime of transport through random media*, Nature Comm. **5**, 3488 (2014).

[Pikovsky 08] A. S. Pikovsky and D. L. Shepelyansky, *Destruction of Anderson localization by a weak nonlinearity*, Phys. Rev. Lett. **100**, 094101 (2008).

[Plisson 13] T. Plisson, T. Bourdel, and C. A. Müller, *Momentum isotropisation in random potentials*, Eur. J. Phys. ST **217**, 79 (2013).

[Polkovnikov 11] A. Polkovnikov, K. Sengupta, A. Silva, and M. Vengalattore, *Colloquium: Nonequilibrium dynamics of closed interacting quantum systems*, Rev. Mod. Phys. **83**, 863 (2011).

[Prat 18] T. Prat, D. Delande, and N. Cherroret, *When Anderson localization makes quantum particles move backward*, arXiv 1704.05241 (2018).

[Prigodin 94] V. N. Prigodin, B. L. Altshuler, K. B. Efetov, and S. Iida, *Mesoscopic dynamical echo in quantum dots*, Phys. Rev. Lett. **72**, 546 (1994).

[Raedt 89] H. De Raedt, Ad Lagendijk, and P. de Vries, *Transverse localization of light*, Phys. Rev. Lett. **62**, 47 (1989).

[Roati 08] G. Roati, C. D'Errico, L. Fallani, M. Fattori, C. Fort, M. Zaccanti, G. Modugno, M. Modugno, and M. Inguscio, *Anderson localization of a non-interacting Bose-Einstein condensate*, Nature **453**, 895 (2008).

[Rosanov 02] N. N. Rosanov, *Spatial hysteresis and optical patterns* (Springer-Verlag, New York, 2002).

[Rosenbaum 94] T. F. Rosenbaum, G. A. Thomas, and M. A. Paalanen, *Critical behavior of Si:P at the metal-insulator transition*, Phys. Rev. Lett. **72**, 2121 (1994).

[Rosny 00] J. de Rosny, A. Tourin, and M. Fink, *Coherent backscattering of an elastic wave in a chaotic cavity*, Phys. Rev. Lett. **84**, 1693 (2000).

[Rotter 17] S. Rotter and S. Gigan, *Light fields in complex media: mesoscopic scattering meets wave control*, Rev. Mod. Phys. **89**, 015005 (2017).

[Sanchez-Palencia 07] L. Sanchez-Palencia, D. Clément, P. Lugan, P. Bouyer, G. V. Shlyapnikov, and A. Aspect, *Anderson localization of expanding Bose-Einstein condensates in random potentials*, Phys. Rev. Lett. **98**, 210401 (2007).

[Sanchez-Palencia 10] L. Sanchez-Palencia and M. Lewenstein, *Disordered quantum gases under control*, Nature Phys. **6**, 87 (2010).

[Saxon 55] D. S. Saxon, *Tensor scattering matrix for the electromagnetic field*, Phys. Rev. **100**, 1771 (1955).

[Scheffold 97] F. Scheffold, W. Hartl, G. Maret, and E. Matijevic, *Observation of long-range correlations in temporal intensity fluctuations of light*, Phys. Rev. B **56**, 10942 (1997).

[Scheffold 98] F. Scheffold and G. Maret, *Universal conductance of light*, Phys. Rev. Lett. **81**, 5800 (1998).

[Scheffold 99] F. Scheffold, R. Lenke, R. Tweer, and G. Maret, *Localization or classical diffusion of light?*, Nature **398**, 206 (1999).

[Schreiber 15] M. Schreiber, S. S. Hodgman, P. Bordia, H. P. Lüschen, M. H. Fischer, R. Vosk, E. Altman, U. Schneider, and I. Bloch, *Observation of many-body localization of interacting fermions in a quasirandom optical lattice*, Science **349**, 842 (2015).

[Schwartz 07] T. Schwartz, G. Bartal, S. Fishman, and M. Segev, *Transport and Anderson localization in disordered two-dimensional photonic lattices*, Nature **446**, 52 (2007).

[Semeghini 15] G. Semeghini, M. Landini, P. Castilho, S. Roy, G. Spagnolli, A. Trenkwalder, M. Fattori, M. Inguscio, and G. Modugno, *Measurement of the mobility edge for 3D Anderson localization*, Nature Phys. **11**, 554 (2015).

[Shapiro 12] B. Shapiro, *Cold atoms in the presence of disorder*, J. Phys. A: Math. Theor. **45**, 143001 (2012).

[Sheng 06] P. Sheng, *Introduction to wave scattering, localization and mesoscopic phenomena*, 2nd edition, Springer-Verlag, Heidelberg, (2006).

[Shepelyansky 89] G. Casati, I. Guarneri, and D. L. Shepelyansky, *Anderson transition in a one-dimensional system with three incommensurate frequencies*, Phys. Rev. Lett. **62**, 345 (1989).

[Sinova 15] J. Sinova, S. O. Valenzuela, J. Wunderlich, C. H. Back, and T. Jungwirth, *Spin Hall effects*, Rev. Mod. Phys. **87**, 1213 (2015).

[Sivan 87] U. Sivan and Y. Imry, *Energy-level correlation function and ac conductivity of a finite disordered system*, Phys. Rev. B **35**, 6074 (1987).

[Skipetrov 07] S. E. Skipetrov, A. Minguzzi, B. A. van Tiggelen, and B. Shapiro, *Anderson localization of a Bose-Einstein condensate in a 3D random potential*, Phys. Rev. Lett. **100**, 165301 (2008).

[Skipetrov 09] S. E. Skipetrov, B. A. van Tiggelen, and J. H. Page, *La localisation forte d'Anderson des ondes classiques*, Images de la physique 2009, 2010, p.75.

[Skipetrov 14] S. E. Skipetrov and I. M. Sokolov, *Absence of Anderson localization of light in a random ensemble of point scatterers*, Phys. Rev. Lett. **112**, 023905 (2014).

[Skipetrov 16] S. E. Skipetrov and J. H. Page, *Red light for Anderson localization*, New J. Phys. **18**, 021001 (2016).

[Slevin 14] K. Slevin and T. Ohtsuki, *Critical exponent for the Anderson transition in the three-dimensional orthogonal universality class*, New J. Phys. **16**, 015012 (2014).

[Sperling 13] T. Sperling, W. Bührer, C. M. Aegerter, and G. Maret, *Direct determination of the transition to localization of light in three dimensions*, Nature Phot. **7**, 48 (2013).

[Sperling 16] T. Sperling, L. Schertel, M. Ackermann, G. J. Aubry, C. M. Aegerter, and G Maret, *Can 3D light localization be reached in 'white paint'?*, New J. Phys. **18**, 013039 (2016).

[Stephen 86] M. Stephen and G. Cwillich, *Rayleigh scattering and weak localization: effects of polarization*, Phys. Rev. B **34**, 7564 (1986).

[Stone 85] A. D. Stone, *Magnetoresistance fluctuations in mesoscopic wires and rings*, Phys. Rev. Lett. **54**, 2692 (1985).

[Störzer 06] M. Störzer, P. Gross, C. M. Aegerter, and G. Maret, *Observation of the critical regime near Anderson localization of light*, Phys. Rev. Lett. **96**, 063904 (2006).

[Sun 12] C. Sun, S. Jia, C. Barsi, S. Rica, A. Picozzi, and J. W. Fleischer, *Observation of the kinetic condensation of classical waves*, Nature Phys. **8**, 470 (2012).

[Thouless 74] D. J. Thouless, *Electrons in disordered systems and the theory of localization*, Phys. Rep. **13**, 93 (1974).

[Tian 05] C. Tian, A. Kamenev, and A. Larkin, *Ehrenfest time in the weak dynamical localization*, Phys. Rev. B **72**, 045108 (2005).

[Tourin 97] A. Tourin, A. Derode, P. Roux, B. A. van Tiggelen, and M. Fink, *Time-dependent coherent backscattering of acoustic waves*, Phys. Rev. Lett. **79**, 3637 (1997).

[Vakulchyk 18] I. Vakulchyk, M. V. Fistul, and S. Flach, *Universal nonlinear disordered wave packet subdiffusion: 12 Decades*, arXiv 1806.06345 (2018).

[van Tiggelen 07] B. A. van Tiggelen, S. E. Skipetrov, N. Cherroret, and S. Kawka, *Self-consistent treatment of Anderson localization. An attempt to engineer with scaling theory*, Advances in Nanophotonics II: International Summer School on Advances in Nanophotonics II. AIP Conference Proceedings **959**, 79 (2007).

[Verma 14] M. Verma, D. K. Singh, P. Senthilkumaran, J. Joseph, and H. C. Kandpal, *Ultrasensitive and fast detection of denaturation of milk by coherent backscattering of light*, Sci. Rep. **4**, 7257 (2014).

[Vermersch 13] B. Vermersch, *Dynamique d'un gaz de bosons ultra-froids dans un milieu désordonné : effets des interactions sur la localisation et sur la transition d'Anderson*, thèse de doctorat, Laboratoire de Physique des Lasers, Atomes et Molécules, Université des Sciences et Technologie de Lille (2013).

[Volchkov18] V. V. Volchkov, M. Pasek, V. Denechaud, M. Mukhtar, A. Aspect, D. Delande, and V. Josse, *Measurement of spectral functions of ultracold atoms in disordered potentials*, Phys. Rev. Lett. **120**, 060404 (2018).

[Vollhardt 80a] D. Vollhardt and P. Wölfle, *Anderson Localization in $d \leqslant 2$ dimensions: a self-consistent diagrammatic theory*, Phys. Rev. Lett. **45**, 842 (1980).

[Vollhardt 80b] D. Vollhardt and P. Wölfle, *Diagrammatic, self-consistent treatment of the Anderson localization problem in $d \leqslant 2$ dimensions*, Phys. Rev. B **22**, 4666 (1980).

[Vollhardt 82] D. Vollhardt and P.Wölfle, *Scaling equations from a self-consistent theory of Anderson localization*, Phys. Rev. Lett. **48**, 699 (1982).

[Vollhardt 92] D. Vollhardt and P. Wölfle, *Self-consistent theory of Anderson localization*, in *Electronic phase transitions*, Elsevier Science, Amsterdam (1992).

[Wang 09] W.-M. Wang and Z. Zhang, *Long time Anderson localization for the nonlinear random Schrödinger equation* J. Stat. Phys. **134**, 953 (2009).

[Weaver 00] R. L. Weaver and O. I. Lobkis, *Enhanced backscattering and modal echo of reverberant elastic waves*, Phys. Rev. Lett. **84**, 4942 (2000).

[Wellens 08] T. Wellens and B. Grémaud, *Nonlinear coherent transport of waves in disordered media*, Phys. Rev. Lett. **100**, 033902 (2008).

[White 09] M. White, M. Pasienski, D. McKay, S. Q. Zhou, D. Ceperley, and B. DeMarco, *Strongly interacting bosons in a disordered optical lattice*, Phys. Rev. Lett. **102**, 1 (2009).

[Wiersma 95] D. S. Wiersma, M. P. Van Albada, B. A. van Tiggelen, and A. Lagendijk, *Experimental evidence for recurrent multiple scattering events of light in disordered media*, Phys. Rev. Lett. **74**, 4193 (1995).

[Wiersma 97] P. Bartolini, A. Lagendijk, R. Righini, and D. S. Wiersma, *Localization of light in a disordered medium*, Nature **390**, 671 (1997).

[Wolf 88] P. E.Wolf, G. Maret, E. Akkermans and R. Maynard, *Optical coherent backscattering by random media : an experimental study*, J. Phys. (France) **49**, 63 (1988).

[Wolfle 10] P. Wölfle and D. Vollhardt, *Self-consistent theory of Anderson localization: general formalism and applications*, Int. J. Mod. Phys. B **24**, 1526 (2010).

[Zharekeshev 95] I. K. Zharekeshev and B. Kramer, *Universal fluctuations in spectra of disordered systems at the Anderson transition*, Jpn J. Appl. Phys. **34**, 4361 (1995).